UNIVERSITY OF LIVERPOOL

Assessing Human Embryonic Stem Cell-Derived Dopaminergic Neuron Progenitor Transplants Using Non-invasive Imaging Techniques

Thesis submitted in accordance with the requirements of the University of Liverpool for the Doctor in Philosophy by

Masoumeh Mousavinejad

March 2021

Abstract

Assessing Human Embryonic Stem Cell-Derived Dopaminergic Neuron Progenitor Transplants Using Non-invasive Imaging Techniques,

by Masoumeh Mousavinejad.

Parkinson's disease (PD) is a neurodegenerative disease that results, in part, from the progressive loss of dopaminergic (DA) neurons in the Substantia Nigra pars compacta (SNpc). Several groups have shown that human Pluripotent Stem Cell (hPSC)-derived dopaminergic neuron Progenitor Cells (DAPCs) can generate mature DA neurons and improve motor function following intrastriatal transplantation in animal models of PD. This has now evolved to the point that the first in human hPSC-based DA neural transplants are being undertaken or are being planned in patients with PD. However, prior to undertaking larger-scale clinical studies, animal experiments are needed to adequately assess the safety of the therapies. Key safety concerns with such therapies for PD and other Central Nervous System (CNS) disorders include the risk that the implanted cells could proliferate and form space-occupying masses and/or migrate to off-target sites within the CNS and/or induce major neuroinflammation. In addition to considering the potential risks, it is also important to monitor the long-term viability and differentiation capacity of implanted cells, as to be effective, they must differentiate into the appropriate phenotype and persist in the brain. Monitoring viability and biodistribution of the DAPCs over time requires non-invasive imaging techniques. In this project, a bimodal imaging strategy based on Bioluminescence (BLI) and Magnetic Resonance Imaging (MRI) to monitor the safety of the human Embryonic Stem Cell (hESC)-based therapy in immunocompromised nude rats has been investigated. BLI is the preferred technique for monitoring viability and proliferation *in vivo*, but spatial resolution is poor, meaning that it cannot be used to assess intracranial biodistribution. However, this can be overcome by labelling cells with Iron Oxide Particles (IOPs) so

that they can be imaged using MRI, a technique that provides very high spatial resolution. RC17 hESCs were transduced with bicistronic Luciferase-ZsGreen lentiviral particles and directed to differentiate to DAPCs. Expression of DAPC markers was assessed to confirm the success of the differentiation. Furthermore, a group of RC17 hESCs were differentiated into DAPCs and labelled using Micron-sized Particles of Iron Oxide (MPIOs) to be visualized using MRI. DAPCs expressing Luciferase-ZsGreen or labelled with MPIOs were transplanted in the striatum of nude rats (n = 6 per group). DAPCs were tracked *in vivo* using BLI and MR imaging modalities. Transgene silencing in differentiating DAPCs accompanied with signal attenuation due to animal growth, rendered the BLI undetectable by week 2 post intrastriatal transplantation. However, MR imaging of MPIO-labelled DAPCs showed that transplanted cells remained at the site of injection for over 120 days. Post-mortem histological analysis of DAPC transplants demonstrated that labelling with either Luciferase-ZsGreen or MPIOs did not affect the ability of cells to differentiate into mature dopaminergic neurons. Importantly, labelled cells did not elicit increased glial reactivity compared to non-labelled cells.

Acknowledgements

First of all, I would like to express my deepest gratitude to my supervisor Professor Patricia Murray, who has guided me through my PhD project- there is no word to express my thanks to you for all your brilliant support, insightful advice and kind patience, and that always placing so much trust in me and my work.

My sincere thanks must also go to my co-supervisors: Professor Harish Poptani and Dr. Antonius Plagge, to offer me feedback and guidance throughout the project.

I would like to thank members in the research lab who inspired me over the past four years. In particular, I am grateful to Dr. Chris Hill for his advice and valuable comments over the course of the research; Dr. Arthur Taylor, for providing the viralparticles to generate reporter gene and his help in the animal experiment, *in vivo* administration and imaging data acquisition; Tamiris Borges Da Silva for her support in undertaking Flow cytometry experiment. I would also like to offer my thanks to Ms. Pam Tyers (University of Cambridge) for *in vivo* cell administration; Pathologist Dr. Rajeev Shukla (Alder Hey Children's NHS Foundation Trust) for his comments on histopathological analysis, and Mr. Chris Law for his help in the cell sorting.

Last but not least, my thanks must go to my parents, husband, son, sister and brothers: you have provided to me endless love, encouragement and support throughout my life; THANKS for everything!

Contents

List of Figures

List of Tables

Abbreviations

AA	L-Ascorbic Acid
AAV	Adeno-associated viral
AC	Adenylyl cyclase
ATP13A2	Adenosine three phosphatase cation transporting 13A2
BARHL1	Barh-like homeobox 1
BBB	Blood-brain-barrier
BDNF	Brain-derived neurotrophic factor
BLI	Bioluminescence
BMP	Bone morphogenetic protein
c-Myc	C-myelocytomatosis
cAMP	Adenosine 3',5'-cyclic monophosphate
CAUD	Caudate nucleus
CED	Convection-enhanced delivery
CNS	Central nervous system
COMT	Catechol-O-methyltransferase
DA	Dopamine
DAPCs	Dopaminergic progenitor cells
DAPI	4',6-diamidino-2-phenylindole
DAT	Dopamine transporter
DBS	Deep brain stimulation
DDC	Dopa decarboxylase
Ddc	L-aromatic amino acid decarboxylase
DJ-1	Parkinson protein 7
EB	Embryoid body
EN1	Engrailed homeobox 1
EN2	Engrailed homeobox 2
ESCs	Embryonic stem cells
FDA	Food and drug administration
FGF8	Fibroblast growth factor 8

FLASH Fast low angle shot

Fluc Firefly luciferas

FOXA1 Forkhead box A1

FOXA2 Forkhead box A2

FP Floor plate

FVM Fetal ventral mesencephalic

GAPDH Glyceraldehyde-3-phosphate dehydrogenase

GBX2 Gastrulation brain homeobox 2

GDNF Glial cell line-derived neurotrophic factor

GFAP Glial fibrillary acidic protein

GFP Green fluorescent protein

Gluc Gaussia luciferase

GMP Good manufacturing practice

GSKi Glycogen synthase kinase inhibitor

hNCAM Human neural cell adhesion molecule

hNuclei Human-specific nuclear antigen

hpESCs Human parthenogenetic embryonic stem cells

HSV Herpes simplex virus

iPSCs Induced pluripotent stem cells

IsO Isthmus organizer

Klf4 Kruppel-like factor 4

L-Dopa L-3,4-dihydroxyphenylalanine

LIN28 Lin-28 homolog

LMX1A Lim homeobox transcription factor 1, alpha

LMX1B Lim Homeobox Transcription Factor 1, beta

LRRK2 Leucine-rich repeat kinase 2

LV Lentiviral

MAOB Oxidation via monoamine oxidase type B

MHC Major histocompatibility complex

MOI Multiplicities of infection

MPIOs Micron-sized particles of iron oxide

MPTP N-methyl-4-phenyl-1, 2, 3, 6-tetrahydropyridine

MRI Magnetic resonance imaging

MSCs Mesenchymal stromal cells

MSX1 Msh homeobox 1

Nanog Nanog homeobox

NPCs Neural progenitor cells

NRTN Neurturin

NT-3 Neurotrophin-3

NT-4 Neurotrophin-4

NTFs Neurotrophic factors

Nurr1 Nuclear receptor related 1 protein

OCT4 Octamer-binding transcription factor 4

OTX2 Orthodenticle homeobox 2

PD Parkinson diseases

PET Positron emission tomography

PINK1 PTEN induced putative kinase 1

PITX2 Paired-like homeodomain 2

PITX3 Pituitary homeobox 3

PKA Phosphoinositide 3-kinase

PUT Putamen

qRT-PCR Quantitative reverse transcriptase polymerase chain reaction

rAAV Recombinant adeno-associated virus

RARE Rapid acquisition with relaxation enhancement

Rluc Renilla luciferase

RNU rat Rowett nude rat

ROS Reactive oxidative stress

SHH Sonic hedgehog

SNCA Synuclein alpha

SNpc Substantia nigra pars compacta

SOX2 Sry-box 2

SPECT Single-photon emission computed tomography

SPIONs Superparamagnetic iron oxide nanoparticles

STN Subthalamic nucleus

TGFβ Transforming growth factor beta

TH Tyrosine hydroxylase

TSPO Translocator protein

USPIONs Ultra-small superparamagnetic iron oxide nanoparticles

VM Ventral midbrain

VMAT Vesicular monoamine transporter

VMAT2 Vesicular monoamine transporter 2

VPS35 Vacuolar protein sorting 35 homolog

VZ	Ventricular zone
Wnt1	Wingless-type 1
ZsGreen	Zoanthus sp. Green fluorescent protein
6-OHDA	6-hydroxy-dopamine

CHAPTER 1

Introduction

1.1 Parkinson's disease

Parkinson's Disease (PD) was first described by Dr. James Parkinson over 200 years ago as a "shaking palsy" that he described as "Paralysis agitans" (DeMaagd and Philip, 2015). Today, PD is the second most common progressive neurodegenerative disorder, affecting 1% of the population over 65 years old. The disease is strongly associated with increased age and likely to become more prevalent as life expectancy increase (Foltynie et al., 2004).

Currently, 4.6 million people suffer from PD worldwide and the European Parkinson Disease Association (EPDA) has estimated that the annual European cost of the disease is approximately 14 billion Euros. The number of people in the UK with PD is estimated to have increased by 27% between 2009 and 2020 (about 162,000 individuals) (DeMaagd and Philip, 2015). Typically, PD appears in the 6th decade of life, although about 20% of patients that are classified as "young-onset", develop PD before age 50 (Mhyre et al., 2012).

1.1.1 Diagnosis and symptoms

Patients with PD are clinically diagnosed with both motor and non-motor systems. The noticeable motor symptoms including altered gait, bradykinesia (slowness of movement), resting tremors, muscle rigidity, and postural instability, usually occur when about 60–80% of DA neurons in the SNpc have degenerated (Parkinson, 1817; Twelves et al., 2003). Typically, the non-motor symptoms such as sleep disorders, depression, cognitive dysfunction, and pain are also important to identify, as early diagnosis of PD could be crucial for effective treatment (Schrag et al., 2015).

Although all patients will not necessarily experience all PD symptoms in the same order, the typical patterns of progression are nevertheless defined in different stages based on symptoms development. During the initial stages, mild symptoms such as changes in gait and posture will occur, but as the disease progresses, more significant motor abnormalities will appear, and patients typically need assistance with their daily activities (Gómez-Esteban et al., 2007). During the final stages, more severe and limiting symptoms prevent the patients from undertaking any movement at all and there can be difficulties with speech and swallowing; in 25-30% of cases, dementia has been reported (Hakim and Mathieson, 1979; Aarsland et al., 2003). Currently, PD is diagnosed on the basis of clinical features. The UK Parkinson's Disease Society Brain Bank has formalized some criteria for PD with a diagnostic accuracy of up to 90%. The bradykinesia is the most common feature which has the strongest correlation with deficiency of dopamine in PD patients.

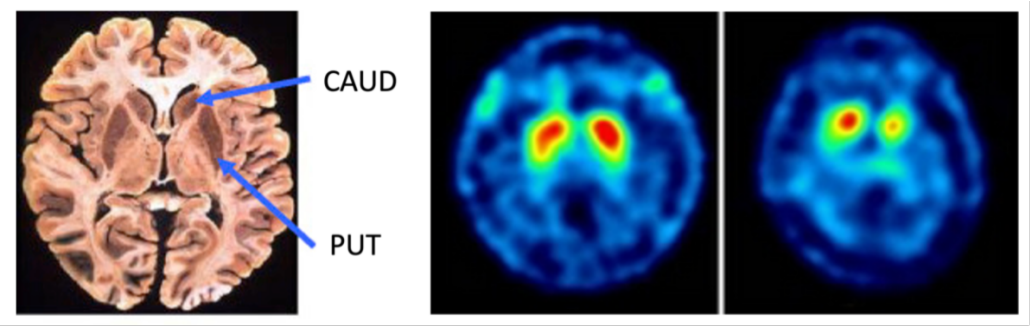

Figure 1.1: Clinical diagnosis of Parkinson's disease using SPECT imaging of [^{99m}Tc]TRODAT-1. [^{99m}Tc]TRODAT-1 is a dopamine transporter imaging agent. Left image shows the histology of the brain to indicate the striatum consisting of Caudate Nucleus (CAUD) and the Putamen (PUT). The middle image is the SPECT image of a normal brain with a typical degree of [^{99m}Tc]TRODAT-1 signal. The right image shows a lower level of [^{99m}Tc]TRODAT-1 signal in a PD patient in the early stages of the disease that indicates dopaminergic neuronal loss, usually with a more pronounced decrease in the putamen rather than in the caudate (Herscovitch, 2014).

The other classic symptoms are hypophonia (soft voice), micrographia (small handwriting) and rigidity (stiffness), which usually affect the upper limbs in the initial stages. Clinical imaging approaches are also available to help diagnose PD (Jankovic and Poewe, 2012). The commonly used imaging techniques are MRI, Positron Emission Tomography (PET) and Single-Photon Emission Computed Tomography (SPECT) (Wang et al., 2012). The nuclear imaging techniques, PET and SPECT typically use

radioactive dopamine ligands to assess dopamine metabolism (Smith et al., 2012; Simonson et al., 2007). A reduction in tracer uptake, or asymmetric uptake in the dorsal or posterior parts of the striatum can be seen in PD patients (Figure 1.1) (Pagano et al., 2016).

1.1.2 Pathology

1.1.2.1 Dopaminergic neurons

PD is characterised by selective degeneration of melanised dopaminergic A9 neurons in the (SNpc) and disruption of the nigrostriatal pathway. The dopaminergic neurons projects axons into the putamen and caudate nucleus that form the striatum in primates to release dopamine (Figure 1.2). The putamen is important for modulation of planning and movement by stimulation of the motor cortex while the caudate nucleus is implicated in cognitive processes (Parkkinen et al., 2011).

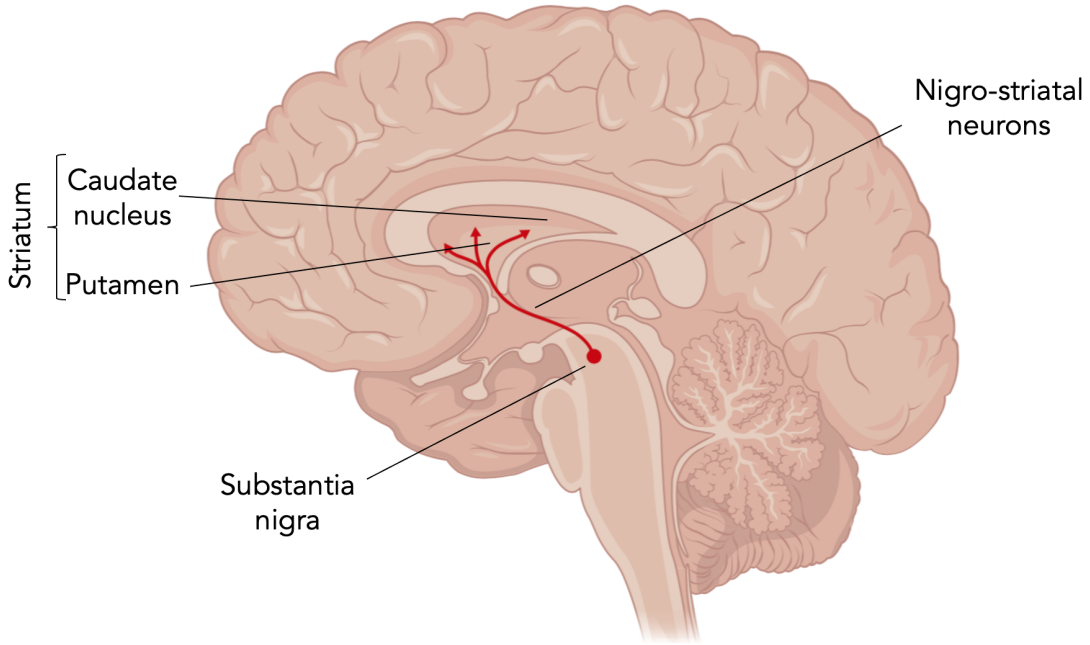

Figure 1.2: The nigrostriatal pathway and projection of dopamine neurons into striatum. Signals that control body movements travel along neurons that project from the substantia nigra to the caudate nucleus and putamen (collectively called the striatum). These "nigro-striatal" neurons (i.e., dopaminergic neurons) release dopamine at their targets in the striatum. In Parkinson's patients, dopamine neurons in the nigro-striatal pathway degenerate for unknown reasons (Bethesda, 2001).

In the DA neurons of the normal adult brain, L-Dopa is synthesized from the amino acid, tyrosine, by the enzyme Tyrosine Hydroxylase *(TH)* that take place in the cytoplasm. L-Dopa is further converted to dopamine by Dopa Decarboxylase (DDC) (Hamanaka et al., 2016). Dopamine is then stored in cytoplasmic vesicles using a

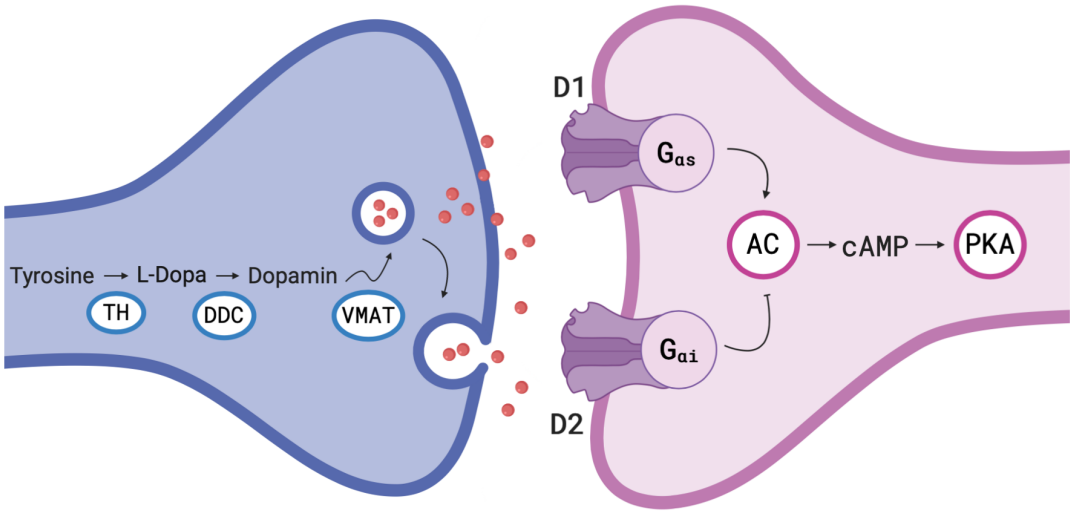

Figure 1.3: Dopamine neurotransmitter signalling in the brain. The schematic figure illustrates the biosynthesis of L-Dopa from Tyrosine using *TH* and further metabolism of Dopamine neurotransmitter by Dopa Decarboxylase (DDC). Realising of Dopamine from presynaptic neuron could be resulted in activation of D1 and D2 receptors in the postsynaptic neuron. D1 receptor signal through G protein to activate Adenylate Ayclase (AC) and formation of cAMP and further stimulation of Phosphoinositide 3-kinase (PKA) while D2 receptor could inhibit this pathway.

Vesicular Monoamine Transporter (VMAT). Release of dopamine neurotransmitter in the presynaptic neuron results in activation of D1 and D2-type dopamine receptors in the postsynaptic neuron. The D1 receptor is coupled to $G\alpha s$ proteins which can activate Adenylyl Cyclase (AC) to raise intracellular cAMP concentrations, leading to activation of the phosphoinositide 3-kinase (PKA) pathway; this, in turn, activates the related transcription factors in the postsynaptic neuron. In contrast, the D2-type receptor inhibits AC and blocks the PKA signalling pathway (Figure 1.3) (Girault and Greengard, 2004).

1.1.2.2 Lewy bodies

In the brain of Parkinson's patients, the degeneration of DA neurons is accompanied by deposition or accumulation of Lewy bodies which are mainly misfolded and insoluble aggregates of α-Synuclein (Mahul-Mellier et al., 2020). α-Synuclein protein is mainly found at the presynaptic terminals of neurons and has a critical role in modulation of synaptic vesicle dynamics to release neurotransmitters. Usually, the α-Synuclein inclusions are originate in the SNpc which is the main location of cell loss in PD patients (Hijaz and Volpicelli-Daley, 2020). Also, the spread of Lewy bodies in the cortex causes the stepwise degeneration of neurons corresponding to an intensification

of disease, associated with the appearance of motor symptoms (Meade et al., 2019). During the late stage of PD, the presence of Lewy bodies was confirmed in the frontal cortex of patient's brains; this could explain why dementia is not uncommon in the late stages of PD (Springer and Kahle, 2011; Spillantini et al., 1998).

In PD cases that have a known genetic basis, it has been established that oligomerisation of α-Synuclein is a common feature (Table 1.1). For instance, mutations in *SNCA*, the gene that encodes α-Synuclein, result in the proteostasis, misfolded and over-expression of α-Synuclein (Park et al., 2018). Mutations in *ATP13A2* (*PARK9*) and *LRRK2* are linked to lysosome dysfunction and/or defective autophagy, leading to reduced *α-Synuclein* degradation (Zimprich et al., 2004; Spataro et al., 2019). In addition, *Parkin*, *PINK1*, and *DJ-1* have roles in the inducing apoptosis, and hence the indirect formation of Lewy bodies. Loss-of-function mutations in *Parkin* and *PINK1* result in mitophagy (a cellular process to clear damaged mitochondria) which is associated with mitochondrial dysfunction (Park et al., 2018; Hu and Wang, 2016). *DJ-1* encodes a putative oxidant known to increase cellular Reactive Oxidative Stress (ROS) in DA neurons (Ariga et al., 2013). *VPS35* gene mutations can result in mitochondrial fragmentation which leads to neurodegeneration in PD patients. Table 1.1 describes the main genes implicated in PD.

Table 1.1: The main genes known to cause PD, their encoded protein and mode of transmission (Lansbury and Brice, 2002; Park et al., 2018).

Gene	Role	Transmission
$\alpha-$Synuclein (SNCA)	Presynaptic protein	Dominant
LRRK2 (PARK8)	Kinase	Dominant
VPS35	Involved in the transport of proteins from endosomes to the Golgi	Dominant
ATP13A2	Lysosomal protein involved in transportation across lysosomal membrane	Recessive
Parkin (PARK2)	Subunit of the E3 ubiquitin ligase	Recessive
PINK1	Mitochondrial kinase	Recessive
DJ1 (PARK7)	Ubiquitin ligase	Recessive

1.1.3 Aetiology and epidemiology

Aetiology of PD is poorly understood, but as mentioned above, it is believed that certain genetic mutations are related to dopaminergic cell death (Table 1.1) (Tanner

et al., 1999). These genetic mutations are well documented and can be inherited or can occur through exposure to environmental neurotoxins (Nandipati and Litvan, 2016). The main environmental neurotoxins that are recognized as a potential cause of PD are MPTP (N-methyl-4-phenyl-1, 2, 3, 6-tetrahydropyridine), pesticides (such as Rotenone, Paraquat and Maneb), and metals (such as iron and manganese) (Nandipati and Litvan, 2016). There is also an inflammatory component to PD, as suggested by animal experiments, and by the presence of activated microglia in the SNpc of PD patients. The activated microglia caused apoptosis by releasing inflammatory cytokines and inducing cell stress (Lecours et al., 2018).

The incidence of PD is associated with different risk factors such as age, sex and ethnicity (Wright Willis et al., 2010). The global age prevalence of PD onset is categorised as "early" and "late" depending on whether symptoms appear before or after the age of 50. PD is rare before the age of 50 and increases sharply after 80 years of age (Van Den Eeden et al., 2003).

The other associated PD risk factor is sex, as several studies have shown that PD is twice as common in men than in women. The protective effects of female sex hormones and more exposer of males to environmental risks might explain this difference. Geography and race are also PD risk factors but the reasons for this are unclear (Wright Willis et al., 2010). For instance, the incidence of PD in Hispanics is 16.6 per 100,000 persons, compared to 13.6 per 100,000 in non-Hispanic Whites, 11.3 per 100,000 in Asians, and 10.2 per 100,000 in Blacks (Van Den Eeden et al., 2003). These differences in PD prevalence could be due to differences in lifestyle and diet between each population (Abbas et al., 2018).

1.1.4 Current therapies for PD

Currently, there is no cure for PD, and mainstay treatments focus on providing symptomatic relief (Jankovic and Aguilar, 2008). However, there is optimism that stem cell therapy could provide a cure for future PD patients by replacing the DA neurons that are lost as a result of the disease (Section 1.2) (Lindvall and Björklund, 2004).

1.1.4.1 Pharmacological approach

The dopamine replacement drug, L-3,4-dihydroxyphenylalanine (L-Dopa), which is the precursor of dopamine, is the most effective drug to treat Parkinson's symptomatically and all patients receive this treatment over time (Schapira, 2005). Unlike dopamine,

L-Dopa is able to cross the Blood Brain Barrier (BBB) and is then converted into dopamine by the DA neurons, thereby restoring dopamine levels in the central nervous system. However, after an initial period of dramatic benefit (about 5 years), the limitation and side effects of L-Dopa become increasingly problematic. "Dopa-resistant" symptoms, such as postural abnormalities, speech impairment, autonomic dysfunction, and/or "drug related" side effects especially development of motor fluctuations and dyskinesias have been reported (Huot et al., 2013; Widnell, 2005; Thanvi and Lo, 2004). In most PD patients who have received L-Dopa orally, peripheral dopa decarboxylase inhibitors (particularly Catechol-O-methyltransferase (COMT) inhibitors) such as carbidopa, or benderizine are administrated to decrease side effects and improve the activity of L-Dopa in the central nervous system (Vassiliou et al., 2019). In addition, developing the new sustained-release formulation of L-Dopa and continuous delivery (via mini pumps subcutaneously or tubes percutaneously) of the drug could overcome the problems associated with the short half-life of L-Dopa, inconsistency in BBB transportation and gastrointestinal absorption (van Wamelen et al., 2018).

Dopaminergic receptor agonists such as bromocriptine, and pergolide are able to target and stimulate the dopamine receptors in the brain and help improve the motor symptoms (Brooks, 2000). Dopamine mimetic receptors have longer half-lives compared to L-Dopa and could delay consuming L-Dopa in patients if used in the early stages of PD development (Perez-Lloret and Rascol, 2010).

Another type of drug used in PD patients are inhibitors of dopamine degradation. Oxidation via Monoamine Oxidase type B (MAOB) is the main mechanism for dopamine clearance in the synapses. Inhibitors of MAOB such as Selegiline and Rasagiline have been found to effectively increase the concentration of synaptic dopamine and are helpful in patients with fluctuations in motor symptoms, especially when used in combination with L-Dopa (Schapira, 2011; Cereda et al., 2017).

1.1.4.2 Neurotrophic factors-based therapies

A vast body of experimental studies suggests that the lack of specific Neurotrophic Factors (NTFs), the secreted proteins that play a critical role in the development, survival, protection, and maturation of neurons, contribute to the pathophysiology of PD (Rodrigues et al., 2014). Two of the dopaminergic NTFs, namely Glial cell line-Derived Neurotrophic Factor (GDNF) and Neurturin (NRTN) have shown great potential in

promoting axon regeneration following damage and protection of nigrostriatal DA neurons *in vitro* (Sullivan and O'Keeffe, 2016). However, the delivery of NTFs to the correct locations in the brain is still a practical challenge because they cannot pass the BBB and will undergo rapid bio-metabolism by endogenous enzymes *in vivo* (Domanskyi et al., 2015).

A recently published clinical trial using a new infusion protocol for GDNF was conducted by a group in Bristol (UK CRN 12085). During the course of the trial, patients were administrated GDNF via a skull-mounted port every 4 weeks using a bilateral intra-putamenal convection-enhanced delivery (CED) (Whone et al., 2019). As the outcome of trial, the extent of benefit in the experimental group was not significantly greater than in the placebo due to the fact that the NTFs need to be delivered more repeatedly.

Gene therapy could be a potential way to bypass the issue of localized delivery of NTFs and is an approach that is being actively explored. Recent studies show that incorporation of therapeutic genes into brain cells using recombinant viral vectors (Adeno-Associated Viral (AAV) or Lentiviral (LV) vectors), stimulate over expression of NTFs (Sullivan and O'Keeffe, 2016). In this regard, assessing the safety and tolerability of AAV-GDNF is one of the ongoing Phase 1 clinical trials for advanced PD (NIH trial No. NCT01621581).

1.1.4.3 Deep brain stimulation

Deep Brain Stimulation (DBS) is a surgical option for advanced PD patients whose symptoms are no longer controlled using medication. DBS involves the surgical implantation of an electrode in the brain, usually in the globus pallidus internus or subthalamic nucleus, without any loss of brain tissue (Montgomery Jr. and Baker, 2000). A pulse generator which is connected to brain electrodes (is placed under the skin of the chest or stomach area) is able to electrically stimulate specific brain targets resulting in the mitigation and dramatic improvement of PD symptoms such as dyskinesia and motor fluctuation for up to about 5 years (Limousin and Foltynie, 2019).

DBS requires high levels of expertise as it is a major surgery in the brain which is usually associated with complications such as intracranial bleeding, infection, or misplacement of the electrode (Rezai et al., 2004). DBS cannot stop the Parkinson's from progressing but in many cases the control of motor symptoms can be highly

improved.

1.1.4.4 Cell-based therapies

Cell transplantation is a therapeutic approach that has generated great interest during recent decades. Current advances in our understanding of the mechanisms and molecular pathways involved in PD, make cell therapy a great candidate to improve the regeneration of dopaminergic neurons (Barker et al., 2015). Particularly, PD is an appropriate neurodegenerative disorder to be considered for cell replacement therapy due to the focal degeneration of a small proportion of DA neurons, making it a relatively easy target. The main objective of cell transplantation is to achieve neurochemical or structural brain repair in PD by replacing the lost cells with DA neurons (Parmar, 2018). In addition, through cell therapy, DA will be secreted locally in a more physiological way that could overcome the unregulated release of DA across the whole brain which is currently associated with the pharmacological approaches for PD treatment (Parmar, 2018).

There are several available cell candidates capable of generating DA neurons for PD treatment including Fetal Ventral Mesencephalic (FVM) cells, induced Pluripotent Stem Cells (iPSCs), Embryonic Stem Cells (ESCs); Mesenchymal stromal Cells (MSCs), Neural Progenitor Cells (NPCs), and human parthenogenetic Embryonic Stem Cells (hpESCs)that are used in clinical trial.

1.1.4.4.1 Fetal ventral midbrain cells

The idea of replacing the degenerated DA neurons in PD was introduced in the 1970s. Several different cell types have been evaluated in clinical trials, including retinal pigmented epithelial cells, porcine fetal ventral midbrain tissue, adrenal medullary cells and carotid body cells (Björklund and Lindvall, 2017). In 1987, the first clinical trial suggested that grafted immature dopaminergic cells derived from the midbrain of aborted fetuses could replace lost DA neurons, restore connectivity as well as reduce PD symptoms (Brundin et al., 2000; Piccini et al., 1999). In this trial, the fetal tissue was transplanted unilaterally or bilaterally into the putamen or caudate-putamen and the patients were on an immunosuppressive regime only for one year. Additionally, long-term follow-up trials have provided strong evidence of graft survival and derivation of functional DA neurons for 24 years with no sign of neuroinflammation (Kefalopoulou et al., 2014; Li et al., 2016). However, further transplantation studies supported by the

National Institute of Health (NIH) in the US found that more than 50% of the treated individuals developed side effects which was mainly graft-induced dyskinesia (Barker et al., 2013). Due to the inconsistent results obtained in different trials, a European group set out to define factors associated with positive graft outcomes and conducted an open trial called TRANSEURO that was initiated in 2009 (Barker et al., 2015). In this trail the patients in the earlier stages of the PD were included in the experimental group because earlier studies had shown very low effectiveness of cell administration for patients in the late stage of disease. 11 patients received bilateral grafts in Cambridge or Lund over 3 years and the last patient was grafted in 2018. Hopefully, the outcome of this trial will be fully released in 2021 (Barker et al., 2019). However, the low availability of human Fetal Ventral Midbrain (hFVM) tissue resulted in the cancellation of more than 80 grafting surgeries during the TRANSEURO trial (Barker et al., 2017). Major shortcomings of hFVM tissues and ethical concerns as well as reported side effects make this kind of clinical transplantation unfeasible for treating larg group of patients.

1.1.4.4.2 Neural stem cells

Primary Neural Stem Cells (NSCs) reside in a particular zone of the brain which is called the "neurogenic niches". These cells permit neurogenesis throughout life as they are self-renewing, multipotent cells (Chou et al., 2015). They can be obtained from fetal, neonatal and adult brains or by the directed differentiation of PSCs. Protocols have been established to isolate NSCs from the adult rat striatal Sub-Ventricular Zone (SVZ) and Sub-Granular Zone (SGZ) of the hippocampus in order to differentiate them into specialised Neural Progenitor Cells (NPCs) (Lois and Alvarez-Buylla, 1993; García-Verdugo et al., 1998). The autologous transplantation of NSC-derived NPCs has shown promising behavioural improvements in rodent models of PD. To date, only one trial involving autologous human NSC transplants has been reported (Levesque et al., 2010). This study was carried out on an individual PD patient and demonstrated the safety and efficacy of using NSC-derived DAPCs. However, procuring adult NSCs residing deep within the brain would require an invasive biopsy, which would not be very feasible due to safety concerns. Furthermore, poor growth potential, unstable phenotype upon repeated passages, and poor survival after transplantation were reported for these cells (Courtois et al., 2010; Ramos-Moreno et al., 2012). Also, clinical

trials aimed at assessing the safety and efficacy of these cells are still ongoing (Table 1.2).

1.1.4.4.3 Mesenchymal stromal cells

Mesenchymal Stromal Cells (MSCs) are adults stromal cells that were initially identified in bone marrow. MSCs can also be isolated from various other sources, including umbilical cord, adipose tissue and peripheral blood (Joyce et al., 2010). Self-renewal and multipotency capacity of differentiation into ectodermal linage make MSCs a good candidate for PD treatment (Chen and Chopp, 2006; Hayashi et al., 2013). Interestingly, MSCs are able to secrete immunomodulatory cytokines (such as Interleukin 6 (IL-6), Prostaglandin E2 (PGE2)) that regulate the intensity of the immune response; and trophic factors (such as GDNF, Brain-Derived Neurotrophic Factor (BDNF), and Nerve Growth Factor (NGF)) that not only have anti-apoptotic and neuro-regenerative effects, but also decrease oxidative stress and stimulate tissue regeneration (Caplan and Correa, 2011). For this reason, MSCs could limit the neuroinflammatory process which can occur following cell transplantation into the brain. Encouraging results obtained in experimental PD models have led to clinical trials using MSCs (Kumar et al., 2016). One of the pioneering studies which was conducted in 2010 involved transplanting autologous MSCs through stereotactic surgery. The patients were followed for a period of 36 months and clinical improvement was observed in 3 out of 7 patients without any serious adverse effects (Inden et al., 2016). Later, a pilot clinical study revealed the feasibility and efficacy of allogeneic MSC transplantation over 12 months in PD patients in early stages of disease (Venkataramana et al., 2012). However, the long-term safety and sustainability of this therapeutic strategy needs to be clarified (Mendes Filho et al., 2018). Other clinical trials involving MSCs for the treatment of PD have not published any results so far.

1.1.4.4.4 Human parthenogenetic embryonic stem cells

Human parthenogenetic Embryonic Stem Cells (hpESCs) are pluripotent cells that are derived from the chemical activation of unfertilized oocytes. In 2014 the US Food and Drug Administration (FDA) cleared the hpESC line used for investigational clinical use (Turovets et al., 2011). hpESCs bypass the ethical concerns associated with hFVM tissue or hESCs because no fetus or viable embryo is used in their derivation, but nevertheless, they show the typical characteristics of ESCs such as pluripotency

and teratoma formation after injection into immunodeficient animals (Wang et al., 2018). In addition, the de novo mutations in hpESCs are much lower compared to iPSCs which reduced the potential risk of tumorigenicity (Barker et al., 2016). In order to use hpESCs in a clinical trial, the stem cells were differentiated into NSCs (Garitaonandia et al., 2018). Animal studies involving rodent and non-human primate models of PD have shown that hpNSCs are able to differentiate into TH^+ neurons and promote behavioural recovery without any uncontrolled proliferation of the implanted cells (Garitaonandia et al., 2018; Gonzalez et al., 2016). However, the first clinical trial involving hpNSCs in PD was just aiming to assess the short-term safety and efficacy and has not been completed yet.

1.1.4.4.5 Pluripotent stem cells

Two main PSCs, ESCs and induced Pluripotent Stem Cells (iPSCs) have gained prominence over the past few years for transplantation as they are less ethically contentious compared to FVM (Medvedev et al., 2010; Amit et al., 2000).

The first mouse ESC line was isolated in 1980s from preimplantation mouse embryos (Evans and Kaufman, 1981) and later in the 1998s, human ESCs were isolated from the inner cell mass of the blastocyst by the Thomson group (Thomson et al., 1998). hESCs are pluripotent and self-renewing cells that are able to differentiate into any cell type and represent a breakthrough for the study of human development and disease (Thomson et al., 1998). However, harvesting hESCs involves destruction of the human embryo, which is ethically controversial (Lo and Parham, 2009).

iPSCs are pluripotent and indefinitely self-renew and are generated via reprogramming of differentiated somatic cells. The ectopic expression of four genes, *OCT4*, *SOX2*, *KLF4*, and *c–Myc*, in both embryonic and adult murine fibroblasts was first reported in 2006 by Yamanaka, who used lentiviral vectors to over-express those genes (Takahashi and Yamanaka, 2006). *OCT4*, *SOX2*, *Nanog*, and *LIN28* were used to generate patient specific iPSCs from individuals with genetic diseases (Liu et al., 2013). The major advantages of using iPSCs in clinical application is that the cultured cells would have an identical genome, theoretically minimising the risk of immune-rejection and increasing the chance of integration into the patient's tissues, while also circumventing the ethical issues associated with hESCs (Takahashi et al., 2007).

Table 1.2: Cell types that currently use in transplantation for PD.

Cell type	Clinical trial	Advantages	Disadvantages
Fetal ventral mesencephalic cells (FVM)	• TRANSEURO (NCT01898390)	• Good long-term graft survival post-transplantation • High efficacy	• Unpredictable and limited supply of cell source • Ethical concerns
Embryonic stem cells (ESCs)	• European-based STEM-PD (Cambridge trial) • China (NCT03119636)	• Indefinite expandability • Good graft survival post transplantation • Advancement in GMP-grade cells	• Ethical concerns • Possible risk of tumorigenesis and immunogenesis
Induced pluripotent stem cells (iPSC)	• Japan (UMIN000033564)	• Indefinite expandability • Easily accessible cell source • Immunologically matching cells • No need of immunosuppression treatment	• High heterogeneity of cell line between individual cell line • Low reprogramming efficiency • High operative cost and Time consuming • Possible risk of tumorigenesis
Mesenchymal stromal cells (MSCs)	• Trial is started at 2020	• Multipotent cells that are able to differentiate into DA cells • Immunomodulatory properties • Diversity of tissues from which they can be extracted • Ability to migrate to sites of injured tissue	• Establishing the best it *in vitro* conditions to grow desire cells is difficult • Safety against tumour formation and long term efficacy is not clear • High risk of thrombosis if administrated intravenously
human parthenogenetic stem cells (hpESCs)	• Australia (NCT02452723)	• Multipotent cells that are able to differentiate into DA cells • No ethical issue • Lower number of de novo coding mutations than iPSCs	• Long term safety and efficacy are not assessed yet
Neural progenitor cells (NPCs)	• USA (NCT03309514)	• Differentiation into specific neural linage including DA neurons • Lower risk of tumour formation and immune rejection comparing to ESCs	• Invasive tissue collection step • Limited proliferation ability • Low graft survivability

1.2 Pluripotent stem cell therapy for PD

The two most common sources of PSCs, namely ESCs and iPSCs, are the cell types that have been most rigorously assessed in regard to their safety and efficacy in PD therapies. Extensive research by different groups around the world have been conducted to differentiate PSCs into functional neural dopaminergic cells *in vitro* as these are the promising specialized cell sources for transplantation in PD patients (Figure 1.4) (Harris et al., 2020).

1.2.1 Neurodevelopment of midbrain DA neurons

DA neurons also known as Ventral Midbrain (VM) dopaminergic neurons are crucial for basic motor and non-motor behaviours. During the early development and regionalization of the neural tube, the position of cells along the dorsal-ventral and rostral-caudal axes is instructed through various signalling centres (Kiecker and Lumsden, 2012). In the neural tube, the gradience of *WNT1*, *FGF8*, and *SHH* signalling pathways provide the required positional information for development of the Isthmus organizer (IsO) and Floor Plate (FP) (Liu and Joyner, 2001). IsO specifies the boundary between the mid and hindbrain using *OTX2* and *GBX2* transcription factors. The DA neurons are generated from radial glia-like cells of the FP along the ventral midbrain (Martinez-Barbera et al., 2001). Extensive studies of transcriptional factors during early brain development have revealed that expression of *LMX1A* and its downstream effector *MSX1* in the mesodiencephalon ventricular zone, are the two earliest genes which determine DA identity along the dorsal-ventral axis. Expression of *FOXA1* and *FOXA2* markers in FP also regulate the development and maturation of midbrain DA neurons (Prakash et al., 2006; Zetterström et al., 1996). In addition to these markers, *EN1*, *EN2*, and *LMX1B* also influence DA differentiation. The expression of *FOXA2*, *OTX2*, and *LMX1A* genes was shown in the early progenitor neurons of the most caudal part of the ventral midbrain and is sustained through the maturation of midbrain DA neurons (Zetterström et al., 1996). However, these three markers are also expressed in the rostral domain of the ventral midbrain that gives rise to the glutamatergic Subthalamic Nucleus (STN) neurons. Also, *PITX2* and *BARHL1* were shown to be expressed in the rostral domain along with *FOXA2*, *OTX2*, and *LMX1A* (Kee et al., 2017).

In the post-mitotic stage of DA progenitor development, the expression of *Nurr1* is initiated which is important in the long-term differentiation and survival of mature DA

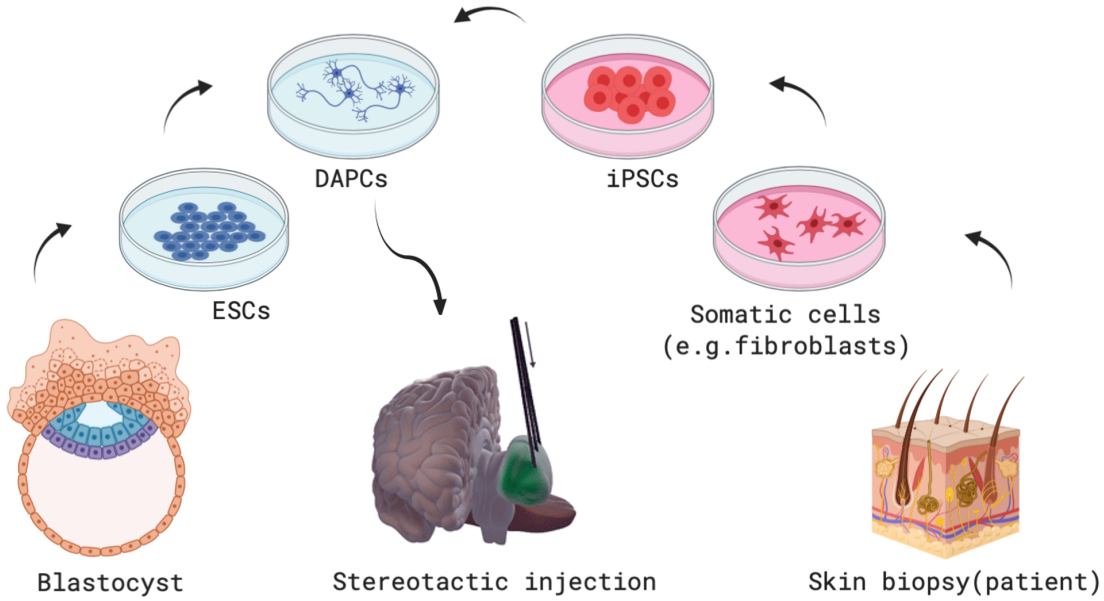

Figure 1.4: Available PSC sources currently be used in the clinical cell therapy for PD. DA neurons can be differentiated from ESCs isolated from preimplantation blastocysts. Somatic cells such as fibroblasts can be reprogrammed into iPSCs and further differentiate into DA neurons for stereotactic injection (Figure is modified from (Parmar, 2018)).

neurons (Hebsgaard et al., 2009). Critically, *Nurr1* is the key regulator of dopamine synthesis through induction of *TH*, Dopamine Transporter (DAT), Vesicular Monoamine Transporter 2 (VMAT2) and L-aromatic amino acid Decarboxylase (DDc) (Saucedo-Cardenas et al., 1998). The *PITX3* transcription factor is also expressed in the post mitotic DA progenitors and induces the expression of *Nurr1*, thereby promoting the terminal differentiation of DA neurons. Members of the neurotrophin family, including GDNF, BDNF, Neurotrophin-3 (NT-3), and Neurotrophin-4 (NT-4) are crucial in the later stage of DA neuron maturation and outgrowth (Jacobs et al., 2009; Nunes et al., 2003).

1.2.2 Strategies for generating hPSC-derived DA neurons

Few years after the first hESCs were isolated by Thompson (Thomson et al., 1998), a study describing the spontaneous differentiation of neural cells generated from hESCs was published (Itskovitz-Eldor et al., 2000). Some of the neural cells that were generated from this system expressed *TH*, but their frequency was quite low. However, the observation that *TH*-expressing neurons could be derived from hESCs in culture attracted a great deal of interest due to the possibility that they could be used to treat PD (Klein et al., 2019).

The first protocols for directing the differentiation of hESCs to DA neurons involved sub-culturing hESCs on murine stromal feeder cells or fetal midbrain cells with or without supplementation of growth factors such as *FGF8* and *SHH*. Although these protocols were quite successful *in vitro* and resulted in the differentiation of relatively high numbers of *TH* neurons, the neurons did not survive following grafting into 6-OHDA–lesioned rats. In addition, tumour formation was frequently reported following engraftment, which was thought to be due to non-synchronised and inefficient differentiation of DA neurons *in vitro* and the fact that the injected cell population contained undifferentiated hESCs (Perrier et al., 2004; Zeng et al., 2004; Roy et al., 2006; Sonntag et al., 2007). Greater understanding of the signalling pathways regulating brain development in the embryo inspired new protocols to drive DA neuron differentiation more effectively. In 2009, a group at the Sloan-Kettering institute reported neural induction through the inhibition of *BMP* and *TGFβ* signalling pathways (Chambers et al., 2009). Follow up studies by this group resulted in an optimised protocol for developing Floor plate cells from hESCs by supplementation of the culture medium with the ventralisation signalling factor, *SHH* (Fasano et al., 2010).

Further studies by Kirkeby et al., 2012 and Kriks et al., 2011, resulted in the generation of Floor plate-derived midbrain DA progenitors from hESCs that co-expressed *OTX2*, *LMX1A*, and *FOXA2* (Kirkeby et al., 2012; Kriks et al., 2011).These initial reports also showed that a Dual-SMAD inhibition protocol, through the addition of Noggin and SB431542 to inhibit BMPs and to block the down-stream pathways of Lefty, Activin and Transforming Growth Factor β (TGFβ), resulted in *TH* expression *in vitro*. Importantly, following engraftment into 6-OHDA lesioned rodents the progenitor cells restored motor function in the absence of tumour formation. These studies demonstrate the feasibility of hESC-derived DA neurons for PD treatment. Later, different groups undertook follow up studies to compare the functionality of the grafted hPSC-derived DA progenitors with hFVM grafts that had shown some efficacy in clinical trials (Chen et al., 2016; Hallett et al., 2015; Niclis et al., 2017). The study by Grealish et al., 2014, become an important landmark in this field, as this report showed similar efficacy and correct target-specific innervation of hESC-derived DA neurons and restoration of DA neurotransmission in the striatum compared with human FVM grafts using PET imaging *in vivo* (Grealish et al., 2014).

The promising results obtained from assessing the potential of hPSC therapies in animal models of PD has led to increased focus on improving differentiation protocols and developing them under Good Manufacture Practice (GMP) condition in order to move hPSCs therapies to the clinical setting for the benefit of PD patients (Section 1.2.3) (Barker et al., 2017).

The functionality of mature DA neurons arising from hPSC-derived DA progenitor cells was analysed using a primate model of PD. The survival of grafted iPSC-derived DA precursor cells in the lesioned primate brain; their maturation into DA neurons capable of secreting dopamine; and extensive innervation were confirmed in studies by Hallett et al., 2015 and Kikuchi et al., 2017. These positive effects were seen regardless of using iPSC from healthy donors or individuals with PD (Kikuchi et al., 2017). The benefit of using iPSCs generated from the patient would be to exclude the necessity of using immunosuppressants post grafting. Another new approach that has been proposed to reduce the need for immunosuppressants is to graft Major Histocompatibility Complex (MHC)-matched allogeneic iPSCs (Morizane et al., 2002). However, long-term graft rejection is still uncertain in this approach, as a study by Badin et al., 2019 shows long term rejection following engraftment of MHC-matched iPSC-derived neurons in a primate model (Aron Badin et al., 2019).

In 2014, the G-FORCE PD organisation (http://www.gforce-pd.com) was formed in order to develop stem cell-based therapy for PD. In 2018, the first human trial was initiated in Japan using iPSC-derived DA progenitors from healthy donor to assess the functionality and safety of the grafted cells (https://www.cira.kyoto-u.ac.jp/e/pressrelease/news/180730-170000.html).

1.2.3 The importance of preclinical studies in developing optimal clinical trial regimes for PD using hPSCs

hPSC-based therapies have the potential to dramatically change how PD patients are treated, because hPSCs can generate DA neurons that are lost in PD. Generally, hPSC therapies for PD involve directing the differentiation of hPSCs to Dopaminergic Progenitor Cells (DAPCs) *in vitro* and implanting these specialised cells into the brain where they undergo further differentiation to mature DA neurons. Although much progress has been made (Table 1.2), safety and efficacy of stem cell therapies in preclinical models needs to be addressed to increase the likelihood that all PD patients can

benefit from these promising therapies. To assess safety, it is important to determine whether the cells generate tumours and/or cause other adverse effects, such as neuroinflammation. To assess efficacy, the viability and functional activity of the cells needs to be monitored, as well as the extent and persistence of any therapeutic response.

In order to develop a safe and functional cell transplantation study, one early decision that needs to be made is which source of pluripotent cells to use: hiPSCs or hESCs? The risk of genetic abnormalities and teratoma formation is higher with iPSCs compared to hESCs which is the consequence of genetic instability due to genetic manipulation (Liang and Zhang, 2013). In addition, significant cost is associated with testing the safety and efficacy of different clonal iPSC lines for each individual patient prior to grafting (Couture and Carpenter, 2015). The only advantage of iPSCs compared to ESCs is that the risk of eliciting an immune response is expected to be lower for iPSCs. However, a clinical report by Li et al., 2016 suggests that allogenic neural transplants with 6-18 months of immunosuppression could survive more than 20 years in the brains of PD patients. Therefore, hESCs appear to have several advantages over iPSCs and have been selected for use in the forthcoming STEM-PD trial (Li et al., 2016). The choice of hESC lines is also important because it is known that hESC lines differ in their propensity to generate specific lineages (Allegrucci and Young, 2007). Studies by Kirkeby et al., 2017 and Nolbrant et al., 2017 showed that for producing a cell product for a PD clinical trial, the most appropriate clinical grade hESC lines are the RC17 line from Roslin Cells, and the HS980 line from the Karolinska Institute. These cell lines fulfil the important criteria of being free of oncogenic mutation and fully GMP-derived as well as generating highly pure populations of DA progenitor cells *in vitro* that later differentiate into mature DA neurons *in vivo* (Kirkeby et al., 2017; Nolbrant et al., 2017).

The next point towards achieving a safer and more efficient PD therapy is optimizing the patterning of hESCs. Several neural induction methods have been described for hESC differentiation that involve culturing the cells under adherent conditions, or in suspension (i.e., as neurospheres). Although these protocols demonstrate the presence of the ventral midbrain neural progenitor cells, the overall efficiency for generating a large and homogeneous population with precisely patterned neurons is variable (Section 1.2.2) (Kirkeby et al., 2012). A published nature protocol which was developed

by Parmar's group at Lund University was utilised in this study to obtain high purity DAPCs from undifferentiated RC17 hESCs. The protocol is relatively short and by day 16 of differentiation, almost 90% of the cells have differentiated to caudal ventral mid-brain progenitors that are able to give rise to mature DA neurons and express TH. Generation of high yields of differentiated DAPCs is relatively important to diminish the risk of contamination of the transplanted population with undifferentiated hESCs or non-DAPCs that can increase the risk of tumour formation and/or make the therapy less efficient. In addition, the protocol excludes the neurosphere phase by shifting the protocol entirely to adherent differentiation in order to diminish batch to batch variation also making the process user friendly and more easy to adapt to GMP (Nolbrant et al., 2017). In line with this point, generating hPSC-derived DAPCs in sufficient numbers for clinical use using the best-available standard protocols is prohibitively expensive. Current methods for generating hPSC-derived DAPCs necessitate expensive recombinant extra-cellular matrix (ECM) substrates and require re-plating steps during the differentiation process. This renders the scale-up process both labour-intensive and very costly, posing a barrier to translation. To address this, our group developed a molecularly engineered protein-based hPSC culture substrate that can be easily and cheaply produced. The substrate comprises a recombinant protein nanofiber carrying a cell-adhesive protein domain. The nanofiber consists of assemblies of two Ig domains, 'Z1Z2', from the human protein titin, which have been molecularly fused into a four-domain tandem (Z1Z2) (Hill et al., 2019). Our preliminary data have shown that one of our current Z1Z2-based substrates, can support the differentiation of hPSCs to DAPCs at high yield, and their subsequent differentiation to *TH*-expressing DA neurons (manuscript in preparation, Figure A.1 in appendix).

Another important parameter that can be assessed using preclinical studies is to determine the most suitable differentiation stage of dopaminergic cells for grafting. Recent studies indicate that injecting DA cells at the progenitor stage, rather than more differentiated DA cells, improves the survival and reinnervation of the graft, allowing it to ameliorate the behavioural deficits. Grafting DA progenitors provides sufficient time for the cells to become adapted to the brain microenvironment and then further maturate to TH^+ cells in response to local signalling factors. Another benefit of transplanting DA progenitors is that following implantation, these cells show

much higher viability than more mature DA neurons that could improve the efficacy of transplantation (Morizane et al., 2002).

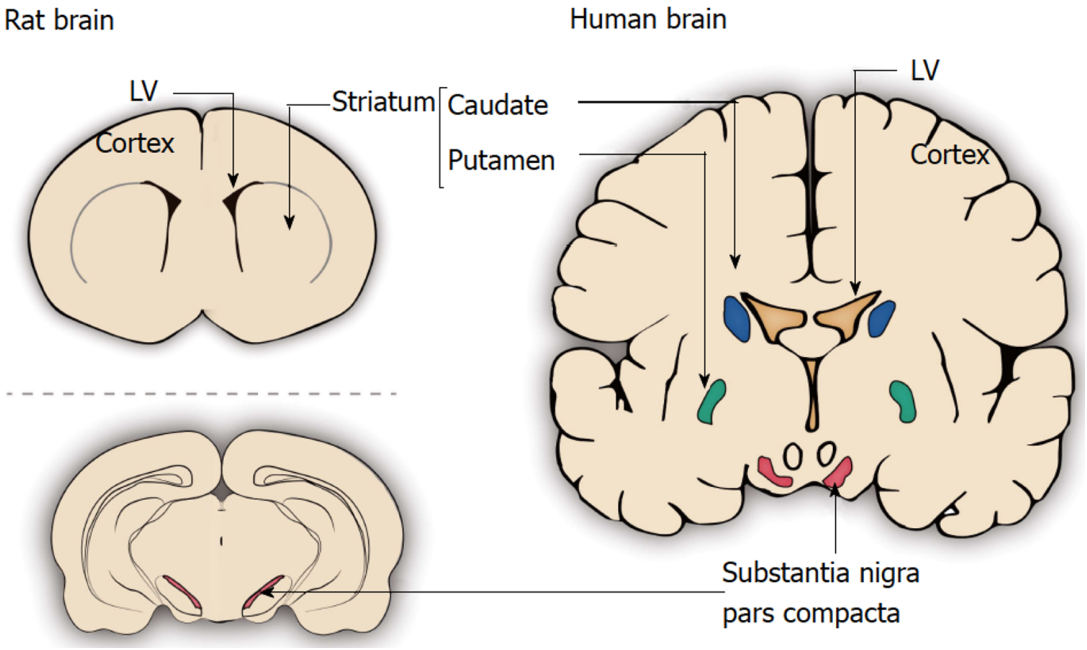

Figure 1.5: Schematic illustration of sites within the rat and human brain used for the engraftment of PD stem cell therapies. The schematic illustrates coronal sections of grafting sites including rat and human striatum together with Substantia nigra pars compacta, Lateral Ventricles (LV).

The advantage of grafting DA progenitors over more immature neural stem cells is that *in vitro* studies have indicated that the progenitors have a very low proliferation rate, which is further reduced following implantation, diminishing to nearly 0% after 2 weeks. This means that transplanted progenitors are likely to be less tumorigenic and therefore safer (Qiu et al., 2017; Liao et al., 2014; Yang et al., 2008). Preclinical studies are also important to find the best site of administration for the cells. There are various sites in the human and rat brain that could be used for grafting cells as a PD cell therapy: lateral ventricles, the striatum (in rat) or caudate nucleus and putamen (in human) and the SNpc (Figure 1.5). Current approaches in clinical trials are mostly focussed on reconstructing the nigrostriatal pathway by transplanting cells into the SNpc. These methods attempt to possibly direct the axonal outgrowth of grafted cells into the striatum to re-stabilise the lost dopaminergic circuitry (Backlund et al., 1985; Lindvall et al., 1987; Madrazo et al., 1987). However, the survival of the grafted cells in the SNpc is less compared to intra-striatal grafts (Grealish et al., 2014). In rodent models of cell therapy for PD, placing neural progenitors into the striatum is

more common compared to grafting directly into the SNpc (Nikkhah et al., 1994b,a). In rodents, reaching the striatum is much more practical through drilling the skull to inject cells. Also, the survival, innervation and maturation rate for progenitor cells is more when they were injected into striatum (Boronat-García et al., 2017).

Following cell implantation, tracking the biodistribution and fate of transplanted cells and determining their effect on the host brain is essential for assessing their safety and efficacy. Key safety concerns include the risk that the cells could form tumours, mal-differentiate, migrate to the wrong target site, or induce neuroinflammation. To be effective, the administered cells need to survive, mature into DA neurons of the right phenotype at high efficiency, innervate the host striatum, display physiological functionality (i.e., show pacemaker potentials, release dopamine), and normalise motor control. At present, cell biodistribution and fate is assessed in rodent PD models using histological analyses at the study endpoint. A drawback with this approach is that it does not allow the cells to be tracked over time in a single animal, instead requiring groups of animals to be culled at multiple time points. Moreover, it is difficult to accurately assess the biodistribution of administered cells across the whole brain from histological sections. Regarding the therapeutic efficacy of transplanted cells, this is typically monitored in rodent PD models using behavioural tests, the most common being the amphetamine-induced rotation assay. Amphetamine induces a pronounced rotation directed ipsilateral to the lesion and lasting about 2-hour in rats bearing a unilateral lesion of the nigrostriatal dopaminergic pathway. Implantation of DAPCs into the lesioned striatum leads to a compensation of this rotation (Herman et al., 1993). A problem with this test, however, is that it has previously shown poor correlation between the rate of amphetamine-induced rotations and the number of DA neurons in the lesioned side of the brain, making it difficult to quantify the extent of recovery following cellular therapy on an individual animal basis (Tronci et al., 2012). Therefore, to accurately assess safety and efficacy, non-invasive imaging strategies are needed that allow the biodistribution and fate of the cells, along with their therapeutic and pathological effects to be assessed in individual animals longitudinally (Section 1.3). A further advantage of this approach is that it obviates the need to cull animals at multiple time-points, thereby reducing the numbers of experimental animals in compliance with the “3 Rs”.

1.2.4 Application of animal models of PD

In recent years, different animal models have been used to recapitulate PD. Reserpine was one of the first pharmacological agents used to induce a reversible loss of DA neurons in the SNpc (Carlsson et al., 1957). Reserpine is able to prevent the uptake of neurotransmitters via blocking the vesicular monoamine transporter. However, there is no nigral dopaminergic cell degeneration using reserpine (Colpaert, 1987; Duty and Jenner, 2011). Later on, neurotoxins that could ablate DA neurons became more popular. Currently, one of the toxins that is extensively used in cell transplant and gene therapy studies using rodent models is 6-Hydroxy-Dopamine (6-OHDA). This neurotoxin penetrates into the cytoplasm of the cells through catecholamine transporters and inhibits mitochondrial complexes I and IV to generate paraquinone and hydrogen peroxide (Tieu, 2011). 6-OHDA is administered directly into the brain as it is not able to cross the BBB. The site of injection can be the terminal area of the striatum, substantia nigra, or nigrostriatal dopaminergic tracts in the medial forebrain bundle (Cannon and Greenamyre, 2010). Bilateral 6-OHDA lesioned animals develop severe movement impairment that affects their feeding and drinking ability, so in most studies, unilateral 6-OHDA lesioned animals are preferred, and this is the most commonly used PD model. Also, the ipsilateral hemisphere can be used for assessing behaviour and can serve as a control (Jagmag et al., 2016).

The compound N-methyl-4-phenyl-1, 2, 3, 6-tetrahydropyridine (MPTP) has been shown to cause permanent Parkinson symptoms by destroying nigral cells (Liu et al., 2008). MPTP is metabolized into MPP^+ via glial cells (mainly astrocytes) using Monoamine Oxidase B (MOB) which can rapidly demolish dopaminergic cells in the SNpc (Jagmag et al., 2016). MPTP has been used in mice and monkey animal models but rats are not sensitive to this neurotoxin as the expression of monoamine oxidase B is lower in rats comparing to mice and monkey. Currently, exposure to MPTP is widely used to generate a non-human primate model of PD which is associated with immunoreactivity to α-Synuclein (Porras et al., 2012).

Some of the endotoxins, such as lipopolysaccharide, can stimulate inflammation in the substantia nigra which results in the death of dopaminergic neuron. This endotoxin could be used to create PD models, but it causes a high death rate in animals (Koprich et al., 2017). Moreover, this PD model is associated with a high degree of variability

because the level of inflammation and cell death can differ considerably between animals (Liu and Bing, 2011).

Genetically modified animals have recently been established to mimic PD. PD Modelling via genetic modification is preferable in mice as the new findings suggest that PD genes and its pathological events are likely to mirror human PD (Breger and Fuzzati Armentero, 2019). In this method, the PD transgene construct such as A30P α-Synuclein and A53T α-Synuclein, will be delivered into desired region of the brain (striatal or intranigral injection) to robustly induce transgene expression throughout the lifetime of the animal (Dawson et al., 2010). The transgenes are typically introduced using viral systems, such as lentivirus, recombinant Adeno-Associated Virus (rAAV), and Herpes Simplex Virus (HSV), according to the purpose of the study and the transgene structure. However, there are significant difficulties associated with using transgenes vectors such as generating sufficient quantities of high-titer vector, random integration into host genome resulted in mutagenesis and oncogenesis. (Koprich et al., 2017).

1.3 Imaging techniques to track stem cell

Stem cell therapy for neurodegenerative diseases is a growing field that is moving toward clinical trials. However, human cell therapy needs innovative and breakthrough methods to analyse cell migration, biodistribution and the viability of transplanted cells, and monitor how the stem cells differentiate and integrate into the host tissue to reconstruct brain function (Sakthiswary and Raymond, 2012). Many labelling, histological, and imaging techniques have been developed to assess both the safety and efficacy of stem cell therapies (Scarfe et al., 2017). Traditional approaches to track stem cells, such as fluorescence imaging of histological sections, requires animals to be culled in order to explore survival and differentiation of grafted cells. On the other hand, non-invasive imaging strategies such as BLI, MRI, PET, and SPECT enable the cells to be monitored longitudinally in the same animal (Jiang et al., 2011). To increase the likelihood that stem cell therapies will be successful in clinical trials, neuroimaging should be used in animal models to enable the therapy to be optimised prior to clinical translation.

Table 1.3: The available *in vivo* imaging modalities for tracking stem cells modified from (Zheng et al., 2017).

Modality	Source of imaging	Type of probe	Spatial resolution	Temporal resolution	Tissue penetrating depth	Sensitivity	Clinical use	Advantages	Disadvantages
MRI									
In vivo labeling	Radiowave	Para-(Gd^{3+}/Mn^{2+}), SPIO or ^{19}F	>25 µm	Min–hrs	No limit	mM–µM	Yes	No radiation, very good tissue contrast, high resolution	Low sensitivity, agent dilution
PET									
Direct labelling	High-energy γ-ray	Radionuclides (e.g., ^{18}F, ^{11}C)	>1mm	Sec–min	No limit	pM	Yes	High sensitivity, deep tissues	Radiation, radiotracer dilution
Indirect labelling	High-energy γ-ray	Reporter genes (e.g., HSV1-tk)						Long-term imaging, avoid false signal,nontoxicity	Exogenous gene risk
SPECT									
Direct labelling	Low energy γ-ray	Radionuclides (e.g., ^{111}In, ^{99m}Tc)	>1mm	Min		pM	Yes	High sensitivity, able to image deep tissues	Radiation, low resolution, radiotracer dilution
Indirect labelling	Low energy γ-ray	Reporter genes (Tyrosinase (TYR))						Long-term imaging, nontoxicity	Exogenous gene risk
Optical imaging									
Fluorescence imaging	Visible light	Fluorescence near-infrared dye, QD light	>2mm	Sec–min	<1 cm	nM-pM	No	Cheap, simple, high sensitivity, activatable	Deep tissue limited, low resolution, tissue damaging
BLI	Visible light	Reporter genes	>2mm	Sec–min	<1 cm	nM	No	Simple, high sensitivity	Deep tissue limited, low resolution

The key parameters that should be assessed in order to determine safety and efficacy are migration, tumorigenicity, immunogenicity, survival, differentiation, innervation, and functionality of grafted cells (Heslop et al., 2015). Table 1.3 lists the available imaging modalities for stem cell tracking *in vivo* (Zheng et al., 2017).

1.3.1 Bioluminescence imaging

Bioluminescence imaging (BLI) is a non-invasive optical imaging technique that offers very high sensitivity, enabling even small numbers of cells to be detected *in vivo*. BLI involves the detection of light emitted following the ATP-dependent enzymatic reaction of a luciferase enzyme and an appropriate substrate in the cells. In order to perform BLI, cells are genetically modified to express luciferase reporter gene (Zhao et al., 2005). So as to label cells of interest, the genes encoding the transcription of luciferase enzymes should be introduced into the genome of cells, usually using a lentiviral vector to facilitate integration into the host genome. The labelled cells with an integrated luciferase gene can be administrated into the animals and will be tracked by BLI. The oxidation process by luciferin requires ATP and oxygen that are only be found in live cells (Figure 1.6).

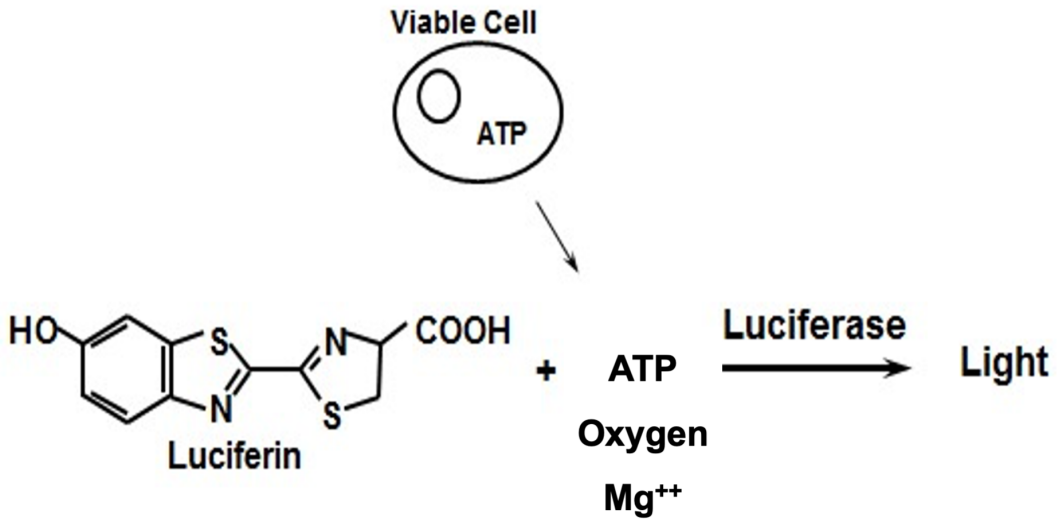

Figure 1.6: Simplified oxidation reaction of light generation luciferin. The diagram is showing ATP and luciferin as substrate for luciferase to generate light which only happen in the viable cells.

There are several kinds of luciferase that can be used in BLI including firefly luciferase (Photinus pyralis, Fluc), Renilla luciferase from North American sea pansy

(Renilla reniformis, Rluc), and Gaussia luciferase from marine copepod (Gaussia princeps, GLuc) (Kim et al., 2004). The exogenously administrated substrate is luciferin in the case of Fluc and coelenterazine in the case of Rluc or GLuc. Fluc is the most commonly used luciferase for BLI, due to its brightness and stronger signal for detection by imaging. The Fluc emits light at red shifted 530–640 nm and peaks at 562 nm wavelength which is not so readily absorbed by endogenous chromophores such as melanin, and haemoglobin compared to Rluc and Gluc, which emit light at around 480 nm that can be readily absorbed by endogenous chromophores (Conway et al., 2020; de Almeida et al., 2011). Furthermore, luciferin has "slow glow" kinetics which emits light around 15 minutes after administration and takes around 2 hours to be cleared after administration. Coelenterazine, has "fast flash" kinetics and is rapidly cleared from body. Also, the substrate, luciferin, can readily reach all bodily tissues including the brain, allowing for while body biodistribution. (Couillard-Despres et al., 2011). Thus, Fluc is an ideal tracking agent to monitor cell survival (Kruttwig et al., 2010). However, the spatial resolution of BLI is lower compared to other non-invasive imaging systems such as MRI. Furthermore, the tissue penetration depth is about 1 cm which makes it difficult to use in large animals (Table 1.3) (Sutton et al., 2008).

1.3.2 Magnetic resonance imaging

One of the important methods for non-invasive and real-time tracking of stem cells that offer high spatial and temporal resolution images is Magnetic resonance imaging (MRI). Gadolinium (III) (Gd^{3+}) is a heavy metal MRI contrast agent which is used in animal and clinical experiments (Wahsner et al., 2019). In many tracking methods, there is a problem of low uptake of (Gd^{3+}) contrast agent by cells (Caravan et al., 1999). In those cases, transfection agents or coupling of the contrast agent to a membrane peptide are available to increase the rate of cell uptake (Estelrich et al., 2015). Manganese is another useful contrast agent which is being used more to study brain function. Manganese is an attractive contrast agent in MRI particularly to study neural activity of transplanted cells as it can enter the cells quite conveniently via calcium/sodium exchanger channels or magnesium binding sites on the nucleic acids or proteins (Silva and Bock, 2008).

Arguably, the most useful MR contrast agents available for cell tracking are iron oxide particles. These are biocompatible as they are typically coated with hydrophilic polymers, including low molecular weight carboxydextran and they generate a much

higher signal than other MR contrast agents, allowing smaller numbers of cells to be detected (Unterweger et al., 2018). Also, compared to manganese or gadolinium, the paramagnetic metal per mole is highly increased in iron oxide particles, which helps to increase the MRI signal-to-noise ratio (Feng et al., 2018).

Iron oxide particles have been classified according to the overall size of the particles as follows: 1) Ultra-Small Superparamagnetic Iron Oxide Nanoparticles (USPIONs) with diameter less than 50 nm, 2) Superparamagnetic Iron Oxide nanoparticles (SPIONs) (100 nm range) and, ultimately, 3) Micron-sized Particles of Iron Oxide (MPIO) with a diameter usually higher than 1 µm (Estelrich et al., 2015).

Many studies have shown that SPION labelling of stem cells has no adverse effect on the survival, migration, and cell function *in vitro* (Wahajuddin and Arora, 2012). More importantly, *in vivo* imaging suggests that the labelled cells can be visualised through MRI up to several weeks after transplantation (Zhu et al., 2006). The two formally approved SPIONs used for stem cell labelling were subsequently removed from the market in 2009 because of economic considerations.

In addition to SPIONs, MPIOs are also available as MR contrast agents and have been used to track a variety of cell types such as neural progenitor cells, mesenchymal stromal cells, macrophages and tumour cells *in vivo* using MRI (Shapiro et al., 2004). MPIOs are multicore microspheres embedded in a carboxyl-modified polystyrene matrix and can be internally loaded with fluorescent dyes, thereby enabling them to be detected on histological samples using confocal fluorescence microscopey (Taylor et al., 2014). MPIOs are now commonly used in preclinical imaging and cell tracking as they are biocompatible and simply require incubation in the culture media for 24 hours before cell administration to be uptaken via spontaneous endocytosis by cells without the need for complexation with transfection agents or potentially harmful electroporation (Shapiro et al., 2005). Furthermore, MPIOs more efficiently package iron due to their bigger volume, facilitating their detection with MRI.

However, there are several limitations associated with stem cell labelling using magnetic contrast agents. Dilution of label due to stem cell proliferation after grafting is one of the common issues, resulting in reduction of MR signal over time (Zheng et al., 2017). In addition, the dead cells can be engulfed by immune cells, especially microglia in the central nervous system, which could lead to false signals on MRI; therefore, it

cannot reveal changes stem cell survival and microenvironment (Margel et al., 2007).

1.3.3 PET and SPECT

Positron Emission Tomography (PET) and Single Photon Emission Computed Tomography (SPECT) are both nuclear medicine imaging techniques that represent a promising imaging modality in experimental and clinical stem cell tracking (Margel et al., 2007). In these techniques, a radiotracer, such as ^{11}C, ^{13}N, ^{15}O, ^{18}F, ^{89}Zr, and ^{111}In is used to label stem cells in order to detect transplanted cells in the host tissue. The PET camera is able to image with relatively high spatial resolution by detecting positron emitting radioisotope (Patrick et al., 2020). SPECT is very similar to PET; however, SPECT uses gamma emitting radioisotopes which are generally less sensitive than those used in PET imaging and the technique is less quantitative (Gleave et al., 2011). SPECT tracers are usually cheaper than PET tracers due to SPECT radioisotopes being more readily available (Kaneta, 2020). The most widely used isotopes in PET imaging are fluorine-18 (^{18}F), and copper-64 (^{64}Cu) half-lives of 110 minutes and 12.7 hours, respectively. Another isotope that has a longer half-life for PET scanning is ^{89}Zr-oxine, with a half-life of about 3 days (Margel et al., 2007; Zheng et al., 2017). The SPECT radiotracers such as ^{99m}Tc-HMPAO, ^{99m}Tc-ECD, ^{123}I-IBZM, and ^{123}I-ioflupane have half-lives of about 6 to 12 hours and are normally used to investigate brain diseases (Martí-Bonmatí et al., 2010).

1.3.4 Assessment of the safety and efficacy of cell transplants using non-invasive techniques

To determine which strategies for manufacturing hPSC-based therapies for PD are safest and most effective, we need to be able to track the fate of the cells longitudinally *in vivo*. Safety and efficacy data are essential for assessing the risk: benefit ratio of hPSC-based therapies so as to identify those that are most appropriate for clinical use (Heslop et al., 2015). To assess safety, it is important to determine whether the cells generate tumours and/or cause other adverse effects, such as neuroinflammation. To assess efficacy, the viability and functional activity of the cells needs to be monitored, as well as the extent and persistence of any therapeutic response (Goldring et al., 2011).

BLI is the preferred technique for monitoring viability and proliferation *in vivo*, due to the fact that it only detects living cells. However, the spatial resolution achievable

with BLI is low, meaning that it cannot be used to assess intracranial biodistribution (Puaux et al., 2011). This can be overcome by labelling cells with iron oxide particles (IOPs) so that they can be imaged using magnetic resonance imaging (MRI), providing very high spatial resolution. MRI enables brain anatomy to be monitored in fine detail allowing an accurate way to visualise tumour formation and biodistribution of transplanted cells (Kraitchman et al., 2008; Stroh et al., 2019).

In order to assess the functionality of the administered cells, measuring dopamine synthesis using PET imaging is the most commonly used non-invasive imaging technique. The tracer 6-[^{18}F]DOPA which is taken up by DA neurons is being clinically developed for this purpose [189]. In addition, to determine whether the administered cells induce inflammation in the host brain, using the PET tracer [^{18}F] DPA-714, a ligand for the 18 kDa Translocator Protein (TSPO) that is upregulated in activated microglia, astroglia and macrophages has been used (Arlicot et al., 2012).

1.4 Aim of the study

A key aim of this study, was to assess the potential of a bimodal BLI/MR imaging strategy to track hESC-derived DAPCs *in vivo* in terms of their viability, biodistribution, and tumourigenicity. In addition to evaluating the effectiveness of the imaging modalities themselves, we also investigated whether the labels used for tracking including, namely, firefly luciferase for BLI and iron oxide particles for MR imaging, affected the differentiation potential of the cells and/or their immunogenicity following implantation into the rat striatum.

CHAPTER 2

Materials and methods

2.1 Cell line

The cell line which has been used in this project is the human embryonic stem cell (hESC) line RC17 (female; passage number 24). RC17 is a clinical grade line obtained from Roslin Cells Ltd (Scotland, UK). As per the description notes by the supplier, the provided cell batch by Roslin CT had already been assessed using karyotyping to show normal chromosome complement and the sex of the cells; phenotyping (through FACS analysis using SSEA4 surface marker); absence of microorganisms and mycoplasma. The cells were used after passaging only 3 to 4 times and it was assumed that in this short time-frame, it would be unlikely that the cell population would contain many cells with an abnormal karyotype. The undifferentiated ESCs were checked for *OCT4* and *Nanog* expression prior to them being differentiated into dopaminergic neurons. The cells were also routinely assessed for the presence of mycoplasma.

2.2 Maintenance of hESCs

RC17 cells were thawed, frozen, expanded, and passaged according to the instructions of the supplier, as described below, using xeno-free media and reagents. Cell culture procedures were performed using sterile culture reagents in a Class II safety cabinet.

2.2.1 Plate coating

To prepare coated plates for undifferentiated cell line, laminin 521 (0.5 µg/cm^2). (Biolamina) was mixed in PBS (+Ca^{2+}/+Mg^{2+}) in a polypropylene conical tube and added to the tissue culture treated plate (Corning Costar). Plates were shaken thoroughly

to ensure homogeneous coating. For urgent cell plating, coating was performed by incubating the plates at 37°C for 2 hour. For slow coating, the plate was wrapped in parafilm and stored at 4°C for 1–7 day. Plates coated at 4°C, were placed at 37°C for 1–2 hour before use.

2.2.2 Thawing and freezing

Cryovials were removed from the liquid nitrogen tank and placed in a water bath (37°C) until partially defrosted. The cell suspension was then transferred to a 15 ml conical tube containing 10 ml of wash which consisted of DMEM/F12 (Gibco) supplemented with 10% Human Serum Albumin solution (Irvine Scientific). After centrifugation $250 \times$ g for 3 minutes) the supernatant was discarded, and the cell pellet resuspended in fresh StemMACS iPS-Brew XF media (StemMACS™), and then seeded in the coated dishes. In order to increase the yield of recovery of the cells, 10 µM of Y-27632 dihydrochloride (StemMACS, Miltenyi) (ROCK inhibitor) was added to the medium of the seeded cells for the first 24 hour after plating. In order to freeze down the cells, the plate was washed once with PBS (without Ca^{2+}/ Mg^{2+}) and incubated for 4 minutes in Versene solution (Thermo Fisher Scientific). Versene was neutralised using wash medium and the cells were gently collected after only one wash. Trituration was avoided to ensure that cells were frozen and passaged as small clumps, rather than as single cells. Cell pellets were collected by centrifuging at ($250 \times$ g for 3 minutes. Cell pellets were resuspended in CryoStor CS10 (StemCell Technology) freezing media and 1 ml of cell suspension was transferred into cryovials. The cryovials were stored in freezing containers (Mr Frosty) filled with 2-propanol at -80°C overnight to ensure freezing occurred, and the day after, were transferred to a liquid nitrogen tank.

In order to freeze down the cells, the plate was washed once with PBS (without Ca^{2+}/ Mg^{2+}) and incubated for 4 minutes in Versene solution (Thermo Fisher Scientific). Versene was neutralised using wash medium and the cells were gently collected after only one wash. Trituration was avoided with both cell lines to ensure that cells were frozen and passaged as small clumps, rather than as single cells. Cell pellets were collected by centrifuging at 250 × g for 3 minutes. Cell pellets were resuspended in CryoStor CS10 (StemCell Technology) freezing media and 1 ml of cell suspension was transferred into cryovials. The cryovials were stored in freezing containers (Mr Frosty) filled with 2-propanol at -80°C overnight to ensure freezing occurred at a rate of , and

the day after, were transferred to a liquid nitrogen tank.

2.2.3 Passaging

Undifferentiated cells were expanded on Laminin 521-coated cell culture plates in the StemMACS iPS-Brew XF media which was pre-warmed to room temperature. The cell medium was changed every day, and when the colonies reached 70-80% confluency, they were incubated for 4 minutes in Versene solution (Thermo Fisher Scientific) and passaged as small clumps. After 3 minutes $250 \times$ g centrifugation, the supernatant was discarded, and cells gently re-suspended in an appropriate amount of StemMACS iPS-Brew XF medium supplemented with 10 µM Y-27632 for the first 24-hour after seeding. To avoid disrupting the small cell clumps during the replating process, trituration was avoided. Cells were always maintained at 37°C under 5% CO2.

2.2.4 Embryoid body formation

In order to make Embryoid Bodies (EBs), the undifferentiated colonies of hESCs (70-80% confluent) were incubated with Accutase (Stem Cell Technologies) for 5 minutes or until partial detachment. $1x10^6$ single cells were suspended in 5 ml APEL 2 (Stem Cell Technologies) media, supplemented with 10 µM of Y-27632 and added into a well of an AggreWell800 plate (Stem Cell Technologies) containing approximately 300 microwells per well with a diameter of 800 µm which was pre-treated with AggreWell rinsing solution (Stem Cell Technologies). AggreWell plates were centrifuged at $100 \times$ g for 3 minutes to deposit the cells in the microwells and incubated at 37°C for 24-hours, during which time spherical aggregates of deposited spheroids were formed. The medium of the AggreWell was changed every 2 days until day 10, when spheroid aggregates were collected by firmly pipetting in the AggreWell plate. EB culture was initiated by seeding spheroids into Matrigel (Corning)-coated cell culture plates for another 10 day with medium being changed every other day.

2.3 Generation of hESC reporter line

The pHIV Lentivirus was used to transduce the undifferentiated cells. The construct encodes a 9320 bp bicistronic element encoding firefly luciferase (luc2) and ZsGreen (via an IRES link) under the control of the constitutive promoter, Elongation Factor α (EF1α). A schematic showing the vector is provided in Figure A.2.

In order to transduce cells, colonies of undifferentiated RC17 cells were dissociated

into small clumps (as they would have very poor survival by seeding as single cells) consisting of about 5-10 cells using Versene solution for 4 minutes. After 3 minutes centrifugation at 250 × g, cells were counted using a haemocytometer and seeded at a density of 5x10^4 cells per well in laminin 521-coated twelve-well plates, in a volume of 500 µl iPS-Brew supplemented with 10 µM Y-27632 per well (to promote cell attachment and inhibit anoikis). Cells were incubated overnight and transduced on the following day. Three Multiplicity Of Infections (MOIs) including 5x10^4, 15x10^4, and 25x10^4 viral particles/µl were tested in order to determine the best concentration for transduction. To enhance the transduction efficiency and virus-cell interaction, the medium was supplemented with Polybrene (Sigma Aldrich) at a concentration of 10 µg/ml. After 24-hour, the medium was replaced with 1 ml of fresh iPS-Brew and cells were cultured routinely, with the medium being changed daily.

2.4 Labelling cells with Micron-sized particles of iron oxide

The 1 µm fluorescent Micron-sized Particles of Iron Oxides (MPIOs) (Bangs Beads laboratories, catalogue No. MESY002) with the fluorophore 'Suncoast yellow' incorporated (exciting maximally at 540 nm and has its greatest emission at 600 nm) were used for direct labelling of DAPCs. The MPIOs of stock concentration 5×10^6/µl were diluted to 1×10^6/µl in B27 basal medium. The DAPCs (1×10^6 cells on day 15 of differentiation) were incubated for 24-hour with the MPIOs at a range of concentrations from 500-8000 particles/µl. On addition of the MPIOs, the plates were shaken to ensure even distribution throughout each well. Cell uptake efficiency was then assessed by flow cytometry.

2.5 Fluorescence-activated cell sorting

Fluorescence-Activated Cell Sorting (FACS) was used to sort transduced hESCs into two different populations of "Dim green" and "Bright green" cells. In order to perform the cell sorting, colonies of RC17 cells were expanded for 4 days until they reached 80% confluency. Cells were dissociated into single cells using TrypLE (Gibco) and 1×10^6 cells were harvested. Then cells were resuspended into Iscove's Modified Dulbecco's Medium (IMDM), no phenol red (Gibco) in round-bottom glass tubes for sorting. A

group of non-transduced cells were used as a baseline control. Sorting was performed using the BD FACSAria (BD Biosciences) flow sorter. The Brightgreen-sorted cells were collected in the iPS-Brew culture medium and seeded with the supplementation of 10 /µM Y-27632 on laminin 521-coated cell culture plates (Corning Costar) for routine expansion.

2.6 Flow cytometry analysis

2.6.1 ZsGreen labelled cells

Cells were dissociated as single cells using TrypLE (Gibco) and resuspended in PBS and finally were transferred into round-bottom glass tubes in ice until analysed. Cells were analysed by BD FACScalibur (BD Biosciences), using 488 nm laser and eGFP fluorescence detector to visualise ZsGreen expression. Each analysis was based on 10,000 to 20,000 events and the negative control was non-transduced RC17 cells. Flow cytometry output was analysed using Flowing Software (TURKU Bioscience).

2.6.2 MPIO labelled cells

Following the 24-hour incubation of DAPCs with MPIOs, cells were treated with minimal volumes of Accutase (Stem cell Technologies) (75 µl/cm^2) at 37°C for 10 minutes to obtain a single cell suspension. Cells were triturated and removed from the wells on addition of PBS and subsequently centrifuged at $250 \times$ g for 3 minutes. The supernatant was removed, and the pellet was resuspended in 1 ml PBS. Cells were then re-centrifuged to remove residual particles that had not been taken up by cells. The pellet was then resuspended in a final 1 ml of PBS and kept on ice until analysed. Fluorescence was detected using BD FACSCalibur (BD Biosciences). In Flowing software, doublets and dead cells were excluded from the analysis and the percentage of the cell population that was positive for fluorescence, i.e., the percentage of the cell population that had uptaken MPIOs, was calculated. Graphs were then plotted in Originlab version 2015.SR1.

2.7 Differentiation of hESCs into DAPCs *In vitro*

In order to differentiate hESCs into caudalized Ventral Midbrain (VM) progenitors, a previously published nature protocol was followed (Nolbrant et al., 2017). The

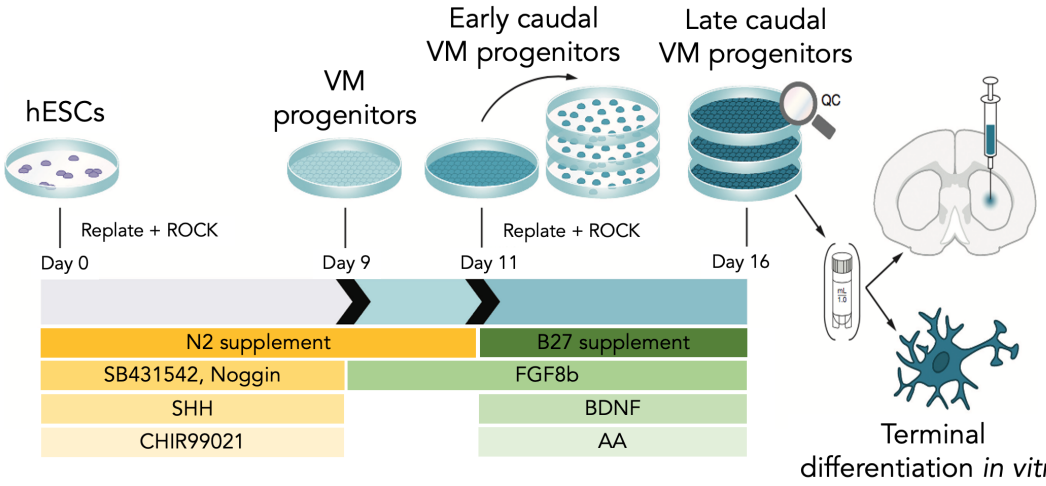

Figure 2.1: Schematic overview of dopaminergic progenitor differentiation protocol. Over 16 days differentiation protocol, DAPCs could terminally differentiate *in vitro* or could be grafted for *in vivo* study (Modified from (Nolbrant et al., 2017))

schematic overview of the protocol steps is shown in Figure 2.1. To optimise the protocol, three different concentrations of the small molecule CHIR99021 (GSK-3 inhibitor) were tested: 0.7, 0.8, and 0.9 µM. The 0.9 µM CHIR99021 was the most effective concentration which was applied in our experiment.

The entire process of VM progenitor differentiation was on laminin 111 (Biolamina). To prepare laminin 111 coated plates, laminin 111 (1 µg/cm^2) was added to a 15 ml polypropylene conical tube containing PBS (+Ca^{2+}/+Mg^{2+}), and after mixing, was transferred to the cell culture plates and stored at 4°C for 1–7 day. To start the differentiation process (day 1), when 70% confluent, the undifferentiated Bright green RC17 cells, were dissociated using Accutase (75 µl/cm^2), and 10,000 cells per cm^2 were seeded on Laminin 111-coated culture plates in 250 µl/cm^2 differentiation medium which consisted of: *N2 medium + 10 µM Y-27632 (StemMACS) + 10 µM SB431542 (StemMACS) + 100 ng/ml Noggin (Miltenyi) + 300 ng/ml Shh-C24II (Miltenyi) and CHIR99021 (0.7, 0.8, and 0.9 µl depending on the condition) (StemMACS). On the following days, day 2, day 4, and day 7, the old medium was removed and replaced with 250, 300, 350 µl/cm^2 of fresh differentiation medium respectively without Y-27632. On day 9, the medium was replaced with 400 µl/cm^2 of N2 medium + 100 ng/ml FGF8b (Miltenyi). On day 11, cells were replated using Accutase (75 µl/cm^2) and were seeded on laminin 111-coated plates at a density of 800,000 cells/cm^2. In this step the medium components were: **B27 medium + 10 µM Y-27632 (StemMACS) + 20 ng/ml BDNF

(Miltenyi) + 0.2 mM L-Ascorbic Acid (AA) (Sigma-Aldrich) + 100 ng/ml FGF8b (Miltenyi). On day 14, the old medium was replaced with 600 µl/cm^2 fresh media which comprised all components which were used on day 11, apart from Y-27632. Table 2.1 describes the timing, media composition, and corresponding volumes for differentiation of DAPCs. On day 16, patterning of VM progenitors was completed and cells were either (i) cryopreserved; (ii) used for transplantation, or (iii) further differentiated into mature DA cells *in vitro*.

Table 2.1: Medium compositions and required volumes per timing of DAPCs differentiation process.

Timing (Day)	**Medium composition (growth factors to be freshly added for each new medium change)**	**Volume (µl/cm^2)**
0	N2 complete: N2*[0] basal medium, Y-27632 (10 µM), SB431542 (10 µM), Noggin (100 ng/ml), Shh-C24II (300 ng/ml) and CHIR99021 (0.7,0.8, 0.9 µM depending on the condition).	250
2	N2 complete: N2 basal medium, SB431542 (10 µM), Noggin (100 ng/ml), Shh-C24II (300 ng/ml) and CHIR99021 (0.7,0.8, 0.9 µM depending on the condition).	250
4	N2 complete: N2 basal medium, SB431542 (10 µM), Noggin (100 ng/ml), Shh-C24II (300 ng/ml) and CHIR99021 (0.7,0.8, 0.9 µM depending on the condition).	300
7	N2 complete: N2 basal medium, SB431542 (10 µM), Noggin (100 ng/ml), Shh-C24II (300 ng/ml) and CHIR99021 (0.7,0.8, 0.9 µM depending on the condition).	350
9	N2 complete: N2 basal medium, FGF8b (100 ng/ml).	400
11	B27 complete: B27** basal medium, Y-27632 10 µM, BDNF (20 ng/ml), Ascorbic acid (0.2mM) and FGF8b (100ng/ml).	570
14	B27 complete: B27 basal medium, BDNF (20 ng/ml), Ascorbic acid (0.2 mM), FGF8b (100 ng/ml).	600

*N2 basal medium, 40 ml of which consists of: 19.6 ml DMEM/F12 (Thermo Fisher Scientific), 19.6 ml of neurobasal CTS medium, 0.4 ml N2 supplement (Thermo Fisher Scientific) (final concentration, 1% (v/v)), 0.4 ml L-glutamine (Thermo Fisher Scientific) (final concentration 2 mM) and 80 µl of penicillin-streptomycin (Thermo Fisher Scientific) (final concentration, 0.2% (v/v)).

**B27 basal medium, 40 ml of which consists of: 38.7 ml of neurobasal CTS medium, 0.8 ml of B27 supplement without vitamin A (Thermo Fisher Scientific) (final concentration,2% (v/v)), 0.4 ml L-glutamine (final concentration 2 mM) and 80 µl of penicillin-streptomycin (final concentration, 0.2% (v/v)).

2.8 Differentiation towards mature DA cells *In vitro*

DAPCs (which were on day 16) were kept in B27 medium + 20 ng/ml BDNF (Miltenyi) + 0.2 mM AA (Sigma-Aldrich) + 100 ng/ml FGF8b (Miltenyi) for 5 days and the medium was replaced every 2 days. On day 21, cells were replated at a density of 155,000 cells/cm^2 on laminin 111-coated plates (2 µg/cm^2) in the B27 media supplemented with 20 ng/ml BDNF (Miltenyi) + 0.2 mM AA (Sigma-Aldrich) + 10 ng/ml GDNF (R&D Systems) + 500 µM db-cAMP (Sigma-Aldrich) + 1 µM DAPT (R&D Systems) + Y-27632 (10 µM). This medium was replaced with 300–500 µl/cm^2 (depending on cell confluency) of fresh medium every 3 days. By day 50, cells were terminally differentiated into mature DA cells.

2.9 Immunostaining

In order to perform immunofluorescence analysis of cultured cells in the plate, the cell medium was removed, and cells washed two times with PBS (without Ca^{2+}/Mg^{2+}). To fix the cells, 4% (w/v) Paraformaldehyde (PFA) (Merck Millipore) was added to the cells, which were then incubated at room temperature for 15 minutes followed by washing twice with PBS. To store the plates for the longer term (maximum of 6 months), they were wrapped in parafilm to avoid evaporation and placed at 4°C. To proceed directly to staining, PBS was removed, and cells were incubated for 20 minutes in 0.1% (v/v) Triton ×100 (Fisher Scientific) at room temperature. Cells were washed twice with PBS and blocked using 1% (w/v) Bovine Serum Albumin (BSA) for 30 minutes at room temperature. After BSA incubation, the primary antibodies (make up to the required concentration using 1:1 volume of 0.1% (v/v) Triton ×100 and 1% (w/v) BSA) were added to the cells and incubated overnight at 4°C. The primary antibody solutions were then removed and after 3 washes with PBS, the appropriate secondary antibodies were added to the cells for 2-hour at room temperature. The plate was wrapped with aluminium foil to avoid bleaching of secondary antibodies. For DAPI (Thermo Fisher Scientific) staining, cells were washed 3 times with PBS to remove the secondary antibodies and DAPI, which was diluted in PBS (1:1000), was added to the cells for 20 minutes at room temperature. Then, cells were washed with PBS and plates wrapped in aluminium foil at 4°C until analysis. A full list of primary and secondary antibodies and the respective dilution factors are listed in Table 2.2.

Table 2.2: Description of primary and secondary antibodies used in immunofluorescence experiments.

Marker	Species	Dilution	Company	Catalog Number	Secondary Antibody
β-III tubulin	Monoclonal Mouse IgG2A	1:1000	Biolegend	801201	AlexaFluor 488 Goat anti Mouse IgG2A
Brachyury	Polyclonal Goat IgG (H+L)	1:500	SantaCruz Biotechnology	sc-17743	AlexaFluor 647 Donkey anti Goat IgG(H+L)
FOXA2	Polyclonal Goat IgG (H+L)	1:200	SantaCruz Biotechnology	sc-655	AlexaFluor 594 Donkey anti Goat IgG(H+L)
GATA6	Polyclonal Rabbit IgG (H+L)	1:500	SantaCruz Biotechnology	sc-9055	AlexaFluor 594 Chicken anti Rabbit IgG(H+L)
GFAP	Polyclonal Rabbit IgG(H+L)	1:1000	DAKO	ZO334	AlexaFluor 647 Chicken anti Rabbit IgG(H+L)
Human NCAM	Monoclonal Mouse IgG1	1:100	SantaCruz Biotechnology	Sc-106	AlexaFluor 488/594 Goat anti Mouse IgG1
Human Nuclei	Monoclonal Mouse IgG1	1:200	Merck	MAB1281	AlexaFluor 594 Goat anti Mouse IgG1
LMX1A	Polyclonal Rabbit IgG(H+L)	1:500	Abcam	Ab139726	AlexaFluor 595 Chicken anti Rabbit IgG(H+L)
Nestin	Polyclonal Rabbit IgG (H+L)	1:250	Abcam	ab92391	AlexaFluor 594 Chicken anti Rabbit IgG(H+L)
OCT4	Monoclonal Mouse IgG2b	1:500	SantaCruz Biotechnology	sc-5279	AlexaFluor 647 Goat anti Mouse IgG2b
OTX2	Polyclonal Goat IgG(H+L)	1:500	R&D Systems	AF-1979	AlexaFluor 594 Donkey anti Goat IgG(H+L)
Tyrosine hydroxylase	Polyclonal Rabbit IgG(H+L)	1:1000	Merck	AB152	AlexaFluor 647 Chicken anti Rabbit IgG(H+L)

2.10 RT-qPCR

Cells were washed twice with PBS and a minimum of 5×10^5 Cells were lysed with 1 ml TRI Reagent (Sigma) for 5 minutes at room temperature. TRI/cell lysate was transferred into a 1.5 ml microfuge tube and following the addition of 200 µl chloroform (Sigma), the tube was shaken vigorously for 15 seconds. Samples were centrifuged 1000×g for 15 minutes, resulting in the formation of three separate phases. The clear top layer that contains the RNA was transferred into a fresh microfuge tube. 100% Isopropanol (75% of the volume of extracted RNA) was added to the sample, and following a 10 minutes incubation at room temperature, was centrifuged at 4°C for 10 minutes at 1000×g. The supernatant was discarded, and the pellet was washed with 75% ethanol and centrifuged for 5 minutes at 800×g. The ethanol was removed, and the pellet was air-dried for a few minutes and then dissolved in 50 µl nuclease-free water. A NanoDrop (Thermofisher) was used to determine the RNA concentration. To remove any contaminating DNA, 8 µl of total RNA was treated with 1 µl DNase1 (Promega) at 37°C for 30 minutes, following which, 1 µl of STOP buffer (Promega) was added and the solution was incubated at 60°C for 15 minutes and placed on the ice for further use (or if not used on the same day, was stored at -80°C). To procced to cDNA synthesis, a maximum of 5 µg of total RNA were added to a solution containing 1 µl of 100 ng/µl of random hexamers (Qiagen), 1 µl of 10 mM deoxyribonucleotide (dNTP) mix and molecular biology water up to 14 µl, denatured at 65°C for 5 minutes, followed by a quick chill on ice. A mix of 5× First Strand Buffer, 0.1 M dithiothreitol (DTT) and 200 U/µl of SuperScript™III-RT (Invitrogen) were then added. The resulting solution was mixed gently and incubated for 5 minutes at room temperature, followed by incubation at 50°C for 60 minutes. Afterwards, the reaction was inactivated by heating up to 70°C for 15 minutes. The solution was stored at -20°C until further use.

qPCR was performed in triplicate using a Bio-Rad CFX system using SYBR Green JumpStart Taq Ready Mix (Sigma) in total 20 µl per reaction. Each 20 µl reaction contains 10 µl of Syber Taq, 1 µl of forward primer (6.25 pmols/µl, 1 µl of reverse primer (6.25 pmols/µl, 1 µl of diluted cDNA (neat cDNA diluted with nuclease-free water (Gibco) according to amount of initial extracted RNA for each gene, typically, 1/50), and 7 µl of nuclease-free water. The No cDNA Template Control (NTC) were used to monitor the false positive results.

Table 2.3: The list of primer sequences.

Genes	Size	Forward sequences	Reverse sequences
GAPDH	119	GTGGAAGGACTCATGACCA	GAGGCAGGGATGATGTTCT
FOXA2	114	CCGTTCTCCATCAACAACCT	GGGGTAGTGCATCACCTGTT
OTX2	122	ACAAGTGGCCAATTCACTCC	GAGGTGGACAAGGGATCTGA
LMX1A	120	CGCATCGTTTCTTCTCCTCT	CAGACAGACTTGGGGCTCAC
BARHL1	113	GTACCAGAACCGCAGGACTAAA	AGAAATAAGGCGACGGGAACAT

GAPDH was used as the housekeeping gene and a sample of undifferentiated hESCs were used to determine the gene expression levels relative to the expression in undifferentiated controls. To calculate of relative gene expression the average Cycle Threshold (CT) values from the three technical replicates were used to analyse the relative gene expression using the ΔΔCT method (Livak and Schmittgen, 2001) (an example of calculation method for *FOXA2* is shown in Equation 2.1). The primer sequences previously known from (Nolbrant et al., 2017) and ordered from Integrated DNA Technologies (listed in Table 2.3).

$$\begin{aligned} \Delta CT_{FOXA2}|_{DAPCs} &= CT_{FOXA2} - CT_{GAPDH} \\ \Delta CT_{FOXA2}|_{UNDIFF\ hESCs} &= CT_{FOXA2} - CT_{GAPDH} \\ \Delta\Delta CT &= \Delta CT_{FOXA2}|_{DAPCs} - \Delta CT_{FOXA2}|_{UNDIFF\ hESCs} \\ Fold\ Change\ over\ Undiff.\ hESCs &= 2^{-\Delta\Delta CT} \end{aligned} \tag{2.1}$$

2.11 Preparation of cells for *In vivo* administration

Cells were administered intra-cranially via stereotactic injection to 3 groups of rats (Table 2.4). The first group was administered undifferentiated hESCs that expressed luciferase and ZsGreen (n=3; positive control for tumour formation); the second group was administered hESC-derived progenitors that expressed luciferase and ZsGreen (n=6); the third group was administered hESC-derived progenitors that were labelled with iron oxide particles (n=6). Modified cells were administered as 2 deposits (each of 75×10^3 cells) into the striatum of the right hemisphere. Unmodified cells were administered as 2 deposits into the striatum of the left hemisphere and served as control cell populations.

On the administration days, corresponding cells were washed twice with PBS and

Table 2.4: Description of experimental groups.

Group	Cells implanted in left hemisphere	Cells implanted in right hemisphere	Number of Animals	Endpoint
1	Undifferentiated hESCs	Undifferentiated hESCs (Fluc-ZsGreen$^+$)	3	day 27
2	DAPCs	DAPCs (Fluc-ZsGreen$^+$)	6	day 91
3	DAPCs	DAPCs (MPIO$^+$)	6	day 127

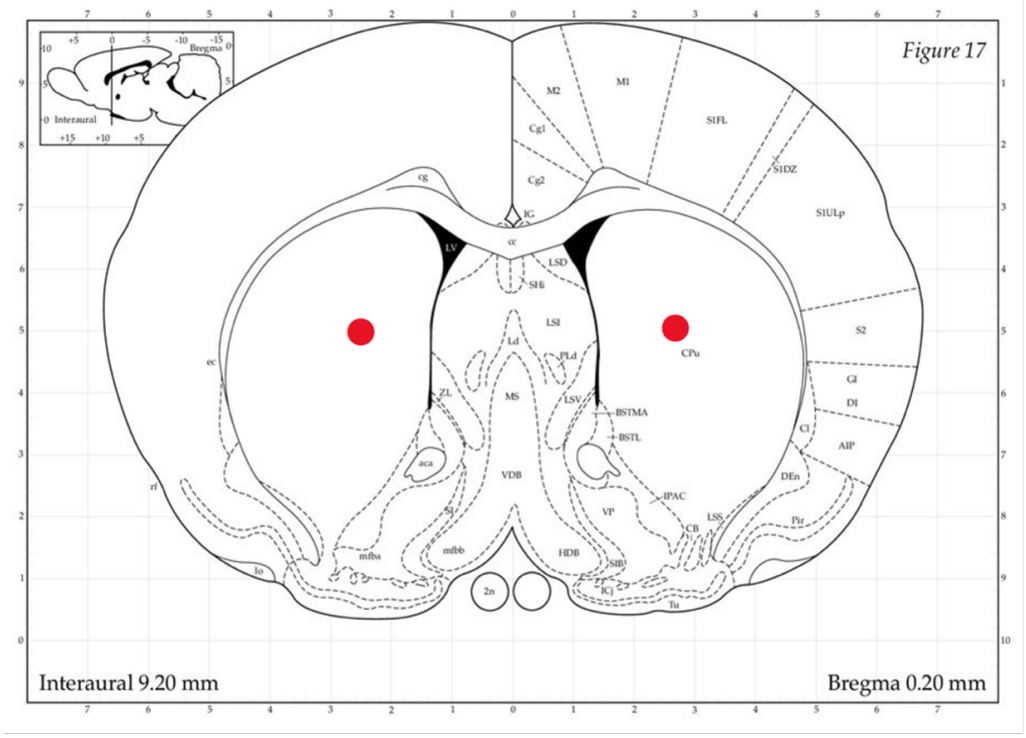

Figure 2.2: Coronal section of rat brain according to bregma. Site of injections were in the rat striatum which shows by red dots.

dissociated using Accutase for 3 minutes or until partial detachment. The single cell suspension was collected and centrifuged at 250×g for 3 minutes. Cells were counted and an appropriate number of cells were diluted in 100 µl of Hanks' Balanced Salrit Solution (HBSS) (Gibco) and stored on ice until transplantation. Single-cell suspensions were implanted stereotactically using bregma as a reference (Figure 2.2). The skull was drilled at 0 mm anteroposterior and +/- 1.5 mm mediolateral, with each hemisphere receiving two deposits of cells using microsyringe (Hamilton) connected to an infusion pump at a depth of -5.0 and -4.3 mm from dura. The injections were performed by Pamela Tyers (Roger Barker group; University of Cambridge).

2.12 Animals

Immune-compromised RNU rats (males, 5-6 weeks old) were purchased from Charles River and housed in individually ventilated cages under a 12 hour light/dark cycle, with ad libitum access to standard food and water. All animal experiments were performed under a licence granted through the UK Animals (Scientific Procedures) Act 1986 and were approved by the University of Liverpool ethics committee (PPL No, 70/8411). All procedures (surgical administration of cells and imaging) were carried out under isoflurane anaesthesia.

2.13 Sectioning and histological analysis

At the experimental endpoint, the rats received an overdose of pentobarbital and were perfused transcranial with PBS followed by 4% formaldehyde. The brains were harvested, postfixed with 4% formaldehyde, equilibrated in 30% sucrose and then embedded using Optimal Cutting Temperature (OCT) embedding medium for frozen tissue specimens (Agar Scientific). Brains were cryosectioned into 10 µm thick sections using a cryostat and superfrost plus slides (Thermo Scientific) and stained with Haematoxylin and eosin (H&E) for morphological analysis or were immunostained and analysed using fluorescence microscopy. In order to perform immunohistochemistry, the frozen tissue sections were washed 2 times with PBS to remove OCT medium and incubated for 10 minutes in 0.1% (v/v) Triton×100 and then 30 minutes in 1% (w/v) BSA followed by primary antibody solution at 4°C overnight. The sections were then washed 3 times with PBS and incubated with secondary antibody solution (1:500) for 2 hours in the dark at RT. After removing the secondary antibody solution and performing 2 times washes (5 minutes each wash), the sections were counterstained with DAPI (1:500) for 10 minutes. After washing with PBS, the section was mounted with fluorescent mounting media (Dako) and cover slipped. (Dr. Chris Hill assisted with brain harvesting.)

2.14 Imaging

2.14.1 Fluorescence microscopy

Imaging was performed using a Leica DM2500 (Leica) fluorescence microscope with the 561 nm, 488 nm, and 405 nm lasers and data were acquired by the Leica Application Suite (LAS, Leica) integrated software and processed with ImageJ, FIJI.

2.14.2 Confocal imaging

Confocal imaging was performed using a 3i spinning disk confocal microscope CSU-X1 (Intelligent Imaging Innovations) with a Zeiss autofocus system and Hamamatsu digital camera using 10×, 20× air or 40× and 63× oil objectives then processed with ImageJ, FIJI.

2.14.3 Bioluminescence

Bioluminescence (BLI) was carried out with an IVIS spectrum system (Perkin Elmer). After inducing anaesthesia, the rats' heads were shaved, and the animals received an intraperitoneal injection of luciferin at a dose of 150 mg/kg body weight. Data was acquired 20 minuets post administration of the substrate with a field of view B (6.5 cm), medium binning, f-stop 1 and exposure time calculated automatically by the acquisition software, up to a maximum of 5 min. All bioluminescence data was normalised to the acquisition conditions and are displayed as radiance (photons/s/cm^2/str).

2.14.4 Magnetic Resonance Imaging

Magnetic Resonance Imaging (MRI) data was acquired with a Bruker Advance III console interfaced to a 9.4T magnet system (Bruker Biospec 94/20 USR). RF excitation was achieved with an 86 mm resonator and signal detection with a 4-channel phased array receive-only rat brain coil. Once the injection site was located using scout images, higher resolution images were acquired with Rapid Acquisition with Relaxation Enhancement (RARE) sequence. Parameters: echo time (TE)= 38 ms, repetition time (TR)= 2700 ms, RARE factor= 8, number of excitations (NEX)= 8, field of view (FOV)= 35×35 mm, matrix size= 350×350 pixels, slices= 20, slice thickness= 500 µm.

(Dr. Arthur Taylor assisted with cell imaging using BLI and MRI; all imaging experiments were overseen by Prof. Harish Poptani.)

2.15 Statistical analysis

Error bars represent standard deviation (SD) using a minimum number (n) of 3 independently conducted experiments (n3). SD were calculated using OriginPro 9.0.0 (OriginLab Corporation). Student T-Test was used to evaluate statistical significances between two groups of samples. The statistical probability is demonstrated in terms of p-value (p), which was considered "significant" when $p<0.05$ (*); "very significant" when $0.01>p>0.001$ (**) and "very highly significant" when $p<0.001$ (***).

CHAPTER 3

Preparation of Fluc-ZsGreen and MPIOs labelled DAPCs

3.1 Introduction

3.1.1 Generating DAPCs from RC17 hESCs

The first part of the study was to optimise the *in vitro* protocol developed by (Nolbrant et al., 2017) for directing the differentiation of hESCs to DAPCs. Since it is known that the Glycogen Synthase Kinase inhibitor (GSKi) concentration is crucial for correct midbrain patterning *in vitro*, and each cell line may have slightly different sensitivity to GSK3i levels (Nolbrant et al., 2017), the optimal concentration of the GSKi (CHIR referred to the chemical form of GSKi) was determined. hESC-derived DAPCs are usually identified by expression of LMX1A, FOXA2 and OTX2A (Kirkeby et al., 2012). However, a problem with relying solely on these 3 markers is that their expression cannot distinguish between progenitors that give rise to Subthalamic Nucleus (STN) neurons and those that generate mature DA neurons. This can be addressed by investigating the expression levels of *BARHL1*, which is only expressed in the STN progenitors. Investigating how the concentration of CHIR affects *BARHL1* expression enables the optimal concentration of CHIR used in the protocol to be established.

Another question that was addressed in this chapter was whether freeze-thawing the DAPCs had any effect on the expression levels of the DAPC markers *FOXA2*, *OTX2A* and *LMX1A*. The reason for doing this was to determine if for future animal experiments, the DAPCs could be prepared in advance and frozen, thereby facilitating the planning of the *in vivo* experiments (Nolbrant et al., 2017).

3.1.2 Generation of Fluc-ZsGreen RC17 reporter hESC line

The next aim of this chapter was to generate a Fluc-ZsGreen RC17 reporter hESC line to enable the hESC-derived DAPCs to be detected in rats *in vivo*. A bicistronic reporter Fluc-ZsGreen was used for this purpose (Figure A.2) because Fluc enables non-invasive bioluminescence imaging *in vivo*, while ZsGreen allows the transduction efficiency to be assessed in cells *in vitro*.

It has previously been reported that reporter gene expression can be reduced over time with passaging (Lippincott-Schwartz and Patterson, 2003; Krishnan et al., 2006). When generating reporter lines, it is therefore important to investigate whether reporter gene expression remains stable. Moreover, it is important to consider that the genetic modification that results from introducing the reporter gene might affect the phenotype of the cells. In the case of pluripotent stem cells, there is a risk that depending on where the reporter genes integrate, it could affect the pluripotency of the cells. Pluripotency of hESCs is assessed by investigating if they can generate derivatives of all 3 embryonic germ layers: endoderm, mesoderm and ectoderm. This is typically done by either implanting the cells into mice to see if they can generate teratomas, or by generating EBs *in vitro* (Allison et al., 2018). In this study, in compliance with NC3Rs principles, pluripotency of the hESC reporters was assessed using the EB system.

Following this, it was important to sort the cells using flow cytometry in order to obtain a pure population of transduced cells that expressed the reporter. It is known that when pluripotent stem cells are modified to express a reporter gene, and then differentiated to a specialised cell type, the reporter gene can become silenced (e.g. cardiomyocyte differentiation of mouse ESC) (Cao et al., 2006). A further aim of this study was therefore to investigate if expression of the ZsGreen and Fluc reporter genes was reduced when the cells were differentiated to DAPCs, and then further differentiated to mature DA neurons.

3.1.3 Labelling hESCs-derived DAPCs with MPIOs for MR imaging

In order to enable *in vivo* cell tracking using MRI, a further aim was to optimise a protocol to label DAPCs using a contrast agent composed of MPIO. This would allow the intercranial biodistribution and fate of the DAPCs to be determined by non-invasive MRI for further investigations (Section 1.3.2).

The objectives of this chapter were as follows:

1. Optimise the protocol for directing the differentiation of RC17 hESCs to DAPCs.
2. Establish a Fluc-ZsGreen RC17 hESC reporter line.
3. Investigate if reporter gene expression is maintained when the Fluc-ZsGreen hESC reporter cell line is differentiated to DAPCs and mature DA neurons.
4. Assess the feasibility of using MPIOs to label hESC-derived DAPCs.

3.2 Results

3.2.1 Optimisation of protocol for directing the differentiation of hESCs to DAPCs

Culturing hESCs of high quality that do not show excessive spontaneous differentiation is a crucial starting point for generating a high yield of DAPCs. Therefore, the RC17 cells were assessed for the expression of stemness markers, *OCT4* and *Nanog*. The immunofluorescence results demonstrate that both *OCT4* and *Nanog* expression (red) in the nuclei (blue) of the undifferentiated colonies of RC17 cells (Figure 3.1).

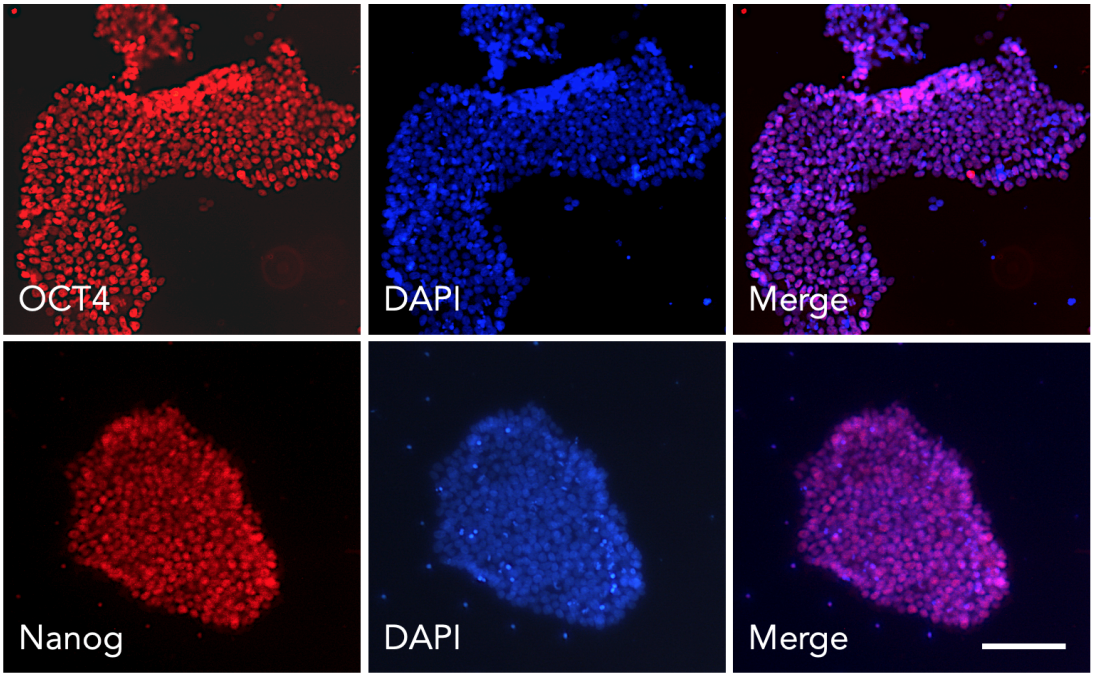

Figure 3.1: Expression of stemness markers in undifferentiated hESCs. RC17 cells cultured for 4 days and fixed and immune stained for *OCT4* and *Nanog* (red channel), counterstained with DAPI (blue channel). The confocal immunofluorescent microscopy detects expression of both markers in the RC17 colonies. Scale bar 100 µm.

To optimise the protocol for differentiating DAPCs from hESCs, the Nolbrant

(2017) protocol was followed over 16 days (Figure 2.2) using the following three different concentration of CHIR: 0.7, 0.8, and 0.9 µM. The hESCs were differentiated in parallel and on day 16, cells were fixed and immunostained for the DAPC markers to assess the success of differentiation and determine the optimum concentration of CHIR. Immunostaining for co expression of *LMX1A*/*FOXA2* and *LMX1A*/*OTX2* indicated the successful patterning of VM progenitors (Figure 3.2 a&b), but differences were observed depending on the concentration of CHIR that was used. For instance, immunostaining revealed a patchy expression of *FOXA2* and *LMX1A* in the presence of 0.7 µM or 0.8 µM CHIR, but a more consistent staining of all markers in the presence of 0.9 µM CHIR. This suggested that 0.9 µM CHIR is the optimal concentration for directing the differentiation of RC17 hESCs to DAPCs.

In order to investigate effects of the freeze-thawing, both fresh and frozen cells which were differentiated into DAPCs using 0.7, 0.8, or 0.9 µM CHIR, were analysed using qRT-PCR for expression of DAPC marker genes *FOXA2*, *LMX1A*, and *OTX2A*. The day 16 frozen DAPCs were defrosted and cultured for 2 days in the media that is used for the cells before freezing to compare with freshly differentiated DAPCs. As Figure 3.3 shows, in the fresh samples, DAPCs differentiated in the presence of 0.9 µM CHIR showed significantly higher expression levels of all three DAPC markers compared to those differentiated in the presence of 0.7 or 0.8 µM CHIR (Figure 3.3 a&b&c). In contrast, cells differentiated in the presence of 0.9 µM CHIR that had been freeze-thawed showed significantly lower expression of DAPC markers.

In order to confirm that 0.9 µM is the optimal concentration for directing the differentiation of RC17 hESCs to DAPCs, immunostaining and qRT-PCR was performed to investigate the expression levels of *BARHL1* at the three CHIR concentrations. In Figure 3.4 (a), the lowest expression of *BARHL1* was observed in the progenitors that were treated with 0.9 µM CHIR. Furthermore, this finding was confirmed by qRT-PCR (Figure 3.4 b).

3.2.2 Establishing Fluc-ZsGreen RC17 reporter hESC line

The lentivirus carrying the bicistronic Fluc-ZsGreen reporter genes was used to transduce the undifferentiated hESCs. Fluc enables non-invasive bioluminescence imaging *in vivo*, while ZsGreen allows the transduction efficiency to be assessed in cells. The full sequence of the construct is provided in Figure A.2. The following 3 multiplicities

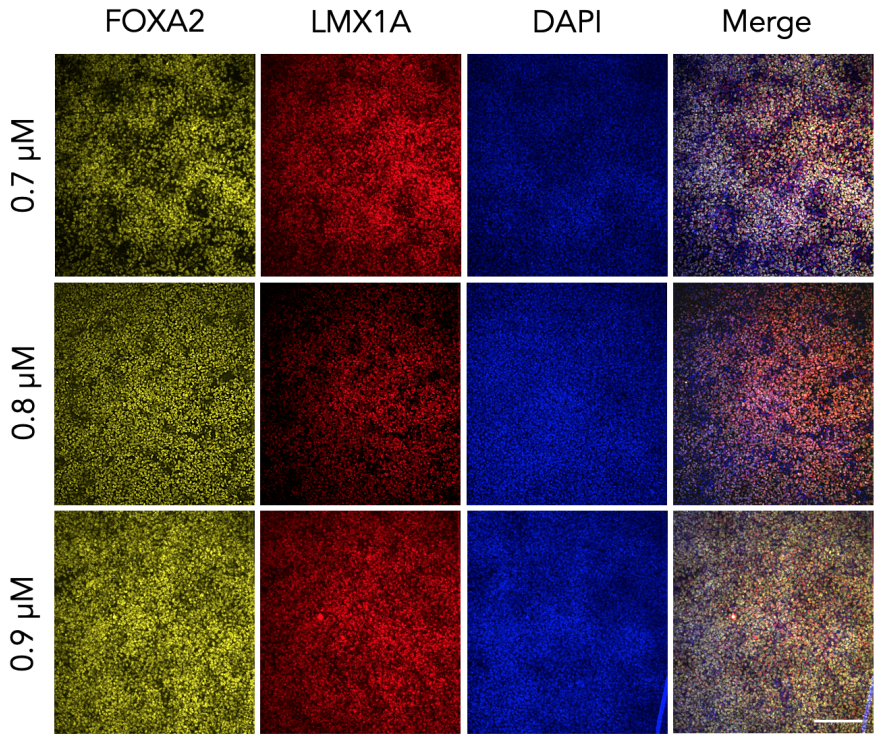

(a)

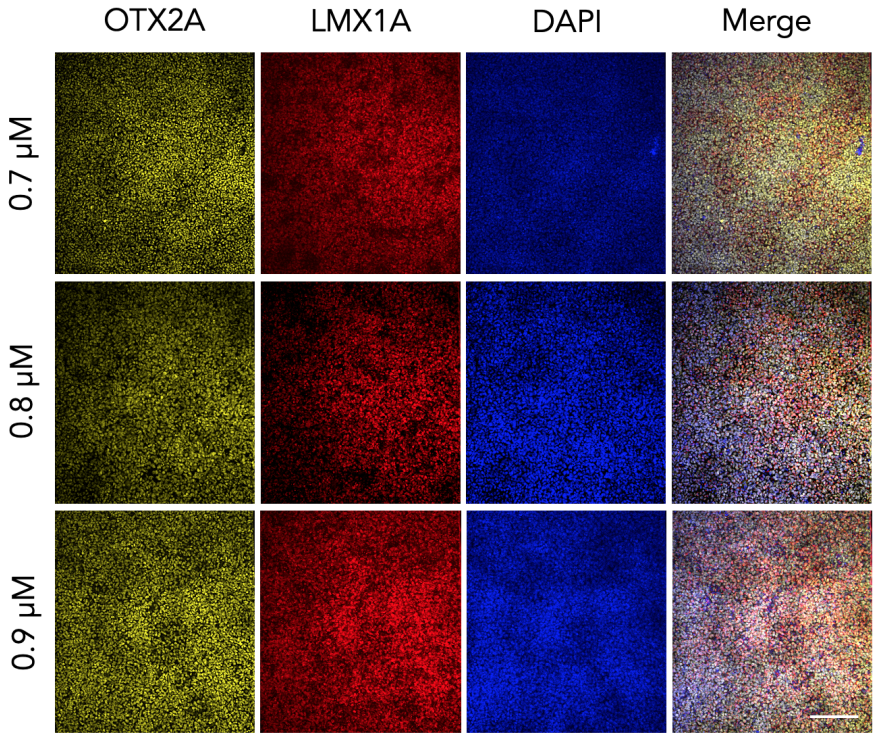

(b)

Figure 3.2: Establishing the optimal concentration of CHIR for directing DAPC differentiation from hESCs. RC17 hESCs were directed to differentiate under the following CHIR concentrations: 0.7, 0.8 and 0.9 µM. Following 16 days, the cells were fixed and immunostained for (a) *FOXA2/ LMX1A* and (b) *OTX2A/ LMX1A*, counterstained with DAPI. At the lower CHIR concentrations of 0.7 and 0.8, patches of unstained cells were observed within the lawn of DAPCs, whereas more consistent staining was observed in the cells cultured in the presence of 0.9 µM. The negative controls provided in Figure A.3. (n=3), Scale bar 100 µm.

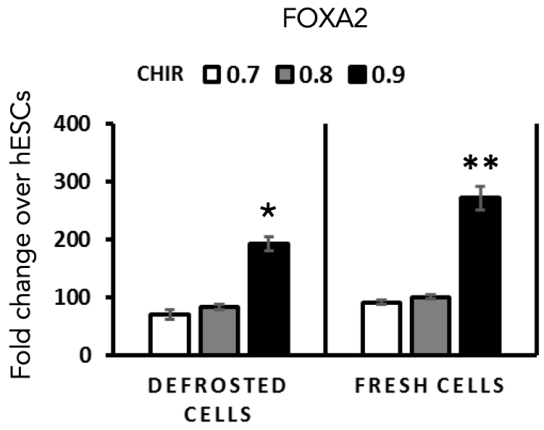

(a)

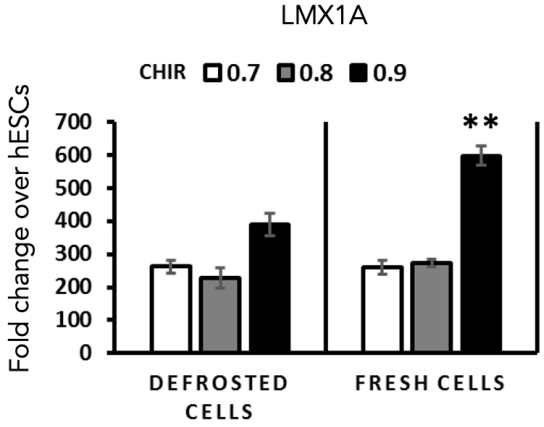

(b)

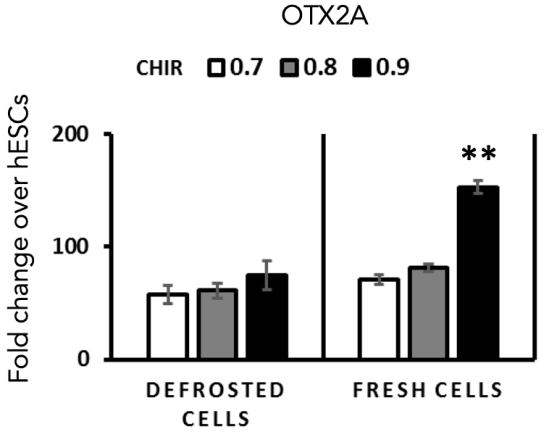

(c)

Figure 3.3: qRT-PCR data of key DAPCs markers from fresh and defrosted DAPCs that was differentiated using 0.7, 0.8, and 0.9 µM **of CHIR.** (a) FOXA2, (b) LMX1A, and (c) OTX2A are expressed in both fresh and defrosted DAPCs with different expression levels. Results are given as fold change over undifferentiated hESCs. *GAPDH* was used as the housekeeping gene and a sample of undifferentiated hESCs were used to determine the gene expression levels relative to the expression in undifferentiated controls. Error bars represent SD, (n=3). $p<0.05$ (*); $0.01>p>0.001$ (**).

of infections (MOIs) were tested: 1,3, and 5, which corresponded to 5×10^4, 15×10^4, and 25×10^4 viralparticles/µl, respectively. The aim was to identify the MOI that gave the highest transduction efficiency without affecting the viability of the hESCs. Phase contrast microscopy showed that cells transduced with all three MOIs, displayed the expected morphology of undifferentiated cells, i.e., colonies comprising a dense monolayer of cells that have a high nuclear: cytoplasmic ratio (Figure 3.5 a). ZsGreen expression was also detected in hESCs transduced with all three different MOIs. The efficiency of transduction was determined by measuring ZsGreen expression with flow cytometry.

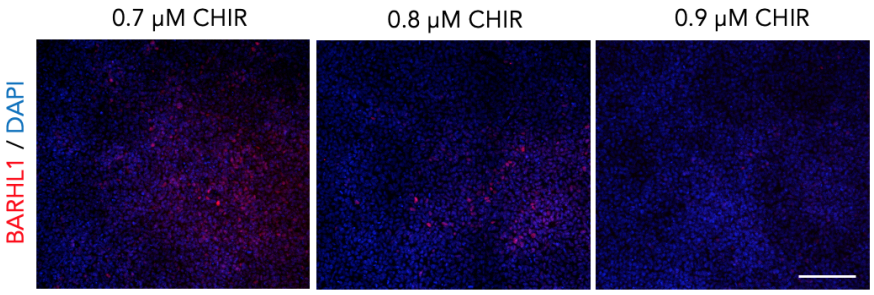

(a)

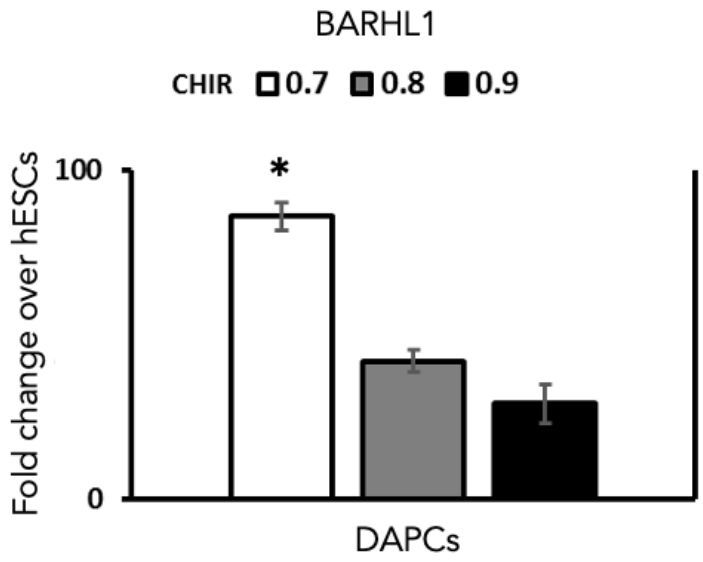

(b)

Figure 3.4: Expression of *BARHL1* in RC17 hESC-derived DAPCs. (a) Immunostaining and (b) qRT-PCR shows lower expression of *BARHL1* in the DAPCs that were treated with 0.9 µM CHIR compared to those treated with 0.7 and 0.8 µM. In (a) *BARHL1* is in red and DAPI represent nuclei is shown with blue colour. In (b) *GAPDH* was used as the housekeeping gene and a sample of undifferentiated hESCs were used to determine the gene expression levels relative to the expression in undifferentiated controls. Error bars represent SD, (n=3), $p<0.05$ (*), Scale bar 100 µm.

Figure 3.2 (b) shows the dot plots of the cytometry data for the baseline control with no detected fluorescence, and the transduced cells with ZsGreen expression for the

three different MOIs. The cytometry data indicate that for the lowest MOI, ZsGreen positivity was only 18%, while increasing the MOI to 3 and 5 increased the proportion of ZsGreen$^+$ hESCs to 35% and 41%, respectively. Also, the similar levels of ZsGreen expression observed with MOIs 3 and 5 suggested that increasing the concentration of viral particles beyond this point would be unlikely to increase the transduction efficacy. Therefore, the undifferentiated RC17 cells that was transduced with MOI 5 were selected for subsequent experiments.

3.2.3 Evaluation of transduced Fluc-ZsGreen$^+$ RC17 reporter line

Given that cytometry data showed that the transduced colonies of RC17 cells were not homogeneous in regard to expression levels of Fluc-ZsGreen and only about 47% of cells expressed the ZsGreen (Figure 3.6 a), cells underwent sorting to obtain a pure homogeneous population with strong expression of the reporters. A group of non-transduced RC17 cells were used as a baseline control and the transduced cells were sorted into two different populations of "Dim-green" and "Bright-green" cells (Figure 3.6 b). The Bright-green sorted cells were collected and routinely cultured and passaged three times to confirm that they maintained their undifferentiated morphology and high levels of ZsGreen expression through subsequent passages. Figure 3.6 c shows the morphology of bright-green sorted cells is indistinguishable from non-transduced cells. To further assess the expression levels of ZsGreen, flow cytometry analysis confirmed the ZsGreen expression was maintained over multiple passages (Figure 3.3 d).

To assess whether the introduction of the reporter and sorting of cells affected pluripotency of transduced cells, EB were generated and immunostained for markers of embryonic germ layer derivatives. The presence of *GATA6* (endoderm), *Brachyury* (mesoderm) and *Nestin* (ectoderm) confirmed that the Fluc-ZsGreen$^+$ hESCs remained pluripotent (Figure 3.7).

3.2.4 Investigating if Fluc-ZsGreen reporter gene expression in maintained in hESC-derived DAPCs and mature DA neurons.

A group of Fluc-ZsGreen RC17 cells was differentiated into DAPCs to assess the effect of transduction on the differentiation patterns and transgene silencing. On Day 16, the differentiated DAPCs were immunostained for *LMX1A*$^+$, *FOXA2*$^+$ and *OTX2A*$^+$. As Figure 3.8 a shows, the successful patterning of VM progenitors was confirmed by

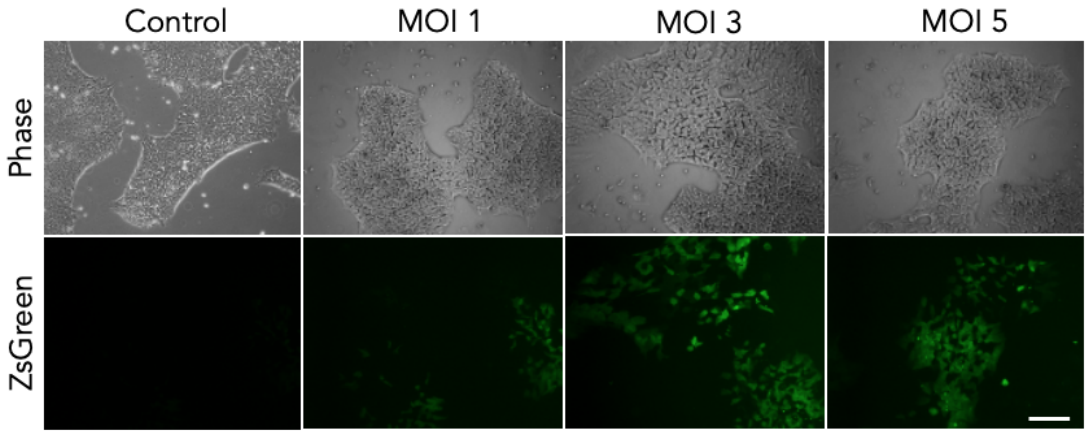

(a)

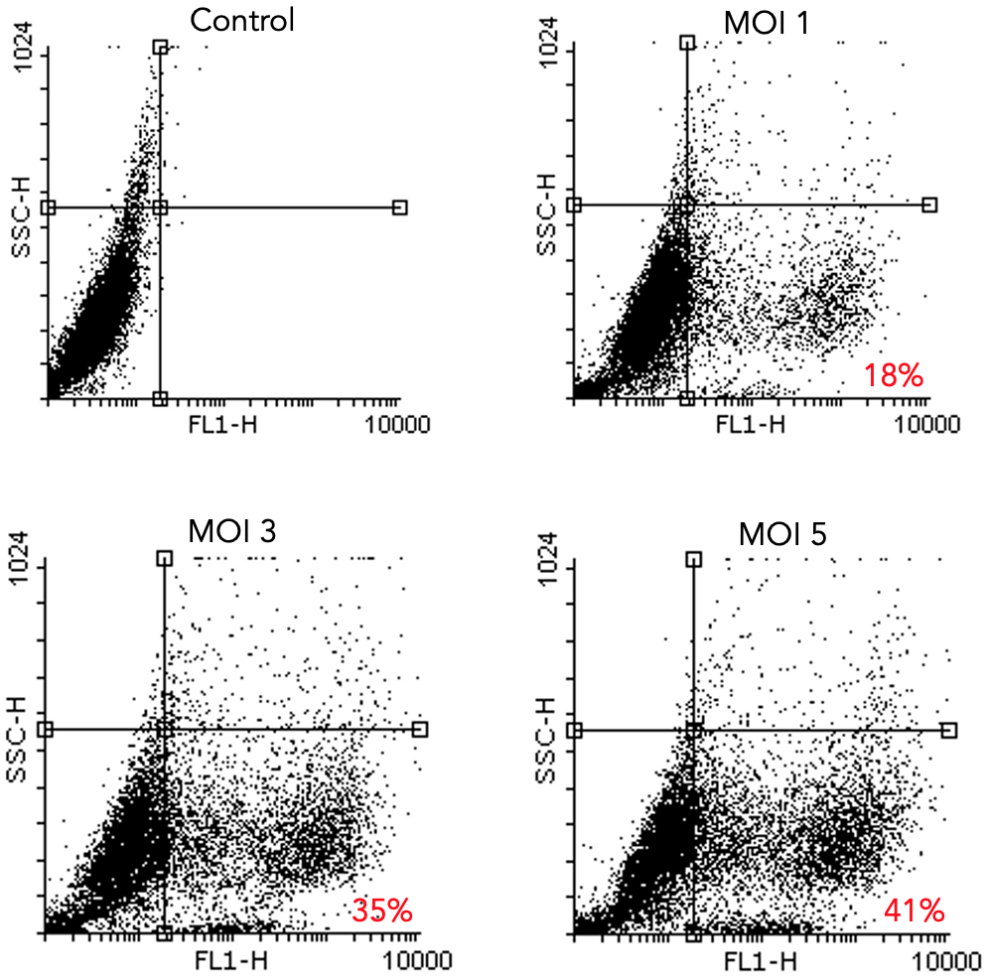

(b)

Figure 3.5: ZsGreen expression in RC17 hESCs transduced with a bicistronic Fluc-ZsGreen construct. (a) The undifferentiated hESCs were transduced using three different concentrations of viral particles (5, 15, and 25×10^4 viral particles/µl), corresponding to MOIs of 1, 3 and 5. The control sample comprised non-transduced hESCs. Following transduction, the hESCs retained their typical morphology. (b) Flow cytometry fluorescence analysis of ZsGreen expression showed the percentage of Fluc-ZsGreen$^+$ hESCs could be increased to 41% by increasing the concentration of lentivirus. Scale bar 100 µm.

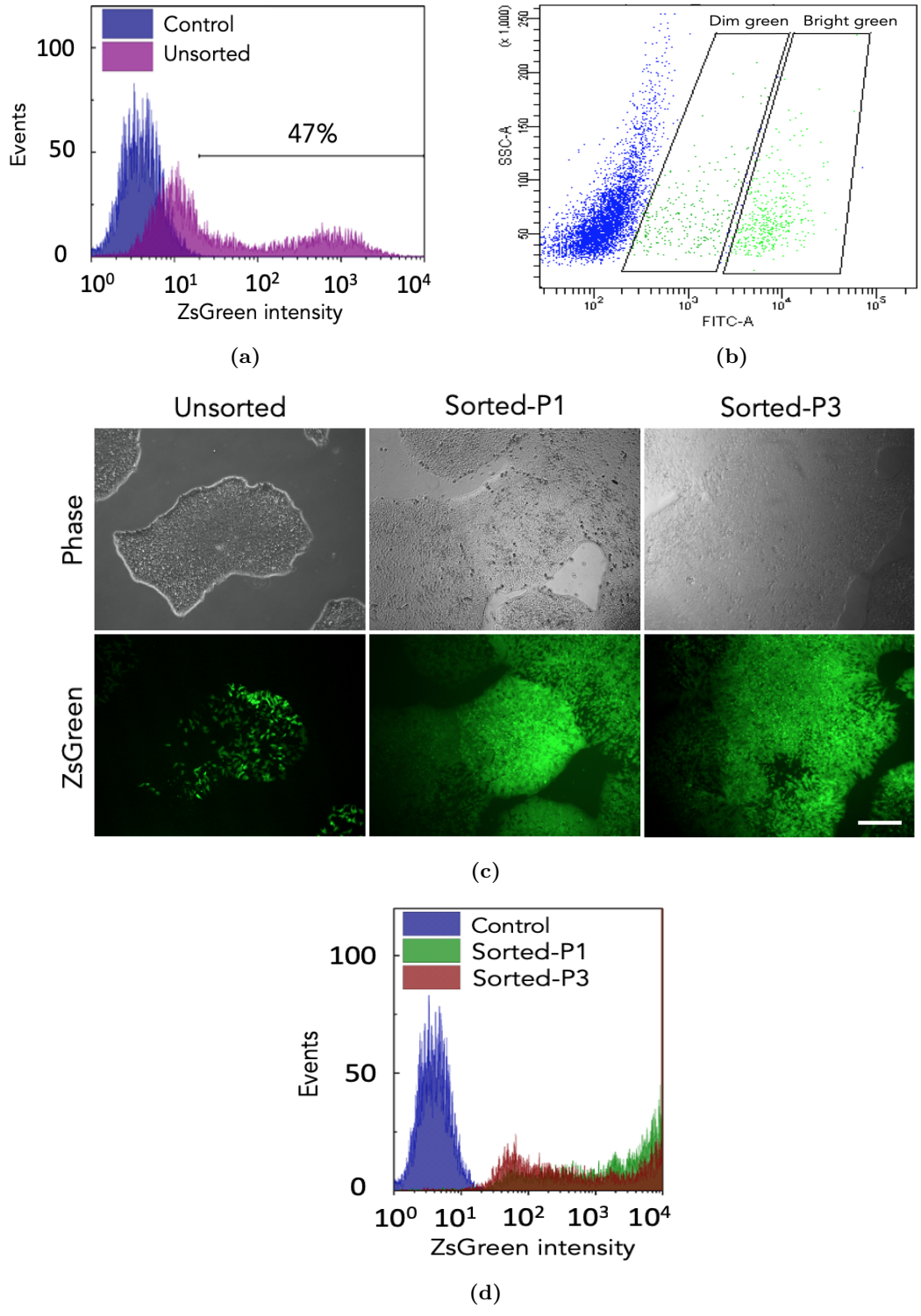

Figure 3.6: Flow-assisted cell sorting (FACS) and evaluation of transduced RC17 hESC Fluc-ZsGreen reporter cells. (a) ZsGreen expression, as measured via flow cytometry, of the control and sorted hESCs. The green fluorescence of the sorted cells is stable for several passages (b) The transduced colonies of RC17 cells were sorted into two different populations of "Dim green" and "Bright green" cells. (c) Phase contrast and immunofluorescent images of unsorted and bright green cells that were cultured for three passages. (d) Flow cytometry confirmed that ZsGreen expression was maintained in the hESC population, with no noticeable decreases observed between passages one and three. Scale bar 100 µm.

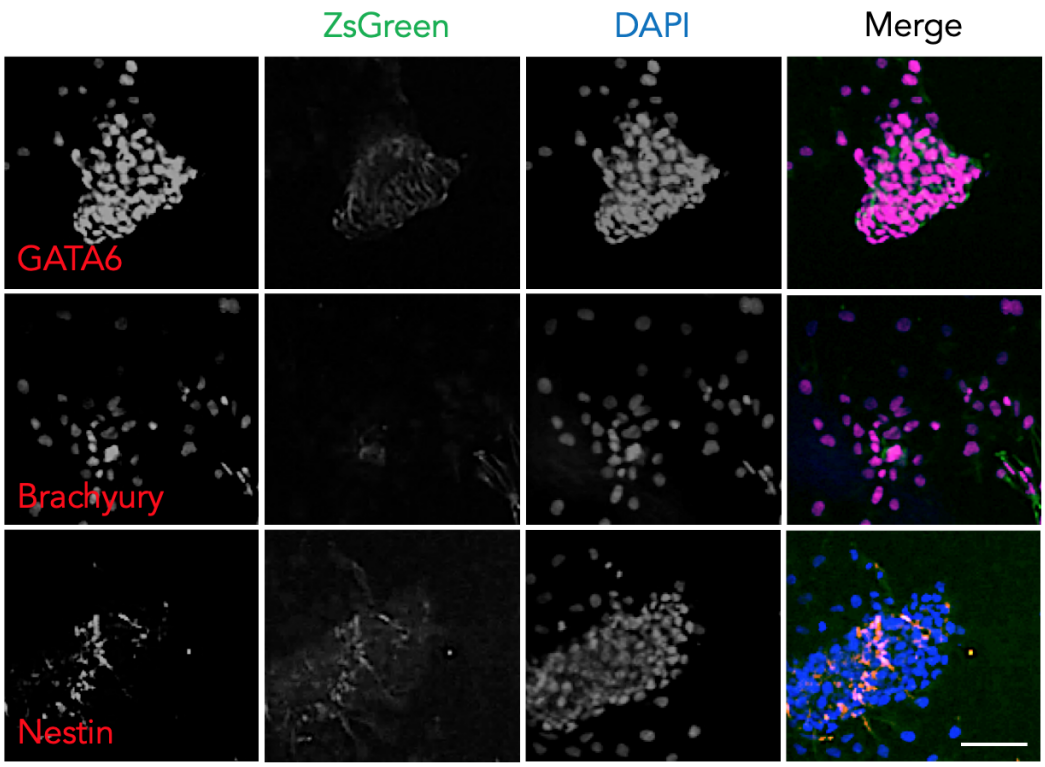

Figure 3.7: Embryoid bodies formed from sorted hESCs were shown to be able to differentiate into all three germ layers. Positive staining for *GATA6* (endoderm), *Brachyury* (mesoderm) and *Nestin* (ectoderm) were detected in the spontaneously differentiated EBs grown from bright green undifferentiated RC17 cells. *GATA6*, *Brachyury* and *Nestin* are shown in red, ZsGreen in green and nuclei of cells counterstained with DAPI using blue colour. Scale bar 100 µm.

expression of all DAPCs associated markers. Also, ZsGreen fluorescence intensity was visible in the progenitors. However, confocal microscopy also revealed that not all cells expressed ZsGreen after differentiation into DAPCs. To further assess the percentage of ZsGreen positive DAPCs flow cytometric analysis was performed and revealed that 51% of these cells expressed ZsGreen, implying a significant loss of reporter gene expression when compared to undifferentiated hESCs (Figure 3.8 b).

In order to apply DAPCs for transplantation, their ability to differentiate into mature DA neurons should be first demonstrated *in vitro*. The key marker for terminally differentiated DAPCs is *TH*, which is co-expressed with *FOXA2* and *OTX2*. A group of VM progenitors were differentiated into mature DA cells according to an established protocol (Section 2.8). This is a long-term differentiation process and takes about 50 days for cells to give rise to DA neurons. Figure 3.9a shows high expression of *FOXA2*, *OTX2A* and *TH* in the immunostained cells on day 50 of differentiation. Of note, ZsGreen was no longer detectable at this differentiation stage (Figure 3.9 b)

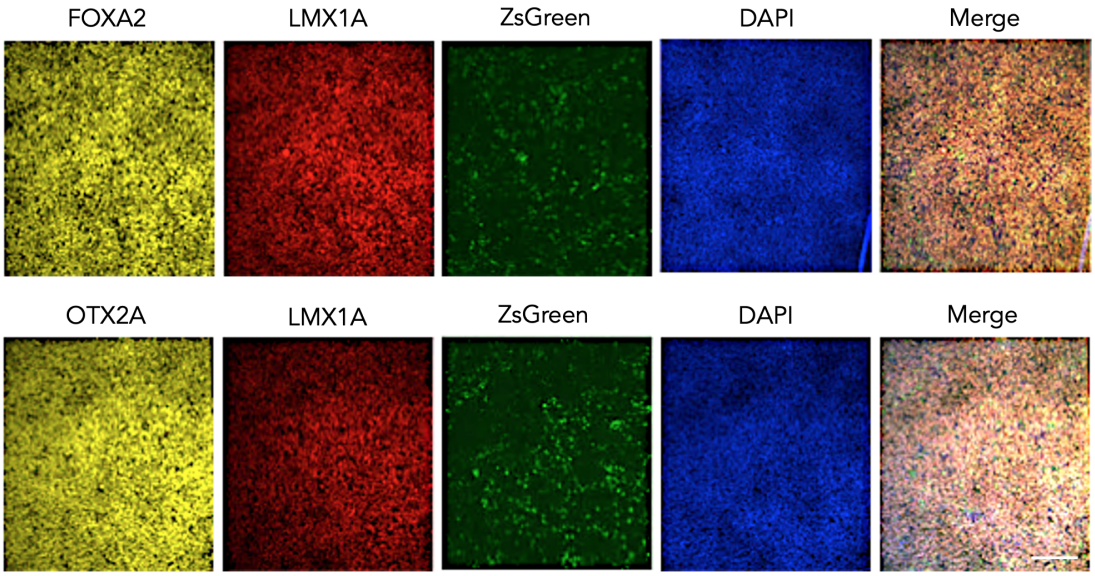

(a)

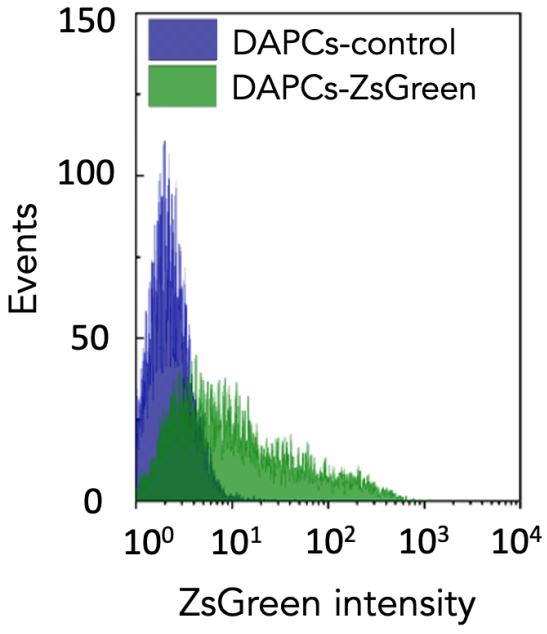

(b)

Figure 3.8: Differentiated Fluc-ZsGreen RC17 express key markers of DAPCs and ZsGreen. (a) Confocal microscopy to show the co-expression of *FOXA2*/*LMX1A* and *OTX2A*/*LMX1A* in the immunostained Fluc-ZsGreen DAPCs. (b) Flow cytometry showed that differentiation into DAPCs reduces ZsGreen expression by approximately 47%. Scale bar 100 µm.

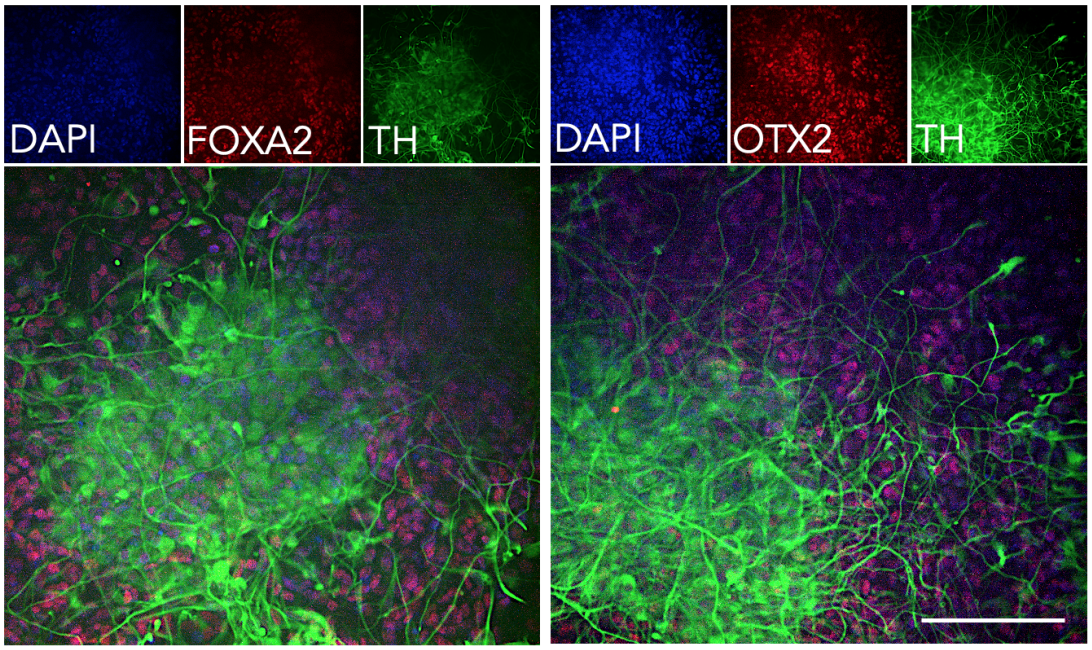

(a)

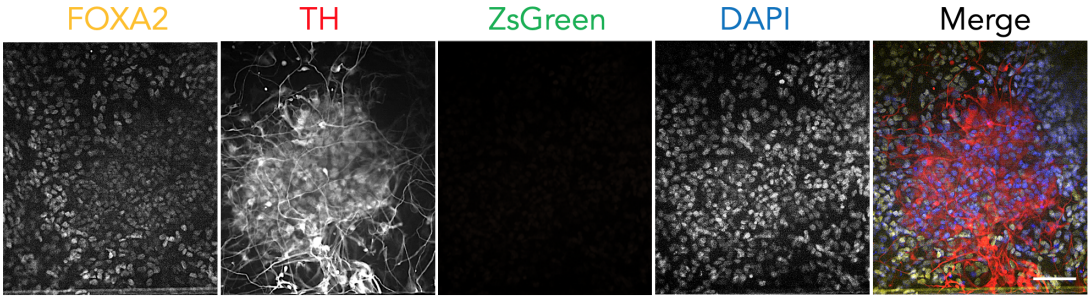

(b)

Figure 3.9: Differentiation towards mature DA cells: Differentiation towards mature DA cells. (a) Fluorescence microscopy of mature DA cells on day 50 of differentiation immunestained for *FOXA2* (red), *OTX2* (red), and *TH* (green). (b) No expression of ZsGreen was detected in the terminally differentiated DA cells that expressed *FOXA2* (yellow) and *TH* (red). All immunestained samples counterstained with DAPI in blue colour. Scale bar 100 µm.

The strength of the bioluminescence signal was assessed using BLI to determine the degree of emitted light by Fluc-ZsGreen labelled cells. Three groups of labelled cells with different seeding density were assessed including undifferentiated hESCs, DAPCs, and mature DA neurons. Measurement of the light output (bioluminescence) revealed that the expression of luciferase was strong before differentiation (37 p/s/cell), but was significantly reduced as cells differentiated towards DAPCs (17 p/s/cell) and extremely weak when they became mature DA neurons (G1 p/s/cell) (Figure 3.10)

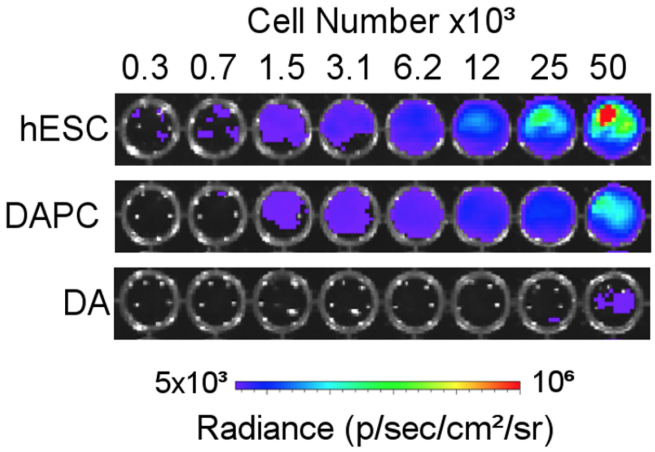

(a)

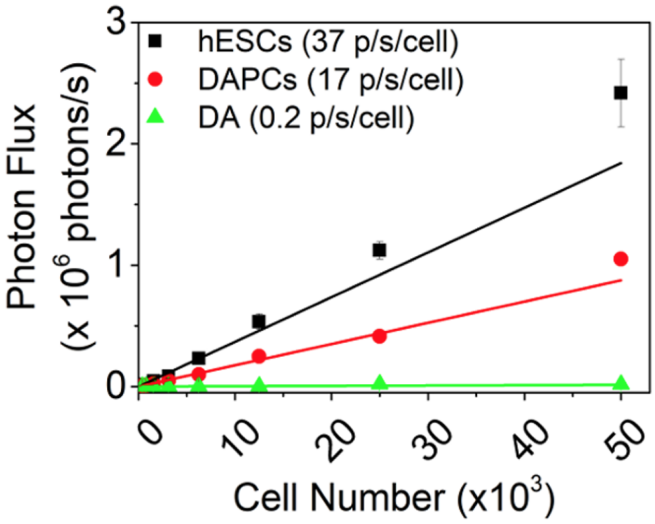

(b)

Figure 3.10: BLI of different numbers of Fluc-ZsGreen$^+$ hESCs, DAPCs, and mature DA cells and the corresponding photon flux. (a) *In vitro* BLI data shows increasing of detected Fluc signal by rising the cell number. (b) Fluc is 37 p/s/cell in hESCs but reduced to 17 p/s/cells in DAPCs. There is significant reduction of signal in mature DA. Expression data are representative of three independent experiments. Error bars represent SD.

3.2.5 Assessing the feasibility of MPIOs labelling of DAPCs

Following a 24-hour incubation with the MPIOs, the DAPCs cells were examined to ascertain if cells appeared to have taken up the particles on visual inspection. Cell uptake efficiency was then quantitatively assessed via flow cytometry. Six concentrations were explored: 500, 1000, 1500, 2000, 4000 and 8000 particles/µl and the percentage of cells in the population that had successfully taken up the fluorescent particles and thus were deemed to be positive, are represented per concentration in Figure 3.11. The control group was unlabelled DAPCs.

The 1500 particles/µl were chosen to label DAPCs for animal experiment. Flow

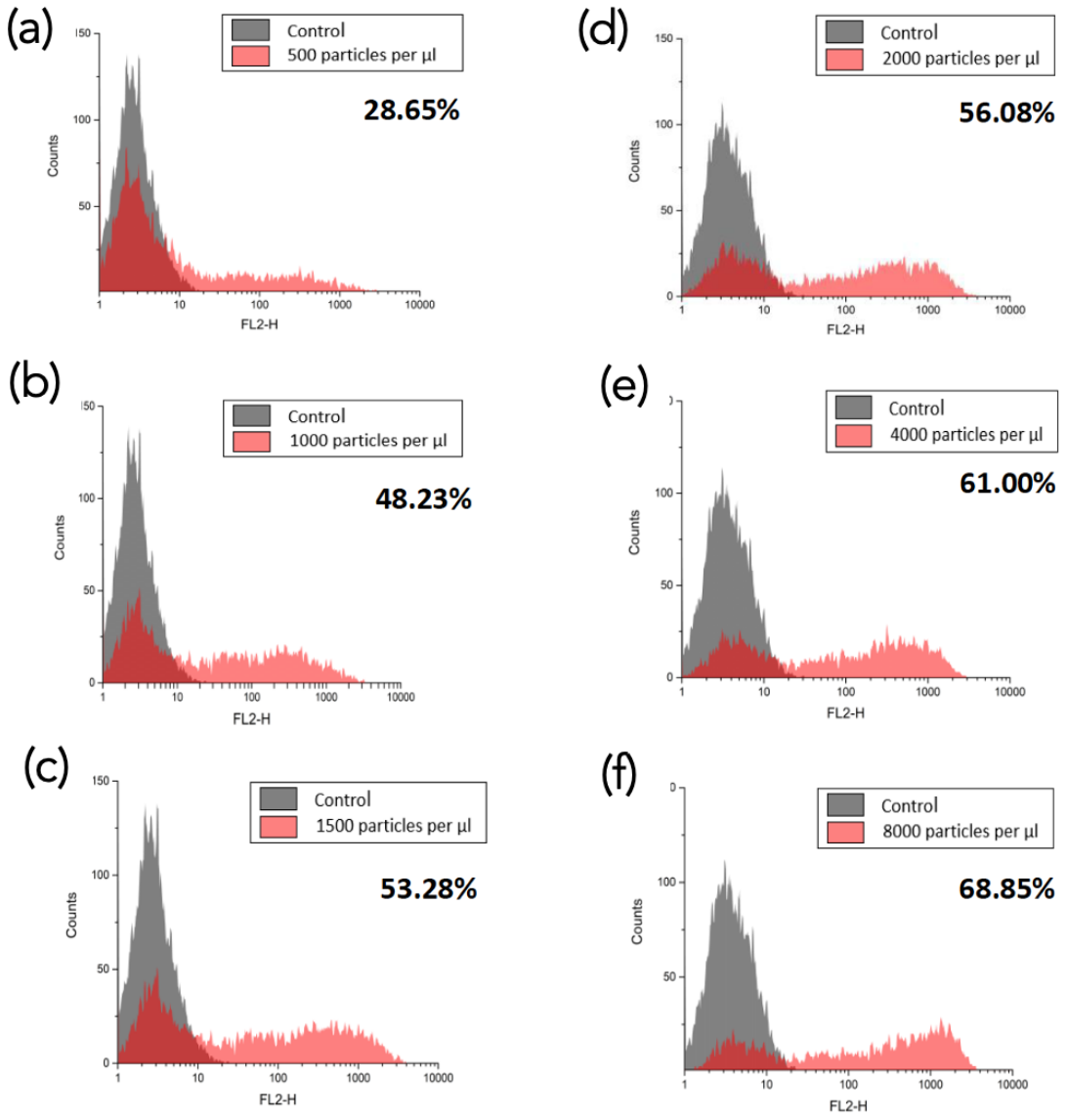

Figure 3.11: Histograms displaying the fluorescence signals detected for MPIOs labelled DAPCs. MPIOs at following concentrations: (a) 500 particles per µl, (b) 1000 particles per µl, (c) 1500 particles per µl, (d). 2000 particles per µl, (e) 4000 particles per µl, (f) 8000 particles per µl. Percentage corresponds to the percentage of the population positive for the signal in each case. Control is in grey colour and selected population of labelled DAPCs is in red colour.

cytometry analysis of MPIO-labelled DAPCs suggested that approximately 72% of DAPCs were labelled with the 1500 particles/µl concentration of MPIOs, as evidenced by yellow fluorescence originating from MPIOs (Figure 3.12).

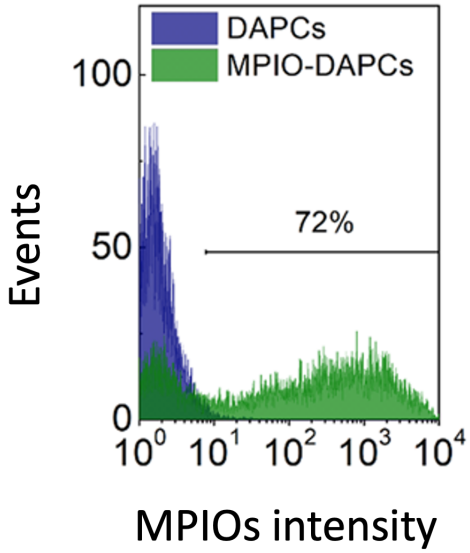

Figure 3.12: Fluorescence signals detected of MPIOs labelled DAPCs using FACS analysis. Yellow fluorescence of unlabelled (blue) and MPIOs-labelled DAPCs (green) shows that approximately 72% of cells uptake the particles.

3.3 Discussion

In this chapter, optimisation of the protocol to direct differentiation of RC17 hESCs towards DAPCs on the basis of GSK inhibitor concentration was investigated. Furthermore, feasibility of the lentiviral vector to transduce RC17 hESCs for BLI, and MPIOs to label DAPCs for MRI tracking have also been evaluated.

Correct patterning of DAPCs is essential to ensure the cells have the potential to give rise to mature and functional mesencephalic DA neurons upon intracerebral transplantation. Efficient and specific neural induction is dependent on finely controlled caudalization using GSKi according to the cell line. All VM progenitors co-express *LMX1A*$^+$, *FOXA2*$^+$ and *OTX2A*$^+$, representing the most caudal triple positive progenitors that generate mature and functional DA neurons. In contrast, triple positive progenitors in the rostral part of the ventral midbrain give rise to glutamatergic STN neurons. In this regard, DAPCs can be distinguished from STN progenitors by the absence of *BARHL1* expression, which serves as a further verification of functional

DAPCs. Taken together, differentiation should be deemed successful where cells express *LMX1A*, *FOXA2* and *OTX2A*, but not *BARHL1*. Here, it was concluded that 0.9 µM CHIR resulted in significant expression of triple DAPC markers while the *BARHL1* expression was minimal.

In addition, the effect of cryopreservation on the differentiated DAPCs was assessed. The data suggest that freezing the cells that were generated under these optimal conditions reduced the expression levels of the DAPC markers *LMX1A*, *FOXA2* and *OTX2A*. Therefore, it was decided that for future animal work, freshly differentiated DAPCs would be used.

In order to perform preclinical bioluminescent modalities, the Fluc-ZsGreen reporter gene was used to label RC17 undifferentiated hESCs. The data indicate that the integrated reporter gene did not affect hESC pluripotency, nor their ability to differentiate to DAPCs and mature DA neurons *in vitro*. However, the reduction of both luciferase and ZsGreen were indicated in the DAPCs *in vitro* followed by transgene silencing in mature DA neurons. The reporter gene silencing in the differentiated cells is mainly considered as the result of DNA methylation followed by attraction of proteins that specifically bind to the transgene and block the other factors required for gene induction (Curradi et al., 2002; Suelves et al., 2016).

Additional assessment in this chapter involved labelling hESC-derived DAPCs using MPIOs for MRI tracking. Generally, the minimum percentage of loading concentration using iron oxide particles to be detectable by MRI is no less than 50%. From our data, it is apparent that the optimum concentration of MPIOs is 1500 particles per µl in order to have at least 50% positive cell uptake. Beyond this concentration, only about 15% difference was observed using up to 8000 particles per µl. This percentage increase could be accounted for by more particles per cell rather than more cells labelled. Furthermore, no morphological changes or any obvious toxic effects were observed in the DAPCs.

CHAPTER 4

In vivo tracking

4.1 Introduction

An effective strategy for monitoring the proliferation, viability and localisation of implanted cells longitudinally is to employ a non-invasive imaging approach comprising different modalities (Lau et al., 2010). In this study, a bi-modal strategy comprising BLI and MRI was used to monitor viability, assess intracranial biodistribution, and monitor tumour formation *in vivo* following administration of cells into the rat striatum. BLI is the most sensitive live animal imaging technique, enabling relatively small numbers of transplanted cells to be detected (Section 1.3.1). This technique requires that the cells express a luciferase reporter, which means that a signal is only emitted if the cells are alive. An increase in BLI signal over time indicates cell proliferation and potential tumour formation, whereas a loss of signal suggests that the cells are no longer viable, or that the reporter is no longer being expressed (Bernau et al., 2014). A drawback with BLI, however, is that spatial resolution is poor, which means that it cannot be used to determine the precise location of the implanted cells and/or any resultant masses within the brain. MR imaging, on the other hand, has a very high spatial resolution and can accurately map the position of intracranial lesions (Denic et al., 2011). Moreover, by labelling cells prior to administration with an appropriate contrast agent, such as iron oxide particles, MRI can be used to plot the biodistribution of the cells over time (Section 1.3.2). Hoehn and co-workers have shown previously that BLI and MR imaging can be used to monitor the viability and intracranial biodistribution of hESC-derived neural stem cells following implantation into the mouse striatum (Tennstaedt et al., 2015). To the best of our knowledge, this bimodal approach has not previously

been used to track the tumourigenicity, viability and biodistribution of hESC-derived DAPCs, following intrastriatal administration into the rat brain. Therefore, in order to assess the potential of this bimodal BLI/ MR strategy to track hESC-derived DAPCs *in vivo*, luciferase-expressing DAPCs and MPIO labelled DAPCs (Chapter 3), were injected intracranially into rats, and the effectiveness of the bimodal imaging strategy for tracking the cells was assessed.

The specific objectives of this chapter were to:

1. Assessing the feasibility of using BLI and MRI to detect undifferentiated hESCs and their derived tumours, respectively.

2. Assessing the feasibility of monitoring the viability and proliferation of FLuc-ZsGreen$^+$ hESC-derived DAPCs longitudinally using BLI.

3. Assessing the feasibility of tracking the biodistribution of MPIO-labelled DAPCs longitudinally using MRI.

4.2 Results

Three experimental group were established. The first experimental group consisted of 3 rats, administrated with undifferentiated RC17 hESCs as the control group. The second and third experimental groups were administrated DAPCs which were labelled with FLuc-ZsGreen and MPIOs respectively (Table 2.4).

4.2.1 Assessing the feasibility of using BLI and MRI to detect undifferentiated hESCs and their derived tumours, respectively

The purpose of this experiment was to assess the feasibility of using the FLuc reporter to monitor the viability and proliferation of implanted cells. For this purpose, undifferentiated hESC were implanted into the rat striatum because it has already been established that undifferentiated hESCs form tumours following intracranial implantation. A further aim was to assess whether any tumours that formed could be detected with MRI. To this end, in this experiment, the cells were not labelled with MPIOs.

Three rats had Fluc-ZsGreen$^+$ RC17 hESCs implanted into the right striatum, and unlabelled hESCs implanted into the left striatum. BLI was performed on the day of administration (day 0) and day 14. On day 27, both BLI and MR imaging were performed before sacrificing the animals (Figure 4.1 a).

(a)

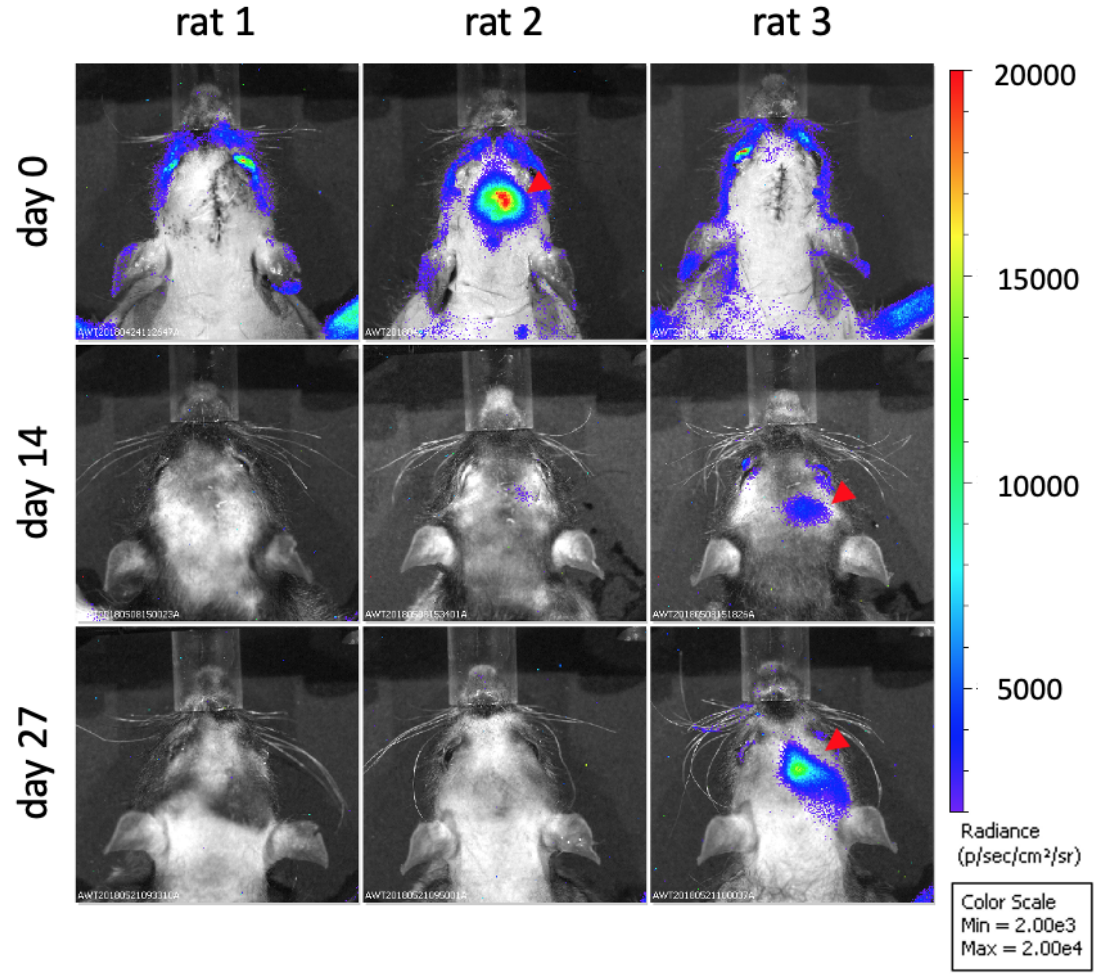

(b)

Figure 4.1: BLI imaging of RC17 hESCs following implantation into the rat brain. (a) Schematic of injection and experimental timeline of hESC administration and imaging. (b) BLI of three rats that received undifferentiated hESCs (left hemisphere: non-transduced cells; right hemisphere Fluc-ZsGreen$^+$ cells). On day 0 only rat 2 exhibited a weak signal (red arrowhead) which was lost on day 14 and 27. Rat 3 revealed a signal on days 14 that became more intense by day 27 (red arrowheads).

BLI of animals that received the undifferentiated hESCs on the day of administration (day 0), day 14, and 27 post-administration revealed great variability in the bioluminescence signal. On day 0, only rat 2 displayed a signal, which was weak and close to background levels (arrowhead) (Figure 4.1 b). This signal was progressively

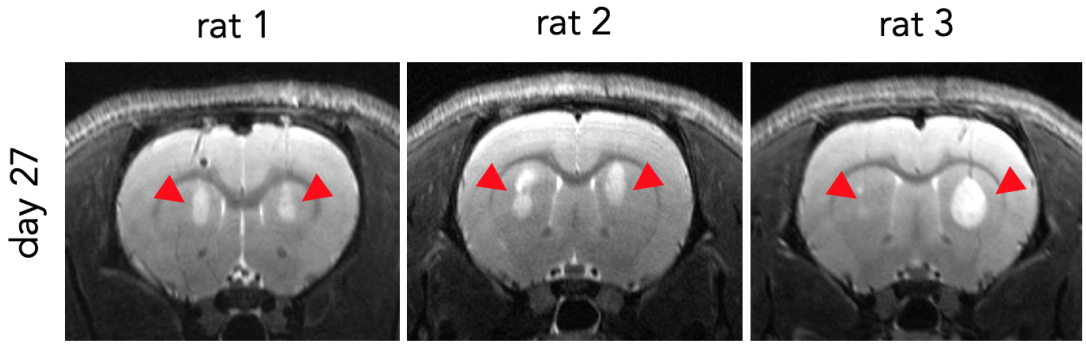

Figure 4.2: MR imaging of RC17 hESCs following implantation into the rat brain. MRI of the brain on day 27 revealed that all rats had developed tumours in both hemispheres (hyperintense contrast).

lost on the subsequent days. Rat 3 displayed a signal only on days 14 and 27 (arrowheads). Due to the weak signal, some non-specific background could be seen around the periphery of the rats' head on day 0 (Figure 4.1 b). Figure 4.2 shows the corresponding MR images of the rat brains on day 27, which was the experimental endpoint. The MR images displayed a large area of atypical hyperintense contrast surrounding the injection site, which was present in both brain hemispheres of all animal, representing tumours of varying sizes irrespective of whether the cells expressed the Fluc-ZsGreen reporter gene.

4.2.2 Assessing the feasibility of monitoring the viability and proliferation of FLuc-ZsGreen$^+$ hESC-derived DAPCs longitudinally using BLI

To assess the ability of BLI and MRI to monitor the viability and tumourigenicity of implanted hESC-derived DAPCs, Fluc-ZsGreen$^+$ RC17 hESCs were differentiated into DAPCs, and after confirming that the DAPCs still expressed the ZsGreen reporter (Chapter 3), they were implanted into right striatum. To ensure that the introduction of the reporter genes did not affect the behaviour of the DAPCs *in vivo*, unlabelled cells were injected into the left side of the brain to serve as a control cell population.

Six rats had Fluc-ZsGreen$^+$ DAPCs implanted into the right striatum, and unlabelled DAPCs implanted into the left striatum. The rats' heads were imaged at day 1, 14, 28, 56 and 91 for BLI (the last session of BLI was performed on the day of sacrificing the animals). MRI were performed on day 90 which was the day before sacrificing the animal (Figure 4.3 a). Although a BLI signal was detected in 4 of the

(a)

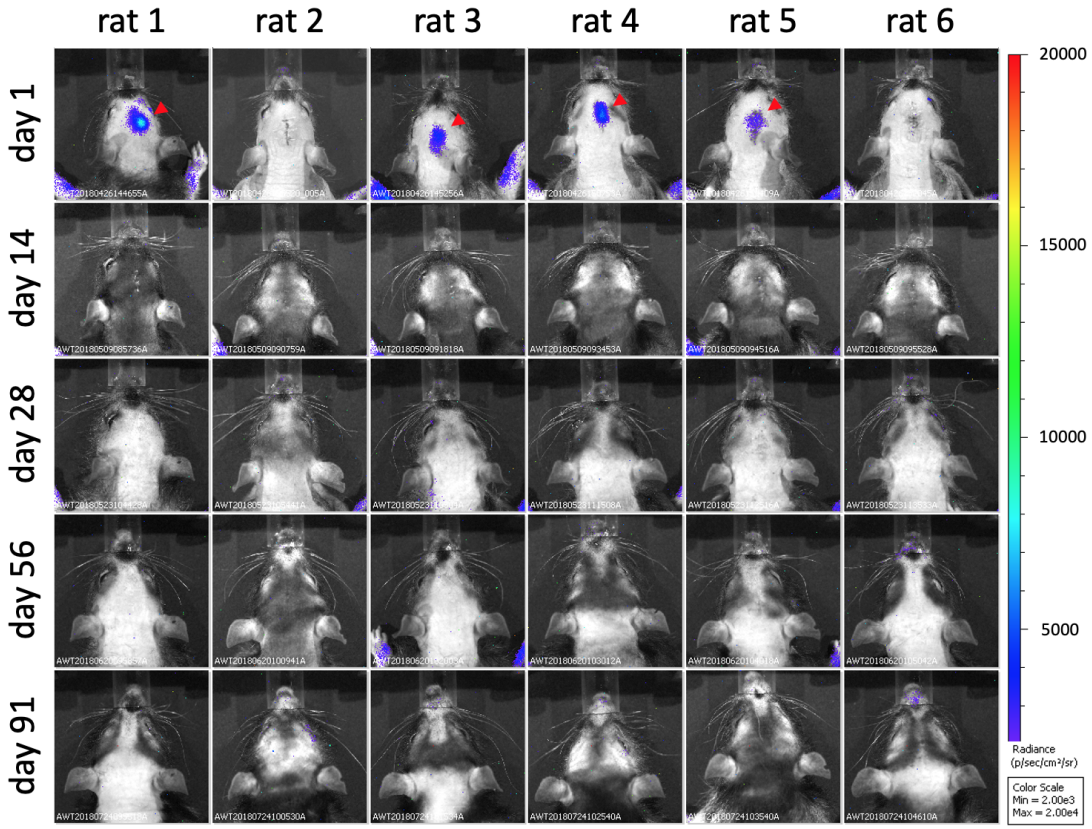

(b)

Figure 4.3: Long-term fate of injected Fluc-ZsGreen$^+$ DAPCs. (a) Schematic of injection and experimental timeline of DAPCs administration and imaging. (b) BLI of the six rats that received DAPCs as imaged on days 1, 14, 28, 56, and 91. Most, but not all rats displayed a signal on the injection day, but this was lost by day 14 and no signal was seen up at any other time points.

6 rats on day 1 (red arrowheads), no signal could be detected in any of the rats on the subsequent days. Note that this rat strain can display cycles of thin hair growth, as seen in some images. In contrast to hESCs (Figure 4.2), administration of DAPCs resulted in no abnormal MR contrast at the experimental endpoint (day 91, Figure 4.4), with all animals exhibiting a normal brain structure and the needle track being

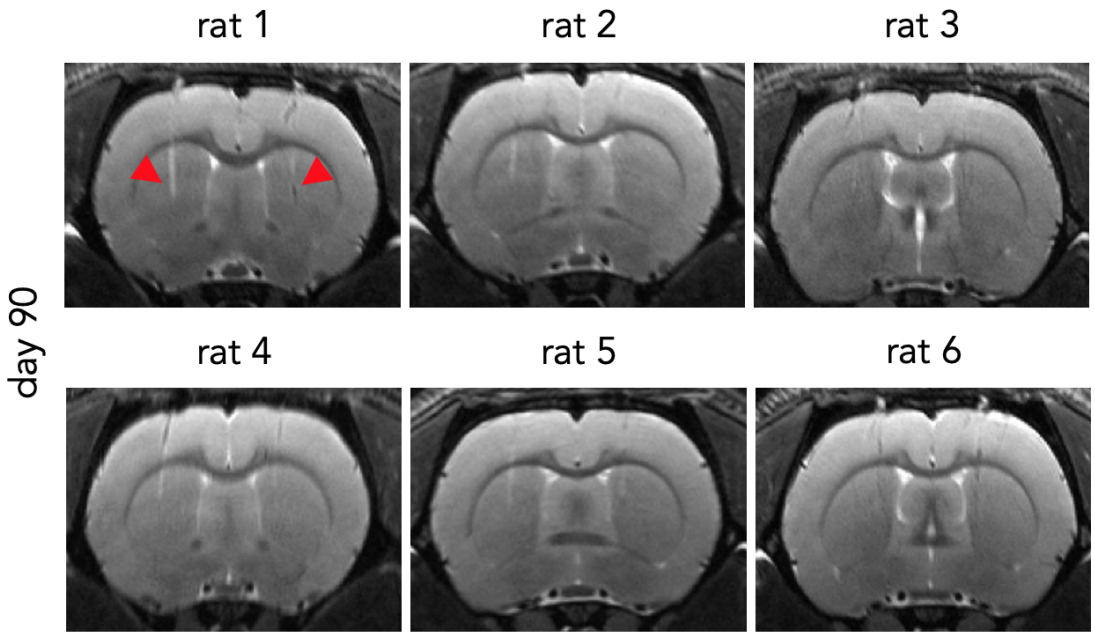

Figure 4.4: MR imaging of grafted Fluc-ZsGreen$^+$ DAPCs at the study endpoint. RARE MRI scans (day 90) of all 6 rats that received DAPCs (left hemisphere: non-transduced, right hemisphere: Fluc-ZsGreen$^+$). No abnormal features are seen, apart from the needle track that is still visible in some animals (indicated arrowheads in the first rat only).

the only remarkable feature (red arrowheads in Figure 4.4).

4.2.3 Assessing the feasibility of tracking the biodistribution of MPIO-labelled DAPCs longitudinally using MRI

To assess the biodistribution of hESC-derived DAPCs with MRI, DAPCs were labelled with fluorescence MPIOs and injected into the right hemisphere of the rat brain. To assess whether the introduction of the MPIOs affected the behaviour of the DAPCs *in vivo*, unlabelled cells were injected into the right side of the brain to serve as a control cell population.

Rats implanted with MPIO-labelled DAPCs were imaged only via MRI, as neither of the hemispheres received cells with the genetic reporter. Figure 4.5 shows Rapid Imaging with Refocused Echoes (RARE) MRI scans of 6 rats that received MPIOs labelled DAPCs (left hemisphere: unlabelled DAPCs; right hemisphere: labelled DAPCs) as imaged on day 1, 14, 28, 42, 70 and 126 post-surgery (Figure 4.5 a). Hypointense contrast (red arrowhead), indicative of a reduction in relaxation time as caused by MPIO labelling, is seen in the right hemisphere throughout the experimental period in all rats apart from rat 5 (Figure 4.5 b). There was no change in the hypointense contrast area during the course of MR imaging.

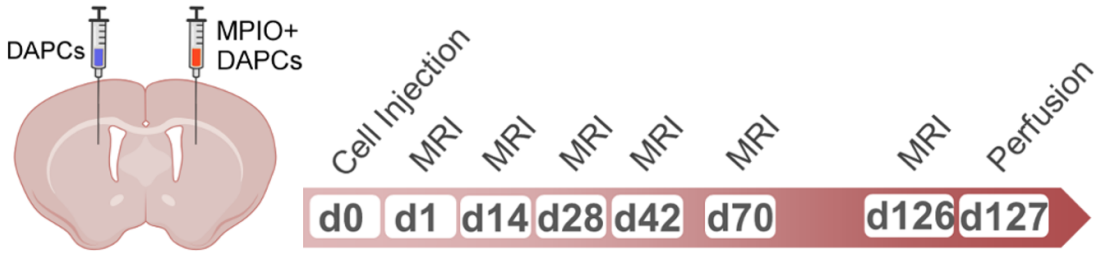

(a)

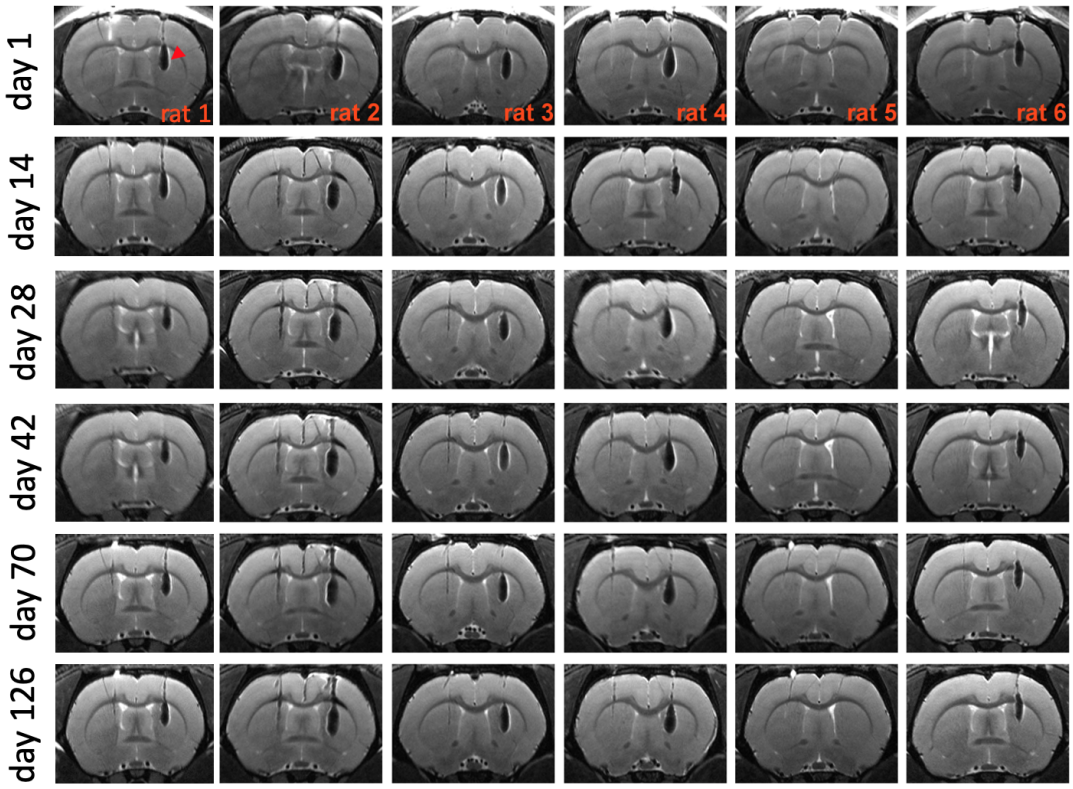

(b)

Figure 4.5: Biodistribution of MPIO-labelled hESC-derived DAPCs over time. (a) Schematic of injection and experimental timeline of DAPC administration and magnetic resonance imaging. (b) Representative RARE MRI scans of 6 rats that received MPIO-labelled DAPCs (left hemisphere: unlabelled DAPCs; right hemisphere: labelled DAPCs) as imaged on day 1, 14, 28, 42, 70 and 126 post administration. Hypointense contrast caused by MPIO labelling, is seen in the right hemisphere throughout the experimental period (indicated with an arrowhead in the first image). No abnormal growth is observed in either of the hemispheres.

By scanning through the brain of rat 5 from anterior-to-posterior, it was found that a hypointense signal was present in the lateral ventricles, rather than in the striatum (Figure 4.6). In the RARE image the needle track is clearly identified in the MR images, revealing an injection angle that led to cells being administered to the ventricle (red arrowheads). Imaging of a different plane reveals hypointense contrast in a different area within the ventricles (arrowheads in top right image), indicating that the cells

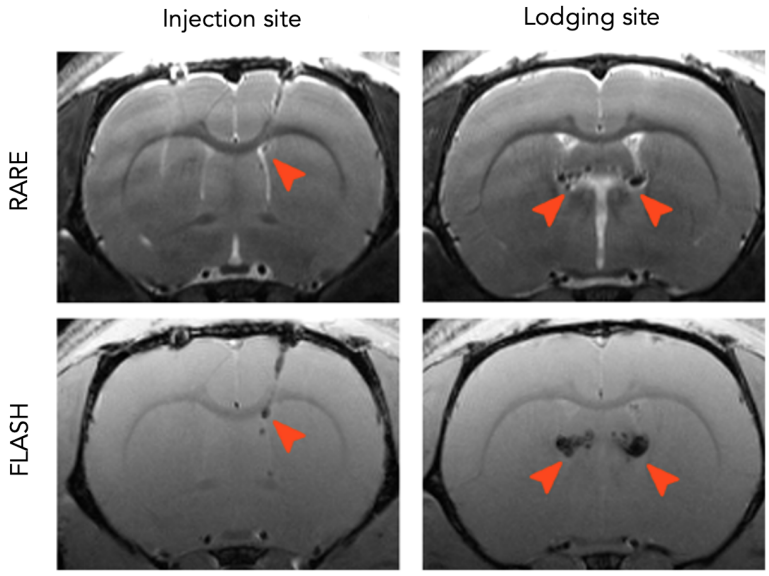

Figure 4.6: RARE and FLASH MRI scan of grafted MPIOs$^+$ DAPCs in rat5. Red arrowheads show needle track in the left images and hypointense contrast in the ventricles in the right images.

migrated and lodged in an unintended site. FLASH images are shown as they provide better contrast between the brain and MPIOs, facilitating the identification of the needle track. Note that hypointense contrast is seen in both hemispheres of the brain of the rat in which cells were mis-injected, which is likely due to the bridged nature of the fluid-filled ventricles.

4.3 Discussion

The main aim of this chapter was to assess the effectiveness of BLI and MR imaging to monitor the tumourigenicity, viability and intracranial biodistribution of hESC-derived DAPCs following stereotactic injection into the rat striatum.

In the animals of the control group that were injected with Fluc-ZsGreen RC17 hESCs, the intensity of BLI signals were different between the three rats of the control group immediately following injection. The reason for this difference might be a due to different levels of cell death after injection. Another reason could be due to the effects of the surgery. There is always a degree of blood clotting at the surgery site, and it would be expected that this would affect the BLI signal. For instance, if the blood clot in one animal is greater than another, it would be expected that this would lead to greater signal attenuation, leading to a reduction in the BLI signal.

MRI was able to detect tumour growth in both the right and left sides of the

brain, indicating that the growth of the tumours was not dependent on the presence of the reporter genes. MRI also showed that the largest mass was in the right striatum of rat 3, which was also the only animal that displayed a signal with BLI. These results therefore suggest that MRI is more sensitive than BLI for detecting hESC-derived tumours in the rat brain (Figure 4.1 & Figure 4.2). In most animals, BLI could only detect Fluc-ZsGreen$^+$ cells shortly after administration and was not effective for monitoring tumourigenicity and cell viability in the longer term.

The inability to detect cells with BLI likely resulted from a number of factors. First, at the initial imaging session, the rats were only 6 weeks old. During the intervening 2 weeks before the next imaging session, the rats grew considerably and became more pigmented (cycles of thin hair growth), causing the intensity of the emitted light to be reduced; this likely explains why after day 1, BLI could only be detected in a rat that had developed a large Fluc-ZsGreen$^+$ hESC-derived mass (Figure 4.1 b). An additional problem was that in comparison with undifferentiated hESCs, we found that the expression levels of the reporter genes decreased by about 50% in Fluc-ZsGreen$^+$ hESC-derived DAPCs and could not be detected at all in the mature DA neurons 3.10. It is well recognised that ESC differentiation is accompanied by increased levels of DNA methylation, leading to gene silencing and that the pattern of silencing is cell type specific (Suelves et al., 2016).

The next factor is the proportion of grafted cells. Bernau et al. found that Fluc$^+$ human foetal neuronal progenitors implanted into the rat striatum could be imaged with BLI for 3 months. However, in this study, 9×10^{5} Fluc$^+$ cells implanted into the left hemisphere compared with only 1.5×10^5 cells in our study (Bernau et al., 2014).

The choice of promoter also affects the extent of silencing the reporter gene. A previous study comparing the activity of five constitutive promoters, EF1α, human β actin (ACT β), Cytomegalovirus (CMV), Phosphoglycerate Kinase (PGK) and Ubiquitin C (UbC) in differentiating hESCs, reported that EF1α was the most stable, with expression levels in EBs being reduced to 50% of those in undifferentiated hESCs (Norman et al., 2010). Our observation that Fluc-ZsGreen expression was undetectable in the mature DA neurons, both *in vitro* and *in vivo*, was unexpected. Tennstaedt et al. have shown that a EF1α: Fluc-GFP$^+$ neural stem cell line derived from hESCs could be detected with BLI for 6 weeks following injection into the mouse brain without any

noticeable decrease in bioluminescence intensity (Tennstaedt et al., 2015). However, the neural stem cells used in the Tennstaedt study have a different phenotype to hESC derived DAPCs, and there is no evidence that they differentiate into the DA lineage (Tennstaedt et al., 2015). Likewise, there is no evidence that the $Fluc^{+}$ human foetal neuron progenitors used in the aforementioned Bernau et al. study differentiate into the DA lineage in the rat brain (Bernau et al., 2014). Indeed, as far as we are aware, there are no studies that show Fluc expression in hESC-derived DA neurons *in vivo* when Fluc is under the control of a constitutive promoter. However, one advantage of our system is that the loss of signal is due to differentiation. This could be used to show that the grafted cells have indeed followed the correct pathway post implantation rather than dedifferentiated back into an ESC-like phenotype.

MR imaging, on the other hand, could detect tumours arising from undifferentiated hESCs and could monitor the intracranial biodistribution of MPIO-labelled hESC-derived DAPCs over the full time-course of our experiments. Monitoring of animals injected for DAPCs labelled by MPIOs using MRI for up to 4 months post implantation confirmed that DAPCs do not appear to generate tumours, with all rats displaying normal brain structures at all time points. In 5 out of 6 rats, hypointense contrast was seen in the right brain hemisphere. This was an expected consequence of the MPIO labelling, which enabled us to monitor the delivery and intracranial distribution of DAPCs. The distribution of the administered DAPCs appeared to remain stable throughout the 4 months that the animals were monitored for, with no obvious change in the area with hypointense contrast, suggesting that the DAPCs were confined to the areas into which they were initially deposited.

The micron sized particles used in this study are much larger than nano-sized particles and contain more iron. Cells labelled with the micron sized particles therefore provide higher contrast in the MR scanner and it has previously been shown that the detection of single cells labelled with these particles can be possible (Shapiro et al., 2005). We therefore feel that it would have been possible for us to detect migrating cells labelled with the micron-sized beads. However, only about 70% of the injected cells were labelled with the particles. Therefore, we cannot rule out the possibility that unlabelled cells might have migrated to other sites within the brain. In rat 5, no hypointense contrast was observed in the target area. Further analysis of the scans

revealed that for this animal, the needle had been inserted at an angle, with the cells delivered to the ventricle leading to them becoming lodged at a different anatomical location (Figure 4.6). This could be an additional advantage of MRI to show and improve the site of injection for transplantation of cells into brain.

CHAPTER 5

Post-mortem analysis

5.1 Introduction

In order to track cells *in vivo*, they need to be labelled with a genetic reporter and/or nanoprobes. However, both types of labelling technique used in this study, including the Fluc-ZsGreen bicistronic genetic reporter and MPIOs, can alter the phenotype of the cells, affect their viability, differentiation potential in the longer term, or render the cells immunogenic (Crabbe et al., 2010; Kostura et al., 2004).

A study by Limberis et al showed that luciferase causes an immunogenic response in the mouse (Limberis et al., 2009). This study indicates that tumour cells expressing luciferase were killed by the host's immune system, but that unlabelled tumour cells were not. This transgene immune recognition could be dependent upon different factors, such as host background, vector dose, and site of injection. If immunogenicity to luciferase were to occur in an *in vivo* study, this could make the results unreliable (Limberis et al., 2009).

Green Fluorescent Protein (GFP) has also been shown to cause apoptosis (Liu et al., 1999). Some studies have shown that cells labelled with GFP do not survive and cannot accurately be tracked over time (Ansari et al., 2016; Gambotto et al., 2000). The immunogenicity response to GFP might be related to the cytotoxicity observed in some cell types, which can result from elevated levels of Reactive Oxygen Stress (ROS) observed in various experiments (Jiang et al., 2014; Choy, 2010). However, it is not clear if ZsGreen, which is a brighter, commercially available GFP, could cause a similar immune response and toxicity in the longer term *in vivo*.

In this study RNU athymic rats are being used that lack T cells. The possible

immune reactivity caused by luciferase and/ or ZsGreen would be expected to be mediated by T cells; therefore, it is expected that the reporter gene would be unlikely to cause an immune response in these particular studies. However, whether there could be any longer-term toxicity issues caused by the expression of ZsGreen, or whether the luciferase and/or ZsGreen reporter genes negatively impact on the differentiation potential of the implanted cells has not previously been explored.

It is documented that iron oxide particle labelling could affect the differentiation capacities of stem cells. A study by Kostura et al revealed that iron oxide labelling of mesenchymal stromal cells markedly diminished *in vitro* differentiation into chondrocytes (Kostura et al., 2004). Furthermore, introduction of iron oxide particles into the CNS induced microglial activation (Wang et al., 2011; Kostura et al., 2004). In fact, brain exposure to iron oxide particles has been associated with significant activation of microglia, corresponding to pathological changes such as inflammation, mitochondrial dysfunction, chromosomal damage, and generation of ROS (Sadeghiani et al., 2005; Veranth et al., 2007). The RNU rats have functional glial cells, so it is important to investigate whether the introduction of cells labelled with MPIOs could trigger an immune response in the brain. In addition to the possibility of a glial response induced by MPIOs, it is also likely that microglia overactivation will be induced by intracerebral transplantation of the cells themselves. So, it is important in this study to establish if the MPIO-labelled cells induce an immune response that is greater than that induced by unlabelled cells (Tomov, 2020).

The specific objectives of this chapter were to use post-mortem samples in order:

1. Assess whether the expression of the Fluc-ZsGreen reporters affect the fate of hESCs following implantation into the rat brain.

2. Assess the influence of Fluc-ZsGreen and MPIO labelling on the survival and differentiation capacity of DAPCs following implantation into the rat striatum.

3. Evaluate the immunogenicity of labelled hESC-derived DAPCs following implantation into the rat striatum.

5.2 Results

5.2.1 Investigating the effect of the Fluc-ZsGreen reporter on hESC fate following implantation into the rat brain

Experiments in Chapter 3 indicated that the introduction of the reporter gene did not inhibit the ability of hESCs to generate mature DA neurons, nor did it affect the ability of cells to generate derivatives of the three embryonic germ layers in EBs derived from the hESC reporter line. Furthermore, experiments in Chapter 4 suggested that the reporter genes did not affect the ability of the implanted hESCs to form tumours. However, a question remains as to whether the presence of the reporters has any noticeable effect on tumour histology. To address this, histological analyses were undertaken of tumours generated by injecting Fluc-ZsGreen$^+$ hESCs or unmodified hESCs into the rat striatum. As shown in Chapter 4 (Figure 4.1 a), Fluc-ZsGreen$^+$ hESCs were injected into the right hemisphere, and unmodified hESCs were injected in the left hemisphere.

At the study end point (day 28) H&E staining was performed on sections of brain tissue containing the hESC-derived tumour and analysed by a pathologist (Figure 5.1).

By eye, it was possible to identify the tumours as they were more intensely stained by H&E (Figure 5.1 a). At low power magnification, the area surrounding the injection site consisted of a large number of tightly packed cells as evidenced by strong nuclear (haematoxylin) staining in the same area suggesting an abnormal growth of cells (black arrowheads in Figure 5.1 a). The tumour cells could clearly be distinguished from the surrounding brain tissue and their position and size correlated well with the MR images (black arrowheads in Figure 5.1 b). Further analysis of H&E sections at higher power magnification shows that most of the tumour typically contains neuroepithelial-like cells in both left and right hemispheres (Figure 5.1 c&d). The normal rat brain tissue is indicated by blue arrows in Figure 5.1 (c&d). Furthermore, in some parts of both the left and right hemispheres, vessel-like structures are observed within the tumours (Figure 5.1 e&f).

Immunofluorescence microscopy revealed that the tumour in both hemispheres consisted of human cells, as evidenced by positive staining for hNuclei compared to the area that is outside the tumour region and has no positivity for hNuclei (Figure 5.2a). In order to determine whether undifferentiated hESCs were present in the tumours,

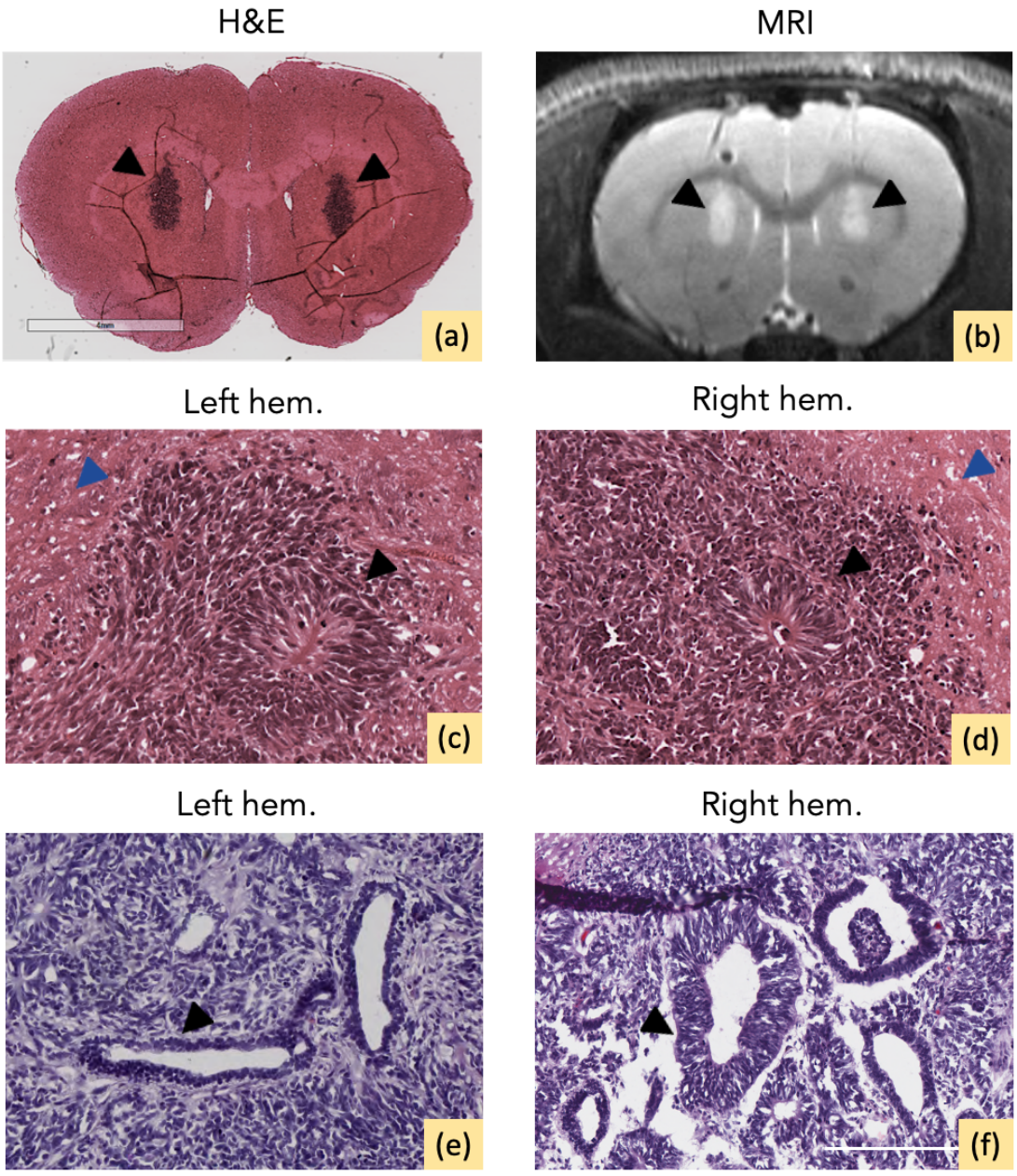

Figure 5.1: Histological analysis of tumours derived from undifferentiated hESCs. (a) H&E staining was performed on frozen sections prepared from the day 27 tumours in rat 1. Black arrowheads show tumour-like structure in the rat brains. (b) Representative image of MRI from rat 1 on day 27 which is corelates with the H&E staining showing the tumour structure in black arrowheads. (c) and (d) high power images of tumour containing neuroepithelial-like cells (arrowheads) in left and right hemispheres. Blue arrowheads indicate the normal rat brain tissue. (e) and (f) Vessel-like structures in the tumours have seen in the left and right hemispheres are indicated by black arrowheads (imaged from rat 2 of control group). Scale bars are 3mm in (a), 200 µm in (c), (d), (e), and (f).

co-staining was undertaken for hNuclei and *OCT4*. However, there is no positive expression of *OCT4* suggesting that the cells within the tumours are not undifferentiated hESCs (Figure 5.2 b). Further immunostaining was performed to investigate which lineages were present within the tumours. Immunostaining for *Brachyury*, *GATA6*

and *β-III-tubulin* were undertaken to detect derivatives of mesoderm, endoderm and ectoderm, respectively. Although *Brachyury* and *GATA6* had been detected in hESC-derived EBs (Figure 3.7), analysis of the tumours showed that these markers were not present (Figure 5.2 c). However, there was an abundance of *β-III-tubulin* staining confirming the presence of the ectodermal linage. Furthermore, some of the cells expressed ZsGreen, suggesting that the ZsGreen might be preferentially silenced in certain lineages but not others. In the vessel-like structures the co-localization of hNuclei and smooth muscle action *αSMA*, a marker that indicates blood vessel myofibers, indicates that they were all derived from the grafted hESCs (Figure 5.2d).

5.2.2 DAPCs express *TH in vivo*, irrespective of the introduction of the reporter gene and MPIOs

In chapter 3, it was shown that the DAPC derived hESCs are able to successfully differentiate into mature DA neurons, expressing *TH in vitro* (Figure 3.9). Therefore, it was anticipated that DAPCs would also mature *in vivo*. Apart from investigating the capacity of DAPCs to differentiate into mature DA neurons, here it was examined whether the labels used for tracking (Fluc-ZsGreen bicistronic vector for BLI and iron oxide particles for MR imaging) affected the differentiation potential of the cells following implantation into the rat striatum. In order to identify this, sections of the right hemisphere that had been injected with Fluc-ZsGreen$^+$ DAPCs, and sections of the left hemisphere that had been injected with nontransduced DAPCs, were immunostained for *TH*. hNuclei and /or hNCAM (two human specific markers that can not recognise the mouse proteins) were also used to confirm the identity of the grafted human cells. Figure 5.3 (a) demonstrates the positivity of hNuclei antigen at the injection site in both hemispheres suggesting the transplanted DAPCs are still alive and integrated with the rat brain and displayed neural lineage commitment, irrespective of whether they had been genetically modified, while there was no positivity for ZsGreen. Importantly, the areas containing human cells were also positive for *TH* (red arrowheads in Figure 5.3 a), suggesting maturation of some DAPCs in the rats' brains within the experimental period (91 days). The injection sites were also positive for a human-specific NCAM (hNCAM) antigen (Figure 5.3 b), providing further evidence that human cells had integrated with the rat brain and displayed neural lineage commitment, irrespective of whether they had been genetically modified.

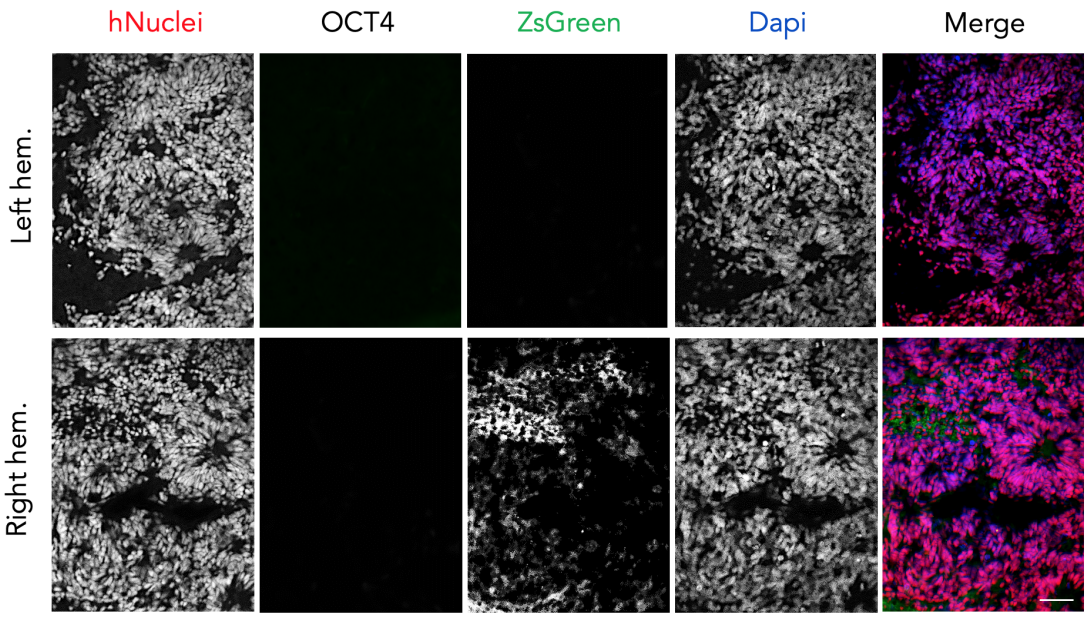
hNuclei
OCT4
ZsGreen
Dapi
Merge
Left hem.
Right hem.

(a)

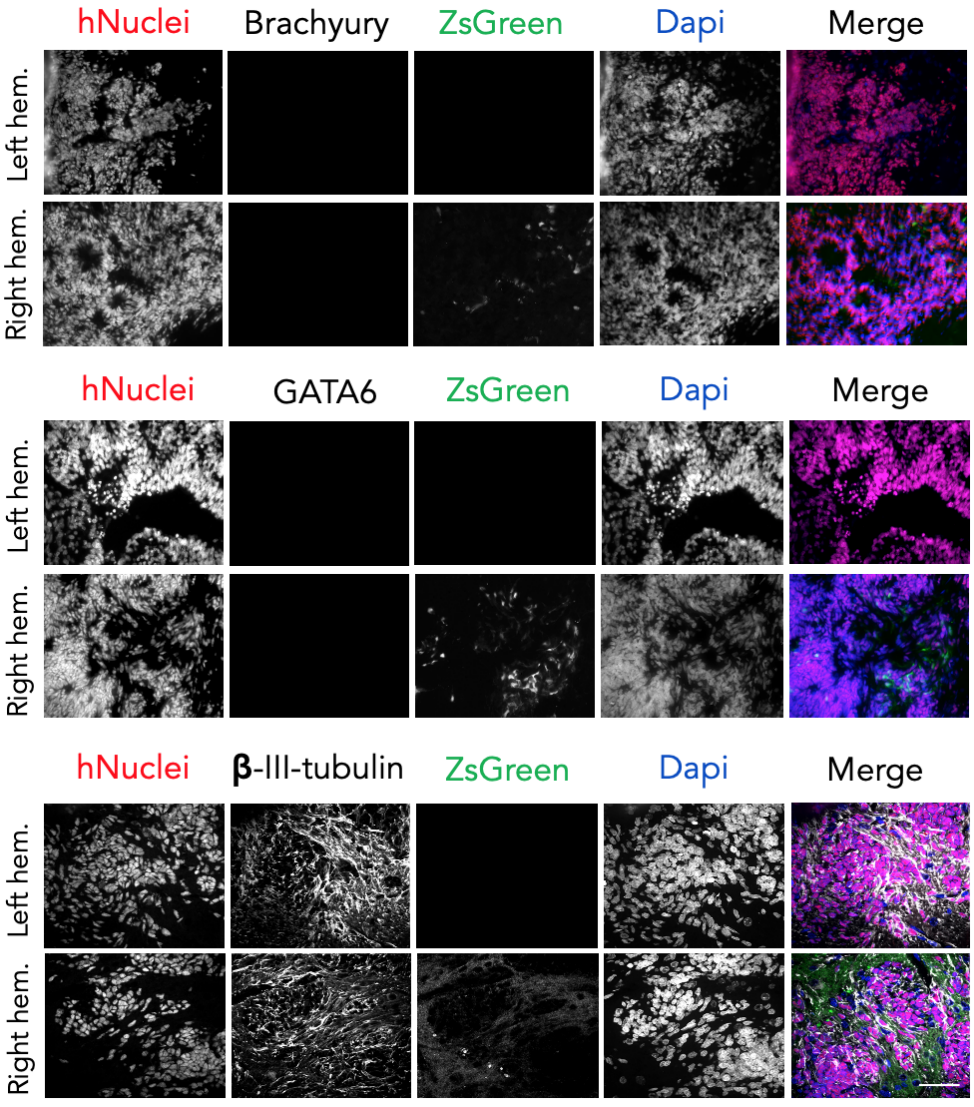
hNuclei
Brachyury
ZsGreen
Dapi
Merge
Left hem.
Right hem.
hNuclei
GATA6
ZsGreen
Dapi
Merge
Left hem.
Right hem.
hNuclei
β-III-tubulin
ZsGreen
Dapi
Merge
Left hem.
Right hem.

(b)

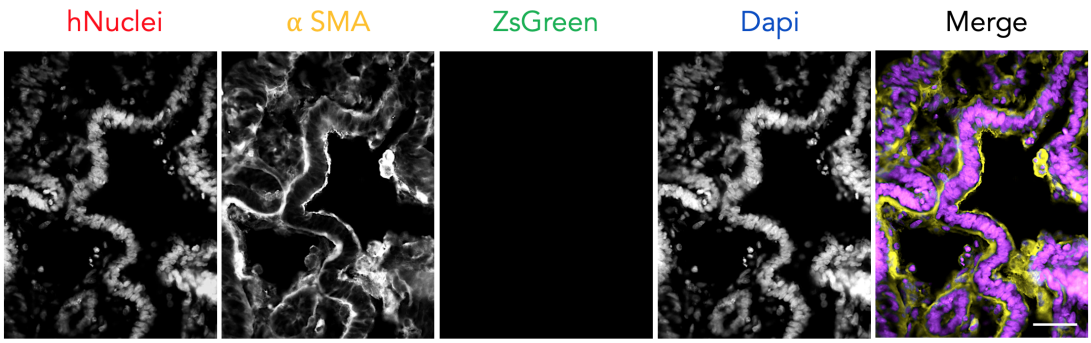

(c)

Figure 5.2: Immunofluorescence analysis of tumours derived from undifferentiated hESCs. (a) Representative micrographs of tumours stained for human nuclei and *OCT4* counterstained with Dapi. Tumour cells are positive for hNuclei but negative for *OCT4*, confirming that all injected hESCs had differentiated in the rat brain. A subpopulation of cells expressing ZsGreen can be observed in the tumours formed from Fluc-ZsGreen$^+$ hESCs injected to the right hemispheres. (b) Images of left and right hemispheres immunostained for *GATA6*, *Brachyury*, and *β-III-tubulin* revels only expression of *β-III-tubulin* in hNuclei positive cells showing that grafted hESCs only differentiated into ectodermal linage. A subpopulation of cells expressing ZsGreen can be observed in the tumours formed from Fluc-ZsGreen$^+$ hESCs. (c) Representative of immunestained section for *αSMA* and hNuclei indicating the presence of vessel-like structures in the tumour derived from grafted cells. Scale bars correspond to 100 µm.

In the rat brain sections that were transplanted with MPIOs$^+$ DAPCs into the right hemisphere, and unlabelled DAPCs into the left hemisphere, the immunofluorescence staining at the injection sites confirmed the presence of human cells that expressed *TH*, reinforcing the point that these cells were able to integrate within the rat brain and differentiated into mature DA neurons, irrespective of the MPIO labelling (Figure 5.4 a). In the right hemisphere, MPIOs were found in the same areas as the administered human cells and appeared to localise to perinuclear regions. It is also of note that in some sections MPIOs were observed in extracellular clusters as shown in Figure 5.4 (b).

5.2.3 Intense staining for *GFAP* is observed surrounding the human cell implants

As previously mentioned, a previous study showed that the implantation of Fluc$^+$ hESC-derived neural stem cells into the mouse striatum caused marked glial reaction in the host brain, as evidenced by intense immunostaining for glial fibrillary acidic protein *(GFAP)*, a marker of reactive astrocytes. To investigate whether Fluc-ZsGreen or MPIOs contributed to this reaction, immunofluorescence staining was performed on sections of rat brains that received MPIO-labelled or Fluc-ZsGreen$^+$ DAPCs (left hemisphere: unlabelled; right hemisphere: labelled).

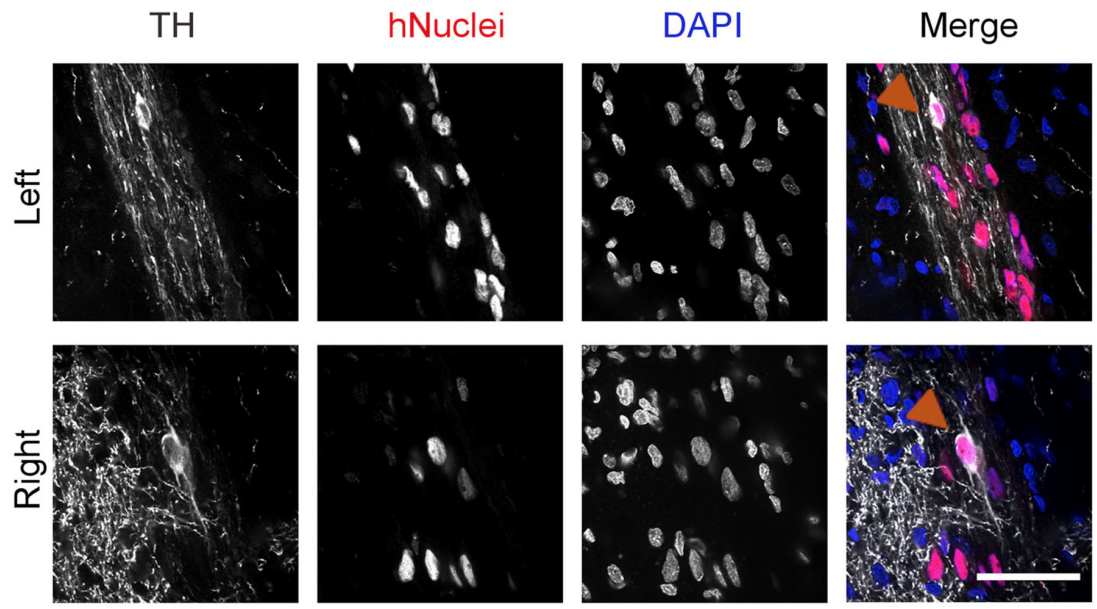

(a)

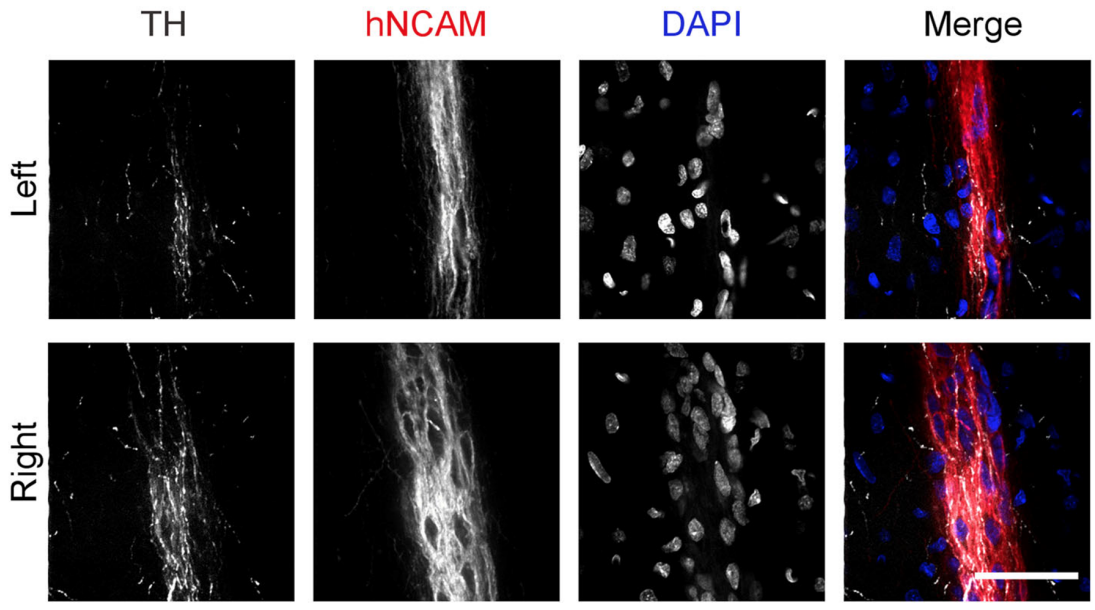

(b)

Figure 5.3: DAPCs integration with the rat brain and *TH* expression. (a) Immunofluorescence microscopy of the injection sites (left hemisphere: nontransduced, right hemisphere: Fluc-ZsGreen^{+}). Cells express a human nuclear antigen, showing that the DAPCs survived in the rats' brains and expressed *TH*, suggesting that they matured into DA neurons. Arrowhead indicates a human cell strongly expressing *TH*. (b) Immunofluorescence of a similar area but using an antibody against human NCAM as a means to confirm the human origin of the cells. In the merged images the *TH* is white, hNuclei/ hNCAM are red, and Dapi is blue. Scale bars correspond to 50 µm.

As Figure 5.5 shows the presence of human cells is identified with hNCAM staining. The intensity of *GFAP* staining is stronger in the regions that show positivity for hNCAM confirming the accumulation of astrocytes surrounding the injection site in the

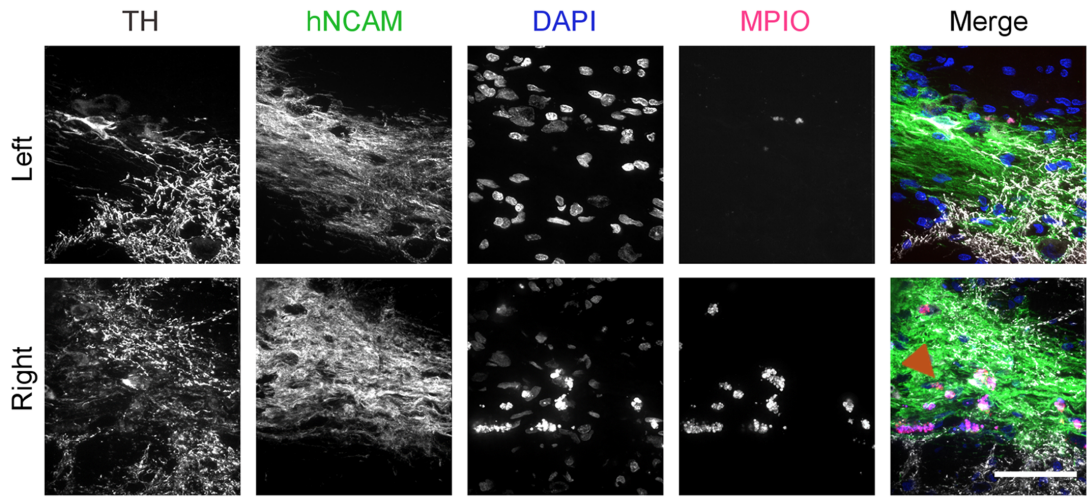

(a)

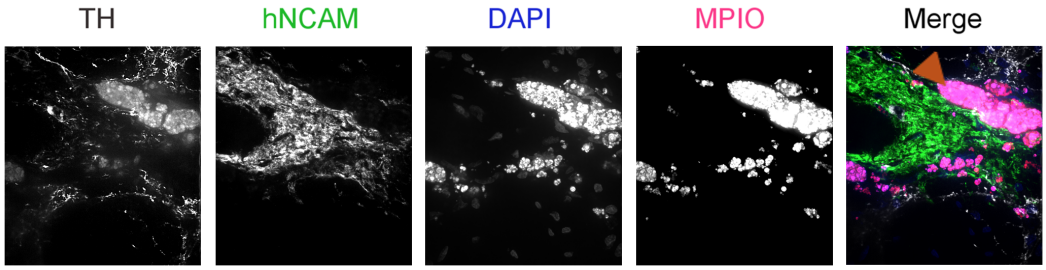

(b)

Figure 5.4: DAPCs integration with the rat brain. (a) Immunofluorescence microscopy of the injection sites (left hemisphere: nonlabelled cells, right hemisphere: MPIOs$^+$ cells). Cells express human NCAM, showing that MPIO labelled DAPCs survived in the rats' brains and *TH*, suggesting that DAPCs matured into DA neurons. MPIO-specific fluorescence is only seen in the right hemisphere and tends to be localised near to the cell nuclei. (b) Representative photomicrographs displaying the clustering and aggregation of MPIOs at the periphery of the graft (red). In the merged images the *TH* is white, hNCAM is green, MPIOs are red and Dapi is blue. Note that the MPIO fluorophore, Suncoast Yellow, is also excited at 405 nm and bleeds into the Dapi channel. Scale bars correspond to 50 µm.

right and left hemispheres (Figure 5.5 a). Further Immunofluorescence microscopy of brains from rats that received Fluc-ZsGreen$^+$ DAPCs (left hemisphere: untransduced control cells, right hemisphere: Fluc-ZsGreen$^+$ cells) also shows the expression of hNCAM and increased *GFAP* staining around the grafted cells both in the right and left hemispheres (Figure 5.5 b).

Furthermore, qualitative analysis showed an increase in *GFAP* staining around the human implants, but no differences in staining intensity were observed around the implants comprising unlabelled human cells or MPIO-labelled cells (Figure 5.5 a) and cells derived from Fluc- ZsGreen$^+$ hESCs (Figure 5.5 b).

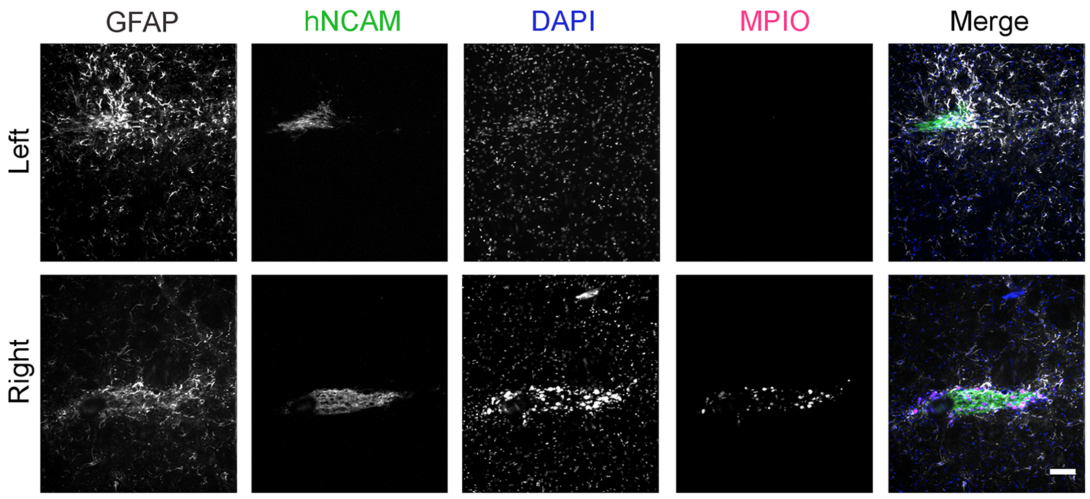

(a)

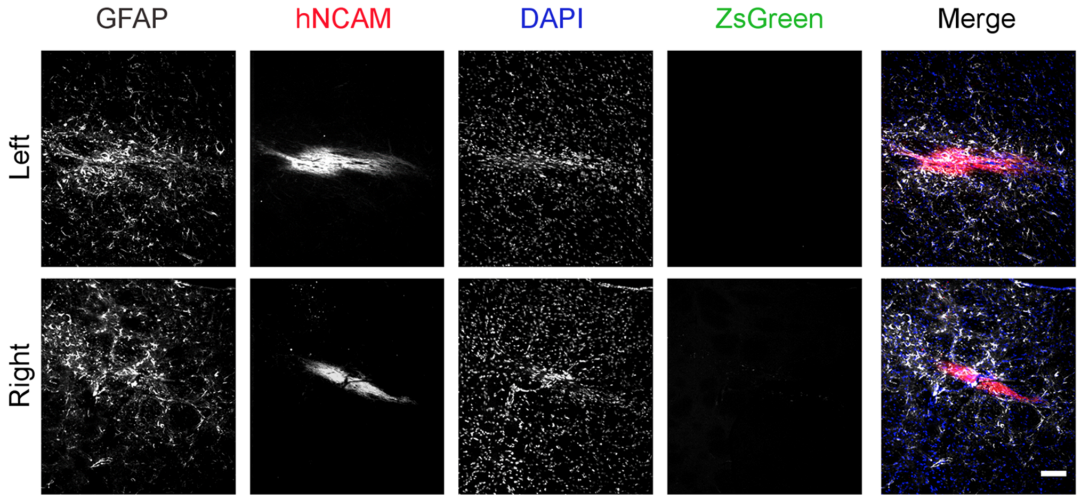

(b)

Figure 5.5: Glial reaction at the injection sites. (a) Immunofluorescence microscopy of brains from rats that received MPIO-labelled DAPCs (left hemisphere: unlabelled; right hemisphere: labelled). The presence of human cells is identified with hNCAM staining, and the intensity of *GFAP* staining is stronger in these areas. MPIOs are only seen in the right hemisphere. (b) Immunofluorescence microscopy of brains from rats that received Fluc-ZsGreen$^+$ DAPCs (left hemisphere: untransduced control cells; right hemisphere Fluc-ZsGreen$^+$ cells). Scale bars correspond to 100 µm.

5.3 Discussion

In order to assess the safety and efficacy of stem cell therapies in preclinical models, it is important to be able to track the fate of the cells *in vivo*. However, before doing this, it is crucial to assess the suitability of the imaging probes themselves in an *in vivo* context. Therefore, the first aim of this chapter was to assess the effects of Fluc-ZsGreen labelling on the fate of hESCs following transplantation into the rat striatum; the second aim of this chapter was to investigate the effect of the Fluc-ZsGreen reporter

gene and MPIOs on hESC-derived DAPCs in terms of viability and their potential to differentiate into mature DA neurons after introduction into the rat striatum; the third aim was to explore whether the labelled cells triggered a more severe immune response than unlabelled cells.

In line with the first aim, H&E histopathological examination of all 3 rats within the control group showed that the grafted cells spontaneous formed tumours, irrespective of whether they expressed the reporter genes or not. Morphologically, the tumour has abundant neuroepithelial cells as evidenced by the high proportion of cells expressing the neuronal marker, *β-III-tubulin*. However, in the EBs that formed from spontaneous differentiation of hESCs the expression of all three germ layers was evident (Figure 3.7). The reason for the dissimilar differentiation capacity of hESCs *in vitro* compared to within the rat brain *in vivo* might be due to the effects of the microenvironment. Recent research findings documented that implanted stem cells are highly affected by the three-dimensional structure of their surrounding microenvironment, the specific extra cellular matrix components, in addition to relevant cytokine signalling, all of which affect their growth and differentiation (Wan et al., 2015). The other typical morphological structures within the hESC-derived tumour was myo-epithelium that stained positively for *αSMA*. However, it is more likely that these myoepithelial cells are of neural crest origin, which is also considered to be part of the ectodermal lineage.

Overall, there was no sign of any difference between the tumours in the left and right hemispheres in terms of morphological structure and marker expression, suggesting the fate of the injected hESCs was not influenced by the presence of Fluc-ZsGreen.

The second aim of this chapter was to assess the viability and maturation of grafted DAPCs. In order to do this, expression of *TH*, a marker gene that is expressed in mature DA neurons (as shown previously in Chapter 3 *in vitro*) was analysed in the brain sections containing the injection site. TH^+ cells were identified within $hNCAM^+/hNuclei^+$ cell populations of labelled and unlabelled human cell cohorts within the rat striatum. Here, there was no evidence that the bicistronic Fluc-ZsGreen reporter or the MPIOs inhibited the differentiation of hESC-derived DAPCs into TH^+ DA neurons. However, in both Fluc-ZsGreen and MPIOs labelled cells, not all human cells robustly expressed *TH*, likely because a period of >20 weeks is necessary for the maturation of all DAPCs.

In order to explore the glial activity of transplanted cells, the expression of *GFAP*

was assessed in the transplanted cells. The transplantation of both labelled and unlabelled DAPCs elicited a marked glial reaction at the injection site, as expected. However, there was no notable difference in the scale of glial response, suggesting that neither Fluc-ZsGreen nor MPIOs increased the glial reaction to the DAPCs. One point that was noted in some of the immunostained brain sections that were injected by $MPIO^{+}$ DAPCs, was the extracellular localisation and aggregation of MPIOs. This might be due to a level of reported cytotoxicity of iron oxide particles that cause cell death and subsequent release of the MPIOs into the extracellular space (Roeder et al., 2014).

CHAPTER 6

Final discussions and future perspectives

The main aim of this thesis was to assess the effectiveness of BLI and MR imaging for monitoring the tumourigenicity, viability and intracranial biodistribution of hESC-derived DAPCs following stereotactic injection into the rat striatum. Furthermore, the study investigated whether the introduction of imaging probes, including a bicistronic luciferase-ZsGreen reporter, and MPIOs, affect the differentiation capacity of transplanted cells and graft immunogenicity. To be considered appropriate for use in the preclinical evaluation of grafted stem cell-derived tissues, it is essential that the integration of imaging probes has no effect on the differentiation capacity of cells. Transgenic induction of luciferase is a well-established method for monitoring stem cell-derived tissues *in vivo* (Bernau et al., 2014; Peng et al., 2018; Huang et al., 2012); therefore, it was not expected that the incorporation of this reporter gene would negatively influence differentiation patterns. In concordance, this study showed that the Fluc-ZsGreen bicistronic reporter gene successfully labelled hESCs without affecting their differentiation capacity *in vitro*.

The labelled cells could differentiate into DAPCs and could also further differentiate into mature DA neurons. Furthermore, there was no noticeable difference in the differentiation ability and immunogenicity between transduced and non-transduced DAPCs *in vivo*. However, during the *in vivo* study, in most rats, BLI could only detect DAPCs during the first few days after cell transplantation. As discussed in Chapter 4 this was likely due to signal attenuation due to the increasing size of the rats' head, and to the silencing of the reporter gene that occurred as the DAPCs differentiated.

In vivo silencing is one of the main bottlenecks of luciferase mediated BLI assays, as the preclinical studies require long-term activity of the transgene. In the discussion of Chapter 4 the possible reasons of silencing Luciferase-ZsGreen reporter gene used in this study were discussed in detail, but in brief, the most likely explanation for the silencing is that the extent of methylation increases as the cells become more differentiated. In future studies, in order to overcome the limitation of very low BLI signal detection, a cell type-specific promoter, such as *FOXA2*, which is expressed in both DAPCs and mature DA neurons (Domanskyi et al., 2014), could prove more effective than the EF1 promoter for monitoring viability longitudinally, especially if used with the highly sensitive AkaLuc luciferase in combination with the substrate Akalumine (Iwano et al., 2018). The discovery of AkaLuc, a red-shifted alternative to Firefly luciferase and its luciferin counterpart, AkaLumine-HCL is a significant improvement for live cell tracking in the brain using BLI. AkaLuc light emission at 677 nm increases tissue penetration, enhancing sensitivity to near single cell detection and increased absorption of AkaLumine-HCL across the BBB makes it highly attractive for neuroimaging (Iwano et al., 2018).

Considering the point of DNA methylation and its effect on silencing the reporter gene through the process of cell differentiation, quantifying the methylation would give a good prediction of the gene silencing over the period of the *in vivo* study. Another potential improvement on the current study in terms of BL imaging could be switching to mice instead of rats, thereby reducing signal attenuation. Apart from the aforementioned problems with the BLI technique, another issue with this modality is that the spatial resolution is poor and does not allow the position of cells within the brain to be accurately mapped.

In the present study, four weeks after implantation of undifferentiated hESCs, MR imaging could detect a cell mass in both cerebral hemispheres, irrespective of whether the cells had been transduced with the Fluc-ZsGreen reporter. However, no cell masses were detected at any time point following administration of hESC-derived DAPCs, suggesting that in contrast to the undifferentiated hESCs, the DAPCs are non-tumourigenic. Cells labelled with MPIOs could be detected at all time points using longitudinal MR imaging. In addition, we found that the cells remained at the injection site and did not appear to migrate to other brain regions. From a safety perspective,

the lack of migration is important to prevent cells integrating into intact neural circuits, causing side effects (e.g., epilepsy) (Wijeyekoon and Barker, 2009). Upon investigation of mature DA neurons that express *TH*, we reported expression of rodent astrocytes at the injection site using the *GFAP* marker. However, no obvious difference in *GFAP* expression was observed between the rats injected with labelled and non-labelled cells, suggesting that the label did not increase the degree of immunogenicity of the cells.

In this study, it is imperative that a high proportion of the grafted cells differentiate into mature DA neurons to allow restoration of motor dysfunction in PD. Therefore, in order to show the graft functionality, investigation of other cell populations, mainly serotonergic neurons in the graft area would be desirable. It is also important to understand the extent to which DAPCs mature and form synapses with host neurons following implantation, as this will give some insight into their therapeutic mechanisms. Few studies have determined the proportion of injected DNPs that generate mature *TH*-expressing DA neurons. However, Kriks et al have shown that this is only 10% and 30% in rats and mice, respectively (Kriks et al., 2011). Furthermore, most studies tend to focus on recovery of motor function and tend not to assess whether the TH^+ neurons form synapses with host neurons. An early study from 1988 showed that human foetal DA neurons could synapse with host rat neurons, but ultrastructural analysis of hESC-derived DNPs is lacking (Clarke et al., 1988). This information is important because limited integration of hESC-derived DNPs might suggest that any observed recovery of motor function in PD animal models might be due, at least in part, to other mechanisms, such as the secretion of paracrine factors. In support of this, mouse ESCs treated with mitomycin C, which are unlikely to generate DNPs *in vivo*, were nevertheless able to significantly improve motor function in a mouse PD model (Acquarone et al., 2015). It is also worth noting that in the most commonly used PD model, where DA neurons are depleted by administering the chemical 6-OHDA, re-innervation can occur with time as long as the injury is not too extreme (Stanic et al., 2003). Thus, it is plausible that paracrine factors derived from administered DNPs might promote the re-growth of host neurons.

Taken together, the preclinical studies indicate that treating PD patient with hESCs-derived DAPCs is likely to be a safe and effective therapy, though this technology requires more maturity in the concept of finding the "universal hPSC line". A

problem, however, is that the pluripotent stem cell lines can vary considerably in their ability to generate the required progenitor cells, and different batches of the progenitor cells may work better than others. Therefore, to give this exciting therapy the best chance of working, we need to be able to screen a range of cell lines before they are used in patients. This will ensure that only the highest-performing cells are implanted. A combined BLI/MRI strategy in preclinical models could be effective for monitoring the viability, biodistribution and tumourigenicity of the different cell lines in animal models longitudinally. Such a strategy could allow for aspects of the therapy to be optimized in the animal model prior to clinical application. For instance, the functional potency of several hPSC lines in generating mature TH^{+} neurons following implantation could be explored. Additionally, preclinical studies could help to explore the potential tumorigenicity of each cell line; the optimal target cell dose to be grafted in the patients; patient-tolerability and efficiency in reversing the symptoms of the disease. Furthermore, such preclinical studies would be useful to explore whether the recovery observed in animal models following cell administration is entirely due to the cells generating dopaminergic neurons, or whether the cells might also stimulate regeneration of host neurons. Also, the idea that the inclusion of specific growth factors, or cocktails of growth factors to enhance survival of post-implantation differentiation could be assessed in such a model. Enhancing our knowledge by using an animal model in this way could help to design the clinical trials more efficiently and mean that the Parkinson's disease patients recruited to the forthcoming clinical trials would have the best chance of experiencing a beneficial outcome.

Bibliography

Aarsland, D., Andersen, K., Larsen, J. P., and Lolk, A. (2003). Prevalence and Characteristics of Dementia in Parkinson Disease: An 8-Year Prospective Study. *Archives of Neurology*, 60(3):387–392.

Abbas, M. M., Xu, Z., and Tan, L. C. S. (2018). Epidemiology of Parkinson's Disease—East Versus West. *Movement Disorders Clinical Practice*, 5(1):14–28.

Acquarone, M., de Melo, T. M., Meireles, F., Brito-Moreira, J., Oliveira, G., Ferreira, S. T., Castro, N. G., Tovar-Moll, F., Houzel, J.-C., and Rehen, S. K. (2015). Mitomycin-treated undifferentiated embryonic stem cells as a safe and effective therapeutic strategy in a mouse model of Parkinson's disease. *Frontiers in cellular neuroscience*, 9(97).

Allegrucci, C. and Young, L. E. (2007). Differences between human embryonic stem cell lines. *Human Reproduction Update*, 13(2):103–120.

Allison, T. F., Andrews, P. W., Avior, Y., Barbaric, I., Benvenisty, N., Bock, C., Brehm, J., Brüstle, O., Damjanov, I., Elefanty, A., Felkner, D., Gokhale, P. J., Halbritter, F., Healy, L. E., Hu, T. X., Knowles, B. B., Loring, J. F., Ludwig, T. E., Mayberry, R., Micallef, S., Mohamed, J. S., Müller, F.-J., Mummery, C. L., Nakatsuji, N., Ng, E. S., Oh, S. K. W., O'Shea, O., Pera, M. F., Reubinoff, B., Robson, P., Rossant, J., Schuldt, B. M., Solter, D., Sourris, K., Stacey, G., Stanley, E. G., Suemori, H., Takahashi, K., Yamanaka, S., and The International Stem Cell, I. (2018). Assessment of established techniques to determine developmental and malignant potential of human pluripotent stem cells. *Nature Communications*, 9(1):1925.

Amit, M., Carpenter, M. K., Inokuma, M. S., Chiu, C.-P., Harris, C. P., Waknitz, M. A., Itskovitz-Eldor, J., and Thomson, J. A. (2000). Clonally Derived Human Embryonic Stem Cell Lines Maintain Pluripotency and Proliferative Potential for Prolonged Periods of Culture. *Developmental Biology*, 227(2):271–278.

Ansari, A. M., Ahmed, A. K., Matsangos, A. E., Lay, F., Born, L. J., Marti, G., Harmon, J. W., and Sun, Z. (2016). Cellular GFP Toxicity and Immunogenicity: Potential Confounders in in Vivo Cell Tracking Experiments. *Stem cell reviews and reports*, 12(5):553–559.

Ariga, H., Takahashi-Niki, K., Kato, I., Maita, H., Niki, T., and Iguchi-Ariga, S. M. M. (2013). Neuroprotective Function of DJ-1 in Parkinson's Disease. *Oxidative Medicine and Cellular Longevity*, 2013:683920.

Arlicot, N., Vercouillie, J., Ribeiro, M.-J., Tauber, C., Venel, Y., Baulieu, J.-L., Maia, S., Corcia, P., Stabin, M. G., Reynolds, A., Kassiou, M., and Guilloteau, D. (2012). Initial evaluation in healthy humans of [18F]DPA-714, a potential PET biomarker for neuroinflammation. *Nuclear Medicine and Biology*, 39(4):570–578.

Aron Badin, R., Bugi, A., Williams, S., Vadori, M., Michael, M., Jan, C., Nassi, A., Lecourtois, S., Blancher, A., Cozzi, E., Hantraye, P., and Perrier, A. L. (2019). MHC matching fails to prevent long-term rejection of iPSC-derived neurons in non-human primates. *Nature Communications*, 10(1):4357.

Backlund, E. O., Granberg, P. O., Hamberger, B., Knutsson, E., Mårtensson, A., Sedvall, G., Seiger, A., and Olson, L. (1985). Transplantation of adrenal medullary tissue to striatum in parkinsonism. First clinical trials. *J Neurosurg*, 62(2):169–173.

Barker, R. A., Barrett, J., Mason, S. L., and Björklund, A. (2013). Fetal dopaminergic transplantation trials and the future of neural grafting in Parkinson's disease. *Lancet Neurol*, 12(1):84–91.

Barker, R. A., Drouin-Ouellet, J., and Parmar, M. (2015). Cell-based therapies for Parkinson disease—past insights and future potential. *Nat Rev Neurol*, 11(9):492–503.

Barker, R. A., Farrell, K., Guzman, N. V., He, X., Lazic, S. E., Moore, S., Morris, R., Tyers, P., Wijeyekoon, R., Daft, D., Hewitt, S., Dayal, V., Foltynie, T., Kefalopoulou, Z., Mahlknecht, P., Lao-Kaim, N. P., Piccini, P., Bjartmarz, H., Björklund, A., Lindvall, O., Nelander-Wahlestedt, J., Parmar, M., Paul, G., Widner, H., Church, A., Dunnett, S., Peall, K., Rosser, A., Gurruchaga, J. M., Palfi, S., Piroth, T., Winkler, C., and Consortium, T. (2019). Designing stem-cell-based dopamine cell replacement trials for Parkinson's disease. *Nature Medicine*, 25(7):1045–1053.

Barker, R. A., Parmar, M., Kirkeby, A., Björklund, A., Thompson, L., and Brundin, P. (2016). Are Stem Cell-Based Therapies for Parkinson's Disease Ready for the Clinic in 2016? *Journal of Parkinson's disease*, 6(1):57–63.

Barker, R. A., Parmar, M., Studer, L., and Takahashi, J. (2017). Human Trials of Stem Cell-Derived Dopamine Neurons for Parkinson's Disease: Dawn of a New Era. *Cell Stem Cell*, 21(5):569–573.

Bernau, K., Lewis, C. M., Petelinsek, A. M., Benink, H. A., Zimprich, C. A., Meyerand, M. E., Suzuki, M., and Svendsen, C. N. (2014). In vivo tracking of human neural progenitor cells in the rat brain using bioluminescence imaging. *Journal of Neuroscience Methods*, 228:67–78.

Bethesda, M. D. (2001). Rebuilding the Nervous System with Stem Cells. chapter 8.

Björklund, A. and Lindvall, O. (2017). Replacing Dopamine Neurons in Parkinson's Disease: How did it happen? *Journal of Parkinson's disease*, 7(s1):S21–S31.

Boronat-García, A., Guerra-Crespo, M., and Drucker-Colín, R. (2017). Historical perspective of cell transplantation in Parkinson's disease. *World journal of transplantation*, 7(3):179–192.

Breger, L. S. and Fuzzati Armentero, M. T. (2019). Genetically engineered animal models of Parkinson's disease: From worm to rodent. *Eur J Neurosci*, 49(4):533–560.

Brooks, D. J. (2000). Dopamine agonists: their role in the treatment of Parkinson's disease. *J Neurol Neurosurg Psychiatry*, 68(6):685–689.

Brundin, P., Pogarell, O., Hagell, P., Piccini, P., Widner, H., Schrag, A., Kupsch, A., Crabb, L., Odin, P., Gustavii, B., Björklund, A., Brooks, D. J., David Marsden, C., Oertel, W. H., Quinn, N. P., Rehncrona, S., and Lindvall, O. (2000). Bilateral caudate and putamen grafts of embryonic mesencephalic tissue treated with lazaroids in Parkinson's disease. *Brain*, 123(7):1380–1390.

Cannon, J. R. and Greenamyre, J. T. (2010). Neurotoxic in vivo models of Parkinson's disease recent advances. *Prog Brain Res*, 184:17–33.

Cao, F., Lin, S., Xie, X., Ray, P., Patel, M., Zhang, X., Drukker, M., Dylla, S. J., Connolly, A. J., Chen, X., Weissman, I. L., Gambhir, S. S., and Wu, J. C. (2006). In vivo visualization of embryonic stem cell survival, proliferation, and migration after cardiac delivery. *Circulation*, 113(7):1005–1014.

Caplan, A. I. and Correa, D. (2011). The MSC: an injury drugstore. *Cell Stem Cell*, 9(1):11–15.

Caravan, P., Ellison, J. J., McMurry, T. J., and Lauffer, R. B. (1999). Gadolinium(III) Chelates as MRI Contrast Agents: Structure, Dynamics, and Applications. *Chemical reviews*, 99(9):2293–2352.

Carlsson, A., Lindqvist, M., and Magnusson, T. (1957). 3,4-Dihydroxyphenylalanine and 5-hydroxytryptophan as reserpine antagonists. *Nature*, 180(4596):1200.

Cereda, E., Cilia, R., Canesi, M., Tesei, S., Mariani, C. B., Zecchinelli, A. L., and Pezzoli, G. (2017). Efficacy of rasagiline and selegiline in Parkinson's disease: a head-to-head 3-year retrospective case-control study. *Journal of neurology*, 264(6):1254–1263.

Chambers, S. M., Fasano, C. A., Papapetrou, E. P., Tomishima, M., Sadelain, M., and Studer, L. (2009). Highly efficient neural conversion of human ES and iPS cells by dual inhibition of SMAD signaling. *Nature Biotechnology*, 27(3):275–280.

Chen, J. and Chopp, M. (2006). Neurorestorative treatment of stroke: cell and pharmacological approaches. *NeuroRX*, 3(4):466–473.

Chen, Y., Xiong, M., Dong, Y., Haberman, A., Cao, J., Liu, H., Zhou, W., and Zhang, S. C. (2016). Chemical Control of Grafted Human PSC-Derived Neurons in a Mouse Model of Parkinson's Disease. *Cell Stem Cell*, 18(6):817–826.

Chou, C.-H., Fan, H.-C., and Hueng, D.-Y. (2015). Potential of Neural Stem Cell-Based Therapy for Parkinson's Disease. *Parkinsonx2019;s Disease*, 2015:571475.

Choy, J. C. (2010). Granzymes and perforin in solid organ transplant rejection. *Cell Death Differ*, 17(4):567–576.

Clarke, D. J., Brundin, P., Strecker, R. E., Nilsson, O. G., Björklund, A., and Lindvall,

O. (1988). Human fetal dopamine neurons grafted in a rat model of Parkinson's disease: ultrastructural evidence for synapse formation using tyrosine hydroxylase immunocytochemistry. *Experimental Brain Research*, 73(1):115–126.

Colpaert, F. C. (1987). Pharmacological characteristics of tremor, rigidity and hypokinesia induced by reserpine in rat. *Neuropharmacology*, 26(9):1431–1440.

Conway, M., Xu, T., Kirkpatrick, A., Ripp, S., Sayler, G., and Close, D. (2020). Real-time tracking of stem cell viability, proliferation, and differentiation with autonomous bioluminescence imaging. *BMC Biology*, 18(1):79.

Couillard-Despres, S., Vreys, R., Aigner, L., and Van der Linden, A. (2011). In vivo monitoring of adult neurogenesis in health and disease. *Front Neurosci*, 5:67.

Courtois, E. T., Castillo, C. G., Seiz, E. G., Ramos, M., Bueno, C., Liste, I., and Martínez-Serrano, A. (2010). In vitro and in vivo enhanced generation of human A9 dopamine neurons from neural stem cells by Bcl-XL. *J Biol Chem*, 285(13):9881–9897.

Couture, L. A. and Carpenter, M. K. (2015). 2005 Donor Eligibility Requirements: Unintended Consequences for Stem Cell Development. *Stem Cells Transl Med*, 4(10):1097–1100.

Crabbe, A., Vandeputte, C., Dresselaers, T., Sacido, A. A., Verdugo, J. M., Eyckmans, J., Luyten, F. P., Van Laere, K., Verfaillie, C. M., and Himmelreich, U. (2010). Effects of MRI contrast agents on the stem cell phenotype. *Cell Transplant*, 19(8):919–936.

Curradi, M., Izzo, A., Badaracco, G., and Landsberger, N. (2002). Molecular mechanisms of gene silencing mediated by DNA methylation. *Molecular and cellular biology*, 22(9):3157–3173.

Dawson, T. M., Ko, H. S., and Dawson, V. L. (2010). Genetic animal models of Parkinson's disease. *Neuron*, 66(5):646–661.

de Almeida, P. E., van Rappard, J. R. M., and Wu, J. C. (2011). In vivo bioluminescence for tracking cell fate and function. *American journal of physiology. Heart and circulatory physiology*, 301(3):H663–H671.

DeMaagd, G. and Philip, A. (2015). Parkinson's Disease and Its Management: Part 1: Disease Entity, Risk Factors, Pathophysiology, Clinical Presentation, and Diagnosis. *P T : a peer-reviewed journal for formulary management*, 40(8):504–532.

Denic, A., Macura, S. I., Mishra, P., Gamez, J. D., Rodriguez, M., and Pirko, I. (2011). MRI in rodent models of brain disorders. *Neurotherapeutics : the journal of the American Society for Experimental NeuroTherapeutics*, 8(1):3–18.

Domanskyi, A., Alter, H., Vogt, M. A., Gass, P., and Vinnikov, I. A. (2014). Transcription factors Foxa1 and Foxa2 are required for adult dopamine neurons maintenance. *Frontiers in cellular neuroscience*, 8:275.

Domanskyi, A., Saarma, M., and Airavaara, M. (2015). Prospects of Neurotrophic Factors for Parkinson's Disease: Comparison of Protein and Gene Therapy. *Human Gene Therapy*, 26(8):550–559.

Duty, S. and Jenner, P. (2011). Animal models of Parkinson's disease: a source of novel treatments and clues to the cause of the disease. *British journal of pharmacology*, 164(4):1357–1391.

Estelrich, J., Sánchez-Martín, M. J., and Busquets, M. A. (2015). Nanoparticles in magnetic resonance imaging: from simple to dual contrast agents. *International journal of nanomedicine*, 10:1727–1741.

Evans, M. J. and Kaufman, M. H. (1981). Establishment in culture of pluripotential cells from mouse embryos. *Nature*, 292(5819):154–156.

Fasano, C. A., Chambers, S. M., Lee, G., Tomishima, M. J., and Studer, L. (2010). Efficient derivation of functional floor plate tissue from human embryonic stem cells. *Cell Stem Cell*, 6(4):336–347.

Feng, Q., Liu, Y., Huang, J., Chen, K., Huang, J., and Xiao, K. (2018). Uptake, distribution, clearance, and toxicity of iron oxide nanoparticles with different sizes and coatings. *Scientific Reports*, 8(1):2082.

Foltynie, T., Brayne, C. E., Robbins, T. W., and Barker, R. A. (2004). The cognitive ability of an incident cohort of Parkinson's patients in the UK. The CamPaIGN study. (3):550.

Gambotto, A., Dworacki, G., Cicinnati, V., Kenniston, T., Steitz, J., Tüting, T., Robbins, P. D., and DeLeo, A. B. (2000). Immunogenicity of enhanced green fluorescent protein (EGFP) in BALB/c mice: identification of an H2-Kd-restricted CTL epitope. *Gene Ther*, 7(23):2036–2040.

García-Verdugo, J. M., Doetsch, F., Wichterle, H., Lim, D. A., and Alvarez-Buylla, A. (1998). Architecture and cell types of the adult subventricular zone: in search of the stem cells. *J Neurobiol*, 36(2):234–248.

Garitaonandia, I., Gonzalez, R., Sherman, G., Semechkin, A., Evans, A., and Kern, R. (2018). Novel Approach to Stem Cell Therapy in Parkinson's Disease. *Stem Cells Dev*, 27(14):951–957.

Girault, J. A. and Greengard, P. (2004). The neurobiology of dopamine signaling. *Arch Neurol*, 61(5):641–644.

Gleave, J. A., Farncombe, T. H., Saab, C., and Doering, L. C. (2011). Correlative single photon emission computed tomography imaging of [123I]altropane binding in the rat model of Parkinson's. *Nuclear Medicine and Biology*, 38(5):741–749.

Goldring, C. P., Duffy, P., Benvenisty, N., Andrews, P., Ben-David, U., Eakins, R., French, N., Hanley, N., Kelly, L., Kitteringham, N., Kurth, J., Ladenheim, D., Laverty, H., McBlane, J., Narayanan, G., Patel, S., Reinhardt, J., Rossi, A., Sharpe, M., and Park, B. (2011). Assessing the Safety of Stem Cell Therapeutics. *Cell Stem Cell*, 8(6):618–628.

Gómez-Esteban, J. C., Zarranz, J. J., Lezcano, E., Tijero, B., Luna, A., Velasco, F., Rouco, I., and Garamendi, I. (2007). Influence of motor symptoms upon the quality of life of patients with Parkinson's disease. *European neurology*, 57(3):161–165.

Gonzalez, R., Garitaonandia, I., Poustovoitov, M., Abramihina, T., McEntire, C., Culp, B., Attwood, J., Noskov, A., Christiansen-Weber, T., Khater, M., Mora-Castilla, S., To, C., Crain, A., Sherman, G., Semechkin, A., Laurent, L. C., Elsworth, J. D., Sladek, J., Snyder, E. Y., Redmond Jr., D. E., and Kern, R. A. (2016). Neural Stem Cells Derived from Human Parthenogenetic Stem Cells Engraft and Promote Recovery in a Nonhuman Primate Model of Parkinson's Disease. *Cell Transplant*, 25(11):1945–1966.

Grealish, S., Diguet, E., Kirkeby, A., Mattsson, B., Heuer, A., Bramoulle, Y., Van Camp, N., Perrier, A. L., Hantraye, P., Björklund, A., and Parmar, M. (2014). Human ESC-derived dopamine neurons show similar preclinical efficacy and potency to fetal neurons when grafted in a rat model of Parkinson's disease. *Cell Stem Cell*, 15(5):653–665.

Hakim, A. M. and Mathieson, G. (1979). Dementia in Parkinson disease. *Neurology*, 29(9 Part 1):1209.

Hallett, P. J., Deleidi, M., Astradsson, A., Smith, G. A., Cooper, O., Osborn, T. M., Sundberg, M., Moore, M. A., Perez-Torres, E., Brownell, A. L., Schumacher, J. M., Spealman, R. D., and Isacson, O. (2015). Successful function of autologous iPSC-derived dopamine neurons following transplantation in a non-human primate model of Parkinson's disease. *Cell Stem Cell*, 16(3):269–274.

Hamanaka, Y., Minoura, R., Nishino, H., Miura, T., and Mizunami, M. (2016). Dopamine- and Tyrosine Hydroxylase-Immunoreactive Neurons in the Brain of the American Cockroach, Periplaneta americana. *PloS one*, 11(8):e0160531–e0160531.

Harris, J. P., Burrell, J. C., Struzyna, L. A., Chen, H. I., Serruya, M. D., Wolf, J. A., Duda, J. E., and Cullen, D. K. (2020). Emerging regenerative medicine and tissue engineering strategies for Parkinson's disease. *npj Parkinson's Disease*, 6(1):4.

Hayashi, T., Wakao, S., Kitada, M., Ose, T., Watabe, H., Kuroda, Y., Mitsunaga, K., Matsuse, D., Shigemoto, T., Ito, A., Ikeda, H., Fukuyama, H., Onoe, H., Tabata, Y., and Dezawa, M. (2013). Autologous mesenchymal stem cell-derived dopaminergic neurons function in parkinsonian macaques. *J Clin Invest*, 123(1):272–284.

Hebsgaard, J. B., Nelander, J., Sabelström, H., Jönsson, M. E., Stott, S., and Parmar, M. (2009). Dopamine neuron precursors within the developing human mesencephalon show radial glial characteristics. *Glia*, 57(15):1648–1658.

Herman, J. P., Rouge-Pont, F., Le Moal, M., and Abrous, D. N. (1993). Mechanisms of amphetamine-induced rotation in rats with unilateral intrastriatal grafts of embryonic dopaminergic neurons: A pharmacological and biochemical analysis. *Neuroscience*, 53(4):1083–1095.

Herscovitch, P. (2014). Single-Photon Emission Computed Tomography (SPECT). In Aminoff, M. J. and Daroff, R. B., editors, *Encyclopedia of the Neurological Sciences (Second Edition)*, pages 173–178. Academic Press, Oxford.

Heslop, J. A., Hammond, T. G., Santeramo, I., Tort Piella, A., Hopp, I., Zhou, J., Baty,

R., Graziano, E. I., Proto Marco, B., Caron, A., Sköld, P., Andrews, P. W., Baxter, M. A., Hay, D. C., Hamdam, J., Sharpe, M. E., Patel, S., Jones, D. R., Reinhardt, J., Danen, E. H. J., Ben-David, U., Stacey, G., Björquist, P., Piner, J., Mills, J., Rowe, C., Pellegrini, G., Sethu, S., Antoine, D. J., Cross, M. J., Murray, P., Williams, D. P., Kitteringham, N. R., Goldring, C. E. P., and Park, B. K. (2015). Concise review: workshop review: understanding and assessing the risks of stem cell-based therapies. *STEM CELLS Translational Medicine*, 4(4):389–400.

Hijaz, B. A. and Volpicelli-Daley, L. A. (2020). Initiation and propagation of α-synuclein aggregation in the nervous system. *Molecular Neurodegeneration*, 15(1):19.

Hill, C. J., Fleming, J. R., Mousavinejad, M., Nicholson, R., Tzokov, S. B., Bullough, P. A., Bogomolovas, J., Morgan, M. R., Mayans, O., and Murray, P. (2019). Self-Assembling Proteins as High-Performance Substrates for Embryonic Stem Cell Self-Renewal. *Adv Mater*, 31(17):e1807521.

Hu, Q. and Wang, G. (2016). Mitochondrial dysfunction in Parkinson's disease. *Translational Neurodegeneration*, 5(1):14.

Huang, N. F., Okogbaa, J., Babakhanyan, A., and Cooke, J. P. (2012). Bioluminescence imaging of stem cell-based therapeutics for vascular regeneration. *Theranostics*, 2(4):346–354.

Huot, P., Johnston, T. H., Koprich, J. B., Fox, S. H., and Brotchie, J. M. (2013). The Pharmacology of l-DOPA-Induced Dyskinesia in Parkinson's Disease. *Pharmacological Reviews*, 65(1):171.

Inden, M., Yanagisawa, D., Hijioka, M., and Kitamura, Y. (2016). Therapeutic Effects of Mesenchymal Stem Cells for Parkinson@ s Disease.

Itskovitz-Eldor, J., Schuldiner, M., Karsenti, D., Eden, A., Yanuka, O., Amit, M., Soreq, H., and Benvenisty, N. (2000). Differentiation of Human Embryonic Stem Cells into Embryoid Bodies Comprising the Three Embryonic Germ Layers. *Molecular Medicine*, 6(2):88–95.

Iwano, S., Sugiyama, M., Hama, H., Watakabe, A., Hasegawa, N., Kuchimaru, T., Tanaka, K. Z., Takahashi, M., Ishida, Y., Hata, J., Shimozono, S., Namiki, K., Fukano, T., Kiyama, M., Okano, H., Kizaka-Kondoh, S., McHugh, T. J., Yamamori, T., Hioki, H., Maki, S., and Miyawaki, A. (2018). Single-cell bioluminescence imaging of deep tissue in freely moving animals. *Science*, 359(6378):935.

Jacobs, F. M. J., van der Linden, A. J. A., Wang, Y., von Oerthel, L., Sul, H. S., Burbach, J. P. H., and Smidt, M. P. (2009). Identification of Dlk1, Ptpru and Klhl1 as novel Nurr1 target genes in meso-diencephalic dopamine neurons. *Development*, 136(14):2363.

Jagmag, S. A., Tripathi, N., Shukla, S. D., Maiti, S., and Khurana, S. (2016). Evaluation of Models of Parkinson's Disease. *Frontiers in Neuroscience*, 9(503).

Jankovic, J. and Aguilar, L. G. (2008). Current approaches to the treatment of Parkinson's disease. *Neuropsychiatric disease and treatment*, 4(4):743–757.

Jankovic, J. and Poewe, W. (2012). Therapies in Parkinson's disease. *Curr Opin Neurol*, 25(4):433–447.

Jiang, H., Cheng, Z., Tian, M., and Zhang, H. (2011). In vivo imaging of embryonic stem cell therapy. *European Journal of Nuclear Medicine and Molecular Imaging*, 38(4):774–784.

Jiang, X., Sung, Y. K., Tian, W., Qian, J., Semenza, G. L., and Nicolls, M. R. (2014). Graft microvascular disease in solid organ transplantation. *J Mol Med (Berl)*, 92(8):797–810.

Joyce, N., Annett, G., Wirthlin, L., Olson, S., Bauer, G., and Nolta, J. A. (2010). Mesenchymal stem cells for the treatment of neurodegenerative disease. *Regen Med*, 5(6):933–946.

Kaneta, T. (2020). PET and SPECT imaging of the brain: a review on the current status of nuclear medicine in Japan. *Japanese Journal of Radiology*, 38(4):343–357.

Kee, N., Volakakis, N., Kirkeby, A., Dahl, L., Storvall, H., Nolbrant, S., Lahti, L., Björklund, Å. K., Gillberg, L., Joodmardi, E., Sandberg, R., Parmar, M., and Perlmann, T. (2017). Single-Cell Analysis Reveals a Close Relationship between Differentiating Dopamine and Subthalamic Nucleus Neuronal Lineages. *Cell Stem Cell*, 20(1):29–40.

Kefalopoulou, Z., Politis, M., Piccini, P., Mencacci, N., Bhatia, K., Jahanshahi, M., Widner, H., Rehncrona, S., Brundin, P., Björklund, A., Lindvall, O., Limousin, P., Quinn, N., and Foltynie, T. (2014). Long-term clinical outcome of fetal cell transplantation for Parkinson disease: two case reports. *JAMA Neurol*, 71(1):83–87.

Kiecker, C. and Lumsden, A. (2012). The role of organizers in patterning the nervous system. *Annu Rev Neurosci*, 35:347–367.

Kikuchi, T., Morizane, A., Doi, D., Magotani, H., Onoe, H., Hayashi, T., Mizuma, H., Takara, S., Takahashi, R., Inoue, H., Morita, S., Yamamoto, M., Okita, K., Nakagawa, M., Parmar, M., and Takahashi, J. (2017). Human iPS cell-derived dopaminergic neurons function in a primate Parkinson's disease model. *Nature*, 548(7669):592–596.

Kim, D. E., Schellingerhout, D., Ishii, K., Shah, K., and Weissleder, R. (2004). Imaging of stem cell recruitment to ischemic infarcts in a murine model. *Stroke*, 35(4):952–957.

Kirkeby, A., Grealish, S., Wolf, D. A., Nelander, J., Wood, J., Lundblad, M., Lindvall, O., and Parmar, M. (2012). Generation of regionally specified neural progenitors and functional neurons from human embryonic stem cells under defined conditions. *Cell Rep*, 1(6):703–714.

Kirkeby, A., Nolbrant, S., Tiklova, K., Heuer, A., Kee, N., Cardoso, T., Ottosson, D. R., Lelos, M. J., Rifes, P., Dunnett, S. B., Grealish, S., Perlmann, T., and Parmar, M. (2017). Predictive Markers Guide Differentiation to Improve Graft Outcome in Clinical Translation of hESC-Based Therapy for Parkinson's Disease. *Cell Stem Cell*, 20(1):135–148.

Klein, M. O., Battagello, D. S., Cardoso, A. R., Hauser, D. N., Bittencourt, J. C., and Correa, R. G. (2019). Dopamine: Functions, Signaling, and Association with Neurological Diseases. *Cellular and Molecular Neurobiology*, 39(1):31–59.

Koprich, J. B., Kalia, L. V., and Brotchie, J. M. (2017). Animal models of α-synucleinopathy for Parkinson disease drug development. *Nature Reviews Neuroscience*, 18(9):515–529.

Kostura, L., Kraitchman, D. L., Mackay, A. M., Pittenger, M. F., and Bulte, J. W. M. (2004). Feridex labeling of mesenchymal stem cells inhibits chondrogenesis but not adipogenesis or osteogenesis. *NMR in Biomedicine*, 17(7):513–517.

Kraitchman, D. L., Gilson, W. D., and Lorenz, C. H. (2008). Stem cell therapy: MRI guidance and monitoring. *Journal of magnetic resonance imaging : JMRI*, 27(2):299–310.

Kriks, S., Shim, J.-W., Piao, J., Ganat, Y. M., Wakeman, D. R., Xie, Z., Carrillo-Reid, L., Auyeung, G., Antonacci, C., Buch, A., Yang, L., Beal, M. F., Surmeier, D. J., Kordower, J. H., Tabar, V., and Studer, L. (2011). Dopamine neurons derived from human ES cells efficiently engraft in animal models of Parkinson's disease. *Nature*, 480(7378):547–551.

Krishnan, M., Park, J. M., Cao, F., Wang, D., Paulmurugan, R., Tseng, J. R., Gonzalgo, M. L., Gambhir, S. S., and Wu, J. C. (2006). Effects of epigenetic modulation on reporter gene expression: implications for stem cell imaging. *FASEB journal : official publication of the Federation of American Societies for Experimental Biology*, 20(1):106–108.

Kruttwig, K., Brueggemann, C., Kaijzel, E., Vorhagen, S., Hilger, T., Löwik, C., and Hoehn, M. (2010). Development of a three-dimensional in vitro model for longitudinal observation of cell behavior: monitoring by magnetic resonance imaging and optical imaging. *Molecular imaging and biology*, 12(4):367–376.

Kumar, A., Dudhal, S., Sundari, T. A., Sunkara, M., Usman, H., Varshney, A., and Mukhopadhyay, A. (2016). Dopaminergic-primed fetal liver mesenchymal stromal-like cells can reverse parkinsonian symptoms in 6-hydroxydopamine-lesioned mice. *Cytotherapy*, 18(3):307–319.

Lansbury, P. T. and Brice, A. (2002). Genetics of Parkinson's disease and biochemical studies of implicated gene products. *Current Opinion in Genetics Development*, 12(3):299–306.

Lau, J. F., Anderson, S. A., Adler, E., and Frank, J. A. (2010). Imaging approaches for the study of cell-based cardiac therapies. *Nature reviews. Cardiology*, 7(2):97–105.

Lecours, C., Bordeleau, M., Cantin, L., Parent, M., Paolo, T. D., and Tremblay, M.-È. (2018). Microglial Implication in Parkinson's Disease: Loss of Beneficial Physiological Roles or Gain of Inflammatory Functions? *Frontiers in cellular neuroscience*, 12:282.

Levesque, M. E., Neuman, T., and Rezak, M. (2010). Therapeutic microinjection of autologous adult human neural stem cells and differentiated neurons for Parkinson's

disease: Five-year post-operative outcome.

Li, W., Englund, E., Widner, H., Mattsson, B., van Westen, D., Lätt, J., Rehncrona, S., Brundin, P., Björklund, A., Lindvall, O., and Li, J.-Y. (2016). Extensive graft-derived dopaminergic innervation is maintained 24 years after transplantation in the degenerating parkinsonian brain. *Proceedings of the National Academy of Sciences*, 113(23):6544.

Liang, G. and Zhang, Y. (2013). Genetic and epigenetic variations in iPSCs: potential causes and implications for application. *Cell Stem Cell*, 13(2):149–159.

Liao, M.-C., Diaconu, M., Monecke, S., Collombat, P., Timaeus, C., Kuhlmann, T., Paulus, W., Trenkwalder, C., Dressel, R., and Mansouri, A. (2014). Embryonic stem cell-derived neural progenitors as non-tumorigenic source for dopaminergic neurons. *World journal of stem cells*, 6(2):248–255.

Limberis, M. P., Bell, C. L., and Wilson, J. M. (2009). Identification of the murine firefly luciferase-specific CD8 T-cell epitopes. *Gene Ther*, 16(3):441–447.

Limousin, P. and Foltynie, T. (2019). Long-term outcomes of deep brain stimulation in Parkinson disease. *Nature Reviews Neurology*, 15(4):234–242.

Lindvall, O., Backlund, E. O., Farde, L., Sedvall, G., Freedman, R., Hoffer, B., Nobin, A., Seiger, A., and Olson, L. (1987). Transplantation in Parkinson's disease: two cases of adrenal medullary grafts to the putamen. *Ann Neurol*, 22(4):457–468.

Lindvall, O. and Björklund, A. (2004). Cell therapy in Parkinson's disease. *NeuroRX*, 1(4):382–393.

Lippincott-Schwartz, J. and Patterson, G. H. (2003). Development and use of fluorescent protein markers in living cells. *Science*, 300(5616):87–91.

Liu, A. and Joyner, A. (2001). Liu, A. Joyner, A.L. Early anterior/posterior patterning of the midbrain and cerebellum. Annu. Rev. Neurosci. 24, 869896. *Annual review of neuroscience*, 24:869–896.

Liu, A., Yu, X., and Liu, S. (2013). Pluripotency transcription factors and cancer stem cells: small genes make a big difference. *Chinese journal of cancer*, 32(9):483–487.

Liu, H. S., Jan, M. S., Chou, C. K., Chen, P. H., and Ke, N. J. (1999). Is green fluorescent protein toxic to the living cells? *Biochem Biophys Res Commun*, 260(3):712–717.

Liu, J., Wang, Y. Y., Liu, L., Wang, Q. D., Yuan, Z. Y., Zhang, Z. X., Gu, P., and Wang, M. W. (2008). Damage to the nigrostriatal system in the MPTP-treated SAMP8 mouse. *Neurosci Lett*, 448(2):184–188.

Liu, M. and Bing, G. (2011). Lipopolysaccharide animal models for Parkinson's disease. *Parkinson's disease*, 2011:327089.

Livak, K. J. and Schmittgen, T. D. (2001). Analysis of relative gene expression data using real-time quantitative PCR and the 2(-Delta Delta C(T)) Method. *Methods*, 25(4):402–408.

Lo, B. and Parham, L. (2009). Ethical Issues in Stem Cell Research. *Endocrine Reviews*, 30(3):204–213.

Lois, C. and Alvarez-Buylla, A. (1993). Proliferating subventricular zone cells in the adult mammalian forebrain can differentiate into neurons and glia. *Proceedings of the National Academy of Sciences of the United States of America*, 90(5):2074–2077.

Madrazo, I., Drucker-Colín, R., Díaz, V., Martínez-Mata, J., Torres, C., and Becerril, J. J. (1987). Open microsurgical autograft of adrenal medulla to the right caudate nucleus in two patients with intractable Parkinson's disease. *N Engl J Med*, 316(14):831–834.

Mahul-Mellier, A.-L., Burtscher, J., Maharjan, N., Weerens, L., Croisier, M., Kuttler, F., Leleu, M., Knott, G. W., and Lashuel, H. A. (2020). The process of Lewy body formation, rather than simply α-synuclein fibrillization, is one of the major drivers of neurodegeneration. *Proceedings of the National Academy of Sciences*, 117(9):4971.

Margel, S., Lublin-Tennenbaum, T., Gura, S., Tsubery, M., Akiva, U., Shpaisman, N., Galperin, A., Perlstein, B., Lapido, P., Boguslavsky, Y., Goldshtein, J., and Ziv, O. (2007). Synthesis and characterization of nano- and micron-sized iron oxide and iron particles for biomedical applications. In *Laboratory Techniques in Biochemistry and Molecular Biology*, volume 32, pages 119–162. Elsevier.

Martí-Bonmatí, L., Sopena, R., Bartumeus, P., and Sopena, P. (2010). Multimodality imaging techniques. *Contrast Media Molecular Imaging*, 5(4):180–189.

Martinez-Barbera, J. P., Signore, M., Boyl, P. P., Puelles, E., Acampora, D., Gogoi, R., Schubert, F., Lumsden, A., and Simeone, A. (2001). Regionalisation of anterior neuroectoderm and its competence in responding to forebrain and midbrain inducing activities depend on mutual antagonism between OTX2 and GBX2. *Development*, 128(23):4789.

Meade, R. M., Fairlie, D. P., and Mason, J. M. (2019). Alpha-synuclein structure and Parkinson's disease – lessons and emerging principles. *Molecular Neurodegeneration*, 14(1):29.

Medvedev, S. P., Shevchenko, A. I., and Zakian, S. M. (2010). Induced Pluripotent Stem Cells: Problems and Advantages when Applying them in Regenerative Medicine. *Acta naturae*, 2(2):18–28.

Mendes Filho, D., Ribeiro, P. D. C., Oliveira, L. F., de Paula, D. R. M., Capuano, V., de Assunção, T. S. F., and da Silva, V. J. D. (2018). Therapy With Mesenchymal Stem Cells in Parkinson Disease: History and Perspectives. *Neurologist*, 23(4):141–147.

Mhyre, T. R., Boyd, J. T., Hamill, R. W., and Maguire-Zeiss, K. A. (2012). Parkinson's disease. *Sub-cellular biochemistry*, 65:389–455.

Montgomery Jr., E. B. and Baker, K. B. (2000). Mechanisms of deep brain stimulation and future technical developments. *Neurol Res*, 22(3):259–266.

Morizane, A., Takahashi, J., Takagi, Y., Sasai, Y., and Hashimoto, N. (2002). Optimal conditions for in vivo induction of dopaminergic neurons from embryonic stem cells through stromal cell-derived inducing activity. *J Neurosci Res*, 69(6):934–939.

Nandipati, S. and Litvan, I. (2016). Environmental Exposures and Parkinson's Disease. *International journal of environmental research and public health*, 13(9):881.

Niclis, J. C., Gantner, C. W., Alsanie, W. F., McDougall, S. J., Bye, C. R., Elefanty, A. G., Stanley, E. G., Haynes, J. M., Pouton, C. W., Thompson, L. H., and Parish, C. L. (2017). Efficiently Specified Ventral Midbrain Dopamine Neurons from Human Pluripotent Stem Cells Under Xeno-Free Conditions Restore Motor Deficits in Parkinsonian Rodents. *Stem Cells Transl Med*, 6(3):937–948.

Nikkhah, G., Bentlage, C., Cunningham, M. G., and Björklund, A. (1994a). Intranigral fetal dopamine grafts induce behavioral compensation in the rat Parkinson model. *J Neurosci*, 14(6):3449–3461.

Nikkhah, G., Cunningham, M. G., Jödicke, A., Knappe, U., and Björklund, A. (1994b). Improved graft survival and striatal reinnervation by microtransplantation of fetal nigral cell suspensions in the rat Parkinson model. *Brain Res*, 633(1-2):133–143.

Nolbrant, S., Heuer, A., Parmar, M., and Kirkeby, A. (2017). Generation of high-purity human ventral midbrain dopaminergic progenitors for in vitro maturation and intracerebral transplantation. *Nature Protocols*, 12(9):1962–1979.

Norrman, K., Fischer, Y., Bonnamy, B., Wolfhagen Sand, F., Ravassard, P., and Semb, H. (2010). Quantitative comparison of constitutive promoters in human ES cells. *PloS one*, 5(8):e12413.

Nunes, M. C., Roy, N. S., Keyoung, H. M., Goodman, R. R., McKhann, G., Jiang, L., Kang, J., Nedergaard, M., and Goldman, S. A. (2003). Identification and isolation of multipotential neural progenitor cells from the subcortical white matter of the adult human brain. *Nature Medicine*, 9(4):439–447.

Pagano, G., Niccolini, F., and Politis, M. (2016). Imaging in Parkinson's disease. *Clinical medicine (London, England)*, 16(4):371–375.

Park, J.-S., Davis, R. L., and Sue, C. M. (2018). Mitochondrial Dysfunction in Parkinson's Disease: New Mechanistic Insights and Therapeutic Perspectives. *Current neurology and neuroscience reports*, 18(5):21.

Parkinson, J. (1817). *An essay on the shaking palsy*. Printed by Whittingham Rowland ..., for Sherwood, Neely Jones ...

Parkkinen, L., O'Sullivan, S. S., Collins, C., Petrie, A., Holton, J. L., Revesz, T., and Lees, A. J. (2011). Disentangling the relationship between lewy bodies and nigral neuronal loss in Parkinson's disease. *Journal of Parkinson's disease*, 1(3):277–286.

Parmar, M. (2018). Towards stem cell based therapies for Parkinson039;s disease. *Development*, 145(1):dev156117.

Patrick, P. S., Kolluri, K. K., Zaw Thin, M., Edwards, A., Sage, E. K., Sanderson, T., Weil, B. D., Dickson, J. C., Lythgoe, M. F., Lowdell, M., Janes, S. M., and Kalber, T. L. (2020). Lung delivery of MSCs expressing anti-cancer protein TRAIL visualised with (89)Zr-oxine PET-CT. *Stem Cell Res Ther*, 11(1):256.

Peng, Y., Xie, M., Duan, X., Hu, L., Yu, J., Zeng, S., Wang, Y., Ouyang, Q., Lu, G.,

Lin, G., and Sun, Y. (2018). Generation of a luciferase-expressing human embryonic stem cell line: NERCe002-A-2. *Stem Cell Res*, 28:172–176.

Perez-Lloret, S. and Rascol, O. (2010). Dopamine Receptor Agonists for the Treatment of Early or Advanced Parkinson's Disease. *CNS Drugs*, 24(11):941–968.

Perrier, A. L., Tabar, V., Barberi, T., Rubio, M. E., Bruses, J., Topf, N., Harrison, N. L., and Studer, L. (2004). Derivation of midbrain dopamine neurons from human embryonic stem cells. *Proceedings of the National Academy of Sciences of the United States of America*, 101(34):12543.

Piccini, P., Brooks, D. J., Björklund, A., Gunn, R. N., Grasby, P. M., Rimoldi, O., Brundin, P., Hagell, P., Rehncrona, S., Widner, H., and Lindvall, O. (1999). Dopamine release from nigral transplants visualized in vivo in a Parkinson's patient. *Nature Neuroscience*, 2(12):1137–1140.

Porras, G., Li, Q., and Bezard, E. (2012). Modeling Parkinson's disease in primates: The MPTP model. *Cold Spring Harbor perspectives in medicine*, 2(3):a009308–a009308.

Prakash, N., Brodski, C., Naserke, T., Puelles, E., Gogoi, R., Hall, A., Panhuysen, M., Echevarria, D., Sussel, L., Weisenhorn, D. M. V., Martinez, S., Arenas, E., Simeone, A., and Wurst, W. (2006). A Wnt1-regulated genetic network controls the identity and fate of midbrain-dopaminergic progenitors in vivo. *Development*, 133(1):89.

Puaux, A.-L., Ong, L. C., Jin, Y., Teh, I., Hong, M., Chow, P. K. H., Golay, X., and Abastado, J.-P. (2011). A Comparison of Imaging Techniques to Monitor Tumor Growth and Cancer Progression in Living Animals. *International Journal of Molecular Imaging*, 2011:321538.

Qiu, L., Liao, M.-C., Chen, A. K., Wei, S., Xie, S., Reuveny, S., Zhou, Z. D., Hunziker, W., Tan, E. K., Oh, S. K. W., and Zeng, L. (2017). Immature Midbrain Dopaminergic Neurons Derived from Floor-Plate Method Improve Cell Transplantation Therapy Efficacy for Parkinson's Disease. *STEM CELLS Translational Medicine*, 6(9):1803–1814.

Ramos-Moreno, T., Lendínez, J. G., Pino-Barrio, M. J., Del Arco, A., and Martínez-Serrano, A. (2012). Clonal human fetal ventral mesencephalic dopaminergic neuron precursors for cell therapy research. *PloS one*, 7(12):e52714.

Rezai, A. R., Phillips, M., Baker, K. B., Sharan, A. D., Nyenhuis, J., Tkach, J., Henderson, J., and Shellock, F. G. (2004). Neurostimulation System Used for Deep Brain Stimulation (DBS): MR Safety Issues and Implications of Failing to Follow Safety Recommendations. *Investigative Radiology*, 39(5).

Rodrigues, T. M., Jerónimo-Santos, A., Outeiro, T. F., Sebastião, A. M., and Diógenes, M. J. (2014). Challenges and Promises in the Development of Neurotrophic Factor-Based Therapies for Parkinson's Disease. *Drugs Aging*, 31(4):239–261.

Roeder, E., Henrionnet, C., Goebel, J. C., Gambier, N., Beuf, O., Grenier, D., Chen,

B., Vuissoz, P. A., Gillet, P., and Pinzano, A. (2014). Dose-response of superparamagnetic iron oxide labeling on mesenchymal stem cells chondrogenic differentiation: a multi-scale in vitro study. *PloS one*, 9(5):e98451.

Roy, N. S., Cleren, C., Singh, S. K., Yang, L., Beal, M. F., and Goldman, S. A. (2006). Functional engraftment of human ES cell-derived dopaminergic neurons enriched by coculture with telomerase-immortalized midbrain astrocytes. *Nat Med*, 12(11):1259–1268.

Sadeghiani, N., Barbosa, L. S., Silva, L. P., Azevedo, R. B., Morais, P. C., and Lacava, Z. G. M. (2005). Genotoxicity and inflammatory investigation in mice treated with magnetite nanoparticles surface coated with polyaspartic acid. *Journal of Magnetism and Magnetic Materials*, 289:466–468.

Sakthiswary, R. and Raymond, A. A. (2012). Stem cell therapy in neurodegenerative diseases: From principles to practice. *Neural regeneration research*, 7(23):1822–1831.

Saucedo-Cardenas, O., Quintana-Hau, J. D., Le, W.-D., Smidt, M. P., Cox, J. J., De Mayo, F., Burbach, J. P. H., and Conneely, O. M. (1998). Nurr1 is essential for the induction of the dopaminergic phenotype and the survival of ventral mesencephalic late dopaminergic precursor neurons. *Proceedings of the National Academy of Sciences*, 95(7):4013.

Scarfe, L., Brillant, N., Kumar, J. D., Ali, N., Alrumayh, A., Amali, M., Barbellion, S., Jones, V., Niemeijer, M., Potdevin, S., Roussignol, G., Vaganov, A., Barbaric, I., Barrow, M., Burton, N. C., Connell, J., Dazzi, F., Edsbagge, J., French, N. S., Holder, J., Hutchinson, C., Jones, D. R., Kalber, T., Lovatt, C., Lythgoe, M. F., Patel, S., Patrick, P. S., Piner, J., Reinhardt, J., Ricci, E., Sidaway, J., Stacey, G. N., Starkey Lewis, P. J., Sullivan, G., Taylor, A., Wilm, B., Poptani, H., Murray, P., Goldring, C. E. P., and Park, B. K. (2017). Preclinical imaging methods for assessing the safety and efficacy of regenerative medicine therapies. *npj Regenerative Medicine*, 2(1):28.

Schapira, A. H. V. (2005). Present and future drug treatment for Parkinson's disease. *Journal of Neurology, Neurosurgery amp; Psychiatry*, 76(11):1472.

Schapira, A. H. V. (2011). Monoamine Oxidase B Inhibitors for the Treatment of Parkinson's Disease. *CNS Drugs*, 25(12):1061–1071.

Schrag, A., Horsfall, L., Walters, K., Noyce, A., and Petersen, I. (2015). Prediagnostic presentations of Parkinson's disease in primary care: a case-control study. *Lancet Neurology*, 14(1):57–64.

Shapiro, E. M., Skrtic, S., and Koretsky, A. P. (2005). Sizing it up: cellular MRI using micron-sized iron oxide particles. *Magn Reson Med*, 53(2):329–338.

Shapiro, E. M., Skrtic, S., Sharer, K., Hill, J. M., Dunbar, C. E., and Koretsky, A. P. (2004). MRI detection of single particles for cellular imaging. *Proceedings of the National Academy of Sciences of the United States of America*, 101(30):10901–10906.

Silva, A. C. and Bock, N. A. (2008). Manganese-enhanced MRI: an exceptional tool in

translational neuroimaging. *Schizophrenia bulletin*, 34(4):595–604.

Simonson, W., Hauser, R. A., and Schapira, A. H. (2007). Role of the pharmacist in the effective management of wearing-off in Parkinson's disease. *Ann Pharmacother*, 41(11):1842–1849.

Smith, Y., Wichmann, T., Factor, S. A., and DeLong, M. R. (2012). Parkinson's disease therapeutics: new developments and challenges since the introduction of levodopa. *Neuropsychopharmacology*, 37(1):213–246.

Sonntag, K. C., Pruszak, J., Yoshizaki, T., van Arensbergen, J., Sanchez-Pernaute, R., and Isacson, O. (2007). Enhanced yield of neuroepithelial precursors and midbrain-like dopaminergic neurons from human embryonic stem cells using the bone morphogenic protein antagonist noggin. *STEM CELLS*, 25(2):411–418.

Spataro, R., Kousi, M., Farhan, S. M. K., Willer, J. R., Ross, J. P., Dion, P. A., Rouleau, G. A., Daly, M. J., Neale, B. M., La Bella, V., and Katsanis, N. (2019). Mutations in ATP13A2 (PARK9) are associated with an amyotrophic lateral sclerosis-like phenotype, implicating this locus in further phenotypic expansion. *Human Genomics*, 13(1):19.

Spillantini, M. G., Crowther, R. A., Jakes, R., Hasegawa, M., and Goedert, M. (1998). alpha-Synuclein in filamentous inclusions of Lewy bodies from Parkinson's disease and dementia with lewy bodies. *Proceedings of the National Academy of Sciences of the United States of America*, 95(11):6469–6473.

Springer, W. and Kahle, P. J. (2011). Regulation of PINK1-Parkin-mediated mitophagy. *Autophagy*, 7(3):266–278.

Stanic, D., Finkelstein, D. I., Bourke, D. W., Drago, J., and Horne, M. K. (2003). Timecourse of striatal re-innervation following lesions of dopaminergic SNpc neurons of the rat. *European Journal of Neuroscience*, 18(5):1175–1188.

Stroh, A., Kressel, J., Coras, R., Dreyer, A. Y., Fröhlich, W., Förschler, A., Lobsien, D., Blümcke, I., Zoubaa, S., Schlegel, J., Zimmer, C., and Boltze, J. (2019). A Safe and Effective Magnetic Labeling Protocol for MRI-Based Tracking of Human Adult Neural Stem Cells. *Frontiers in Neuroscience*, 13(1092).

Suelves, M., Carrió, E., Núñez-Álvarez, Y., and Peinado, M. A. (2016). DNA methylation dynamics in cellular commitment and differentiation. *Brief Funct Genomics*, 15(6):443–453.

Sullivan, A. M. and O'Keeffe, G. W. (2016). Neurotrophic factor therapy for Parkinson's disease: past, present and future. *Neural regeneration research*, 11(2):205–207.

Sutton, E. J., Henning, T. D., Pichler, B. J., Bremer, C., and Daldrup-Link, H. E. (2008). Cell tracking with optical imaging. *Eur Radiol*, 18(10):2021–2032.

Takahashi, K., Tanabe, K., Ohnuki, M., Narita, M., Ichisaka, T., Tomoda, K., and Yamanaka, S. (2007). Induction of Pluripotent Stem Cells from Adult Human Fibroblasts by Defined Factors. *Cell*, 131(5):861–872.

Takahashi, K. and Yamanaka, S. (2006). Induction of pluripotent stem cells from mouse

embryonic and adult fibroblast cultures by defined factors. *Cell*, 126(4):663–676.

Tanner, C. M., Ottman, R., Goldman, S. M., Ellenberg, J., Chan, P., Mayeux, R., and Langston, J. W. (1999). Parkinson disease in twins: an etiologic study. *Jama*, 281(4):341–346.

Taylor, A., Herrmann, A., Moss, D., Sée, V., Davies, K., Williams, S. R., and Murray, P. (2014). Assessing the efficacy of nano- and micro-sized magnetic particles as contrast agents for MRI cell tracking. *PloS one*, 9(6):e100259–e100259.

Taylor, A., Sharkey, J., Harwood, R., Scarfe, L., Barrow, M., Rosseinsky, M. J., Adams, D. J., Wilm, B., and Murray, P. (2020). Multimodal Imaging Techniques Show Differences in Homing Capacity Between Mesenchymal Stromal Cells and Macrophages in Mouse Renal Injury Models. *Molecular imaging and biology*, 22(4):904–913.

Tennstaedt, A., Mastropietro, A., Nelles, M., Beyrau, A., and Hoehn, M. (2015). In Vivo Fate Imaging of Intracerebral Stem Cell Grafts in Mouse Brain. *PloS one*, 10(12):e0144262–e0144262.

Thanvi, B. R. and Lo, T. C. N. (2004). Long term motor complications of levodopa: clinical features, mechanisms, and management strategies. *Postgraduate Medical Journal*, 80(946):452.

Thomson, J. A., Itskovitz-Eldor, J., Shapiro, S. S., Waknitz, M. A., Swiergiel, J. J., Marshall, V. S., and Jones, J. M. (1998). Embryonic stem cell lines derived from human blastocysts. *Science*, 282(5391):1145–1147.

Tieu, K. (2011). A guide to neurotoxic animal models of Parkinson's disease. *Cold Spring Harbor perspectives in medicine*, 1(1):a009316–a009316.

Tomov, N. (2020). Glial cells in intracerebral transplantation for Parkinson8217;s disease. *Neural regeneration research*, 15(7):1173–1178.

Tronci, E., Shin, E., Björklund, A., and Carta, M. (2012). Amphetamine-induced rotation and l-DOPA-induced dyskinesia in the rat 6-OHDA model: A correlation study. *Neuroscience Research*, 73(2):168–172.

Turovets, N., Semechkin, A., Kuzmichev, L., Janus, J., Agapova, L., and Revazova, E. (2011). Derivation of human parthenogenetic stem cell lines. *Methods Mol Biol*, 767:37–54.

Twelves, D., Perkins, K. S. M., and Counsell, C. (2003). Systematic Review of Incidence Studies of Parkinson's Disease. (1):19.

Unterweger, H., Dézsi, L., Matuszak, J., Janko, C., Poettler, M., Jordan, J., Bäuerle, T., Szebeni, J., Fey, T., Boccaccini, A. R., Alexiou, C., and Cicha, I. (2018). Dextran-coated superparamagnetic iron oxide nanoparticles for magnetic resonance imaging: evaluation of size-dependent imaging properties, storage stability and safety. *International journal of nanomedicine*, 13:1899–1915.

Van Den Eeden, S. K., Tanner, C. M., Bernstein, A. L., Fross, R. D., Leimpeter, A., Bloch, D. A., and Nelson, L. M. (2003). Incidence of Parkinson's disease: variation by age, gender, and race/ethnicity. *Am J Epidemiol*, 157(11):1015–1022.

van Wamelen, D. J., Grigoriou, S., Chaudhuri, K. R., and Odin, P. (2018). Continuous Drug Delivery Aiming Continuous Dopaminergic Stimulation in Parkinson's Disease. *Journal of Parkinson's disease*, 8(s1):S65–S72.

Vassiliou, A. G., Siaterli, M.-Z., Frakolaki, E., Gkogkosi, P., Paspaltsis, I., Sklaviadis, T., Vassilacopoulou, D., and Vassilaki, N. (2019). L-Dopa decarboxylase interaction with the major signaling regulator 3 in tissues and cells of neural and peripheral origin. *Biochimie*, 160:76–87.

Venkataramana, N. K., Pal, R., Rao, S. A., Naik, A. L., Jan, M., Nair, R., Sanjeev, C. C., Kamble, R. B., Murthy, D. P., and Chaitanya, K. (2012). Bilateral transplantation of allogenic adult human bone marrow-derived mesenchymal stem cells into the subventricular zone of Parkinson's disease: a pilot clinical study. *Stem Cells Int*, 2012:931902.

Veranth, J. M., Kaser, E. G., Veranth, M. M., Koch, M., and Yost, G. S. (2007). Cytokine responses of human lung cells (BEAS-2B) treated with micron-sized and nanoparticles of metal oxides compared to soil dusts. *Part Fibre Toxicol*, 4:2.

Wahajuddin and Arora, S. (2012). Superparamagnetic iron oxide nanoparticles: magnetic nanoplatforms as drug carriers. *International journal of nanomedicine*, 7:3445–3471.

Wahsner, J., Gale, E. M., Rodríguez-Rodríguez, A., and Caravan, P. (2019). Chemistry of MRI Contrast Agents: Current Challenges and New Frontiers. *Chemical reviews*, 119(2):957–1057.

Wan, P.-X., Wang, B.-W., and Wang, Z.-C. (2015). Importance of the stem cell microenvironment for ophthalmological cell-based therapy. *World journal of stem cells*, 7(2):448–460.

Wang, L., Zhang, Q., Li, H., and Zhang, H. (2012). SPECT molecular imaging in Parkinson's disease. *Journal of biomedicine biotechnology*, 2012:412486.

Wang, Y., Wang, B., Zhu, M.-T., Li, M., Wang, H.-J., Wang, M., Ouyang, H., Chai, Z.-F., Feng, W.-Y., and Zhao, Y.-L. (2011). Microglial activation, recruitment and phagocytosis as linked phenomena in ferric oxide nanoparticle exposure. *Toxicology Letters*, 205(1):26–37.

Wang, Y. K., Zhu, W. W., Wu, M. H., Wu, Y. H., Liu, Z. X., Liang, L. M., Sheng, C., Hao, J., Wang, L., Li, W., Zhou, Q., and Hu, B. Y. (2018). Human Clinical-Grade Parthenogenetic ESC-Derived Dopaminergic Neurons Recover Locomotive Defects of Nonhuman Primate Models of Parkinson's Disease. *Stem Cell Reports*, 11(1):171–182.

Whone, A. L., Boca, M., Luz, M., Woolley, M., Mooney, L., Dharia, S., Broadfoot, J., Cronin, D., Schroers, C., Barua, N. U., Longpre, L., Barclay, C. L., Boiko, C., Johnson, G. A., Fibiger, H. C., Harrison, R., Lewis, O., Pritchard, G., Howell, M., Irving, C., Johnson, D., Kinch, S., Marshall, C., Lawrence, A. D., Blinder, S., Sossi, V., Stoessl, A. J., Skinner, P., Mohr, E., and Gill, S. S. (2019). Extended Treatment

with Glial Cell Line-Derived Neurotrophic Factor in Parkinson's Disease. *Journal of Parkinson's disease*, 9:301–313.

Widnell, K. (2005). Pathophysiology of motor fluctuations in Parkinson's disease. *Movement Disorders*, 20(S11):S17–S22.

Wijeyekoon, R. and Barker, R. A. (2009). Cell replacement therapy for Parkinson's disease. *Biochimica et Biophysica Acta (BBA) - Molecular Basis of Disease*, 1792(7):688–702.

Wright Willis, A., Evanoff, B. A., Lian, M., Criswell, S. R., and Racette, B. A. (2010). Geographic and ethnic variation in Parkinson disease: a population-based study of US Medicare beneficiaries. *Neuroepidemiology*, 34(3):143–151.

Yang, D., Zhang, Z.-J., Oldenburg, M., Ayala, M., and Zhang, S.-C. (2008). Human Embryonic Stem Cell-Derived Dopaminergic Neurons Reverse Functional Deficit in Parkinsonian Rats. *STEM CELLS*, 26(1):55–63.

Zeng, X., Cai, J., Chen, J., Luo, Y., You, Z.-B., Fotter, E., Wang, Y., Harvey, B., Miura, T., Backman, C., Chen, G.-J., Rao, M. S., and Freed, W. J. (2004). Dopaminergic Differentiation of Human Embryonic Stem Cells. *STEM CELLS*, 22(6):925–940.

Zetterström, R. H., Williams, R., Perlmann, T., and Olson, L. (1996). Cellular expression of the immediate early transcription factors Nurr1 and NGFI-B suggests a gene regulatory role in several brain regions including the nigrostriatal dopamine system. *Molecular Brain Research*, 41(1):111–120.

Zhao, H., Doyle, T. C., Coquoz, O., Kalish, F., Rice, B. W., and Contag, C. H. (2005). Emission spectra of bioluminescent reporters and interaction with mammalian tissue determine the sensitivity of detection in vivo. *J Biomed Opt*, 10(4):41210.

Zheng, Y., Huang, J., Zhu, T., Li, R., Wang, Z., Ma, F., and Zhu, J. (2017). Stem Cell Tracking Technologies for Neurological Regenerative Medicine Purposes. *Stem Cells International*, 2017:2934149.

Zhu, J., Zhou, L., and XingWu, F. (2006). Tracking neural stem cells in patients with brain trauma. *N Engl J Med*, 355(22):2376–2378.

Zimprich, A., Biskup, S., Leitner, P., Lichtner, P., Farrer, M., Lincoln, S., Kachergus, J., Hulihan, M., Uitti, R. J., Calne, D. B., Stoessl, A. J., Pfeiffer, R. F., Patenge, N., Carbajal, I. C., Vieregge, P., Asmus, F., Müller-Myhsok, B., Dickson, D. W., Meitinger, T., Strom, T. M., Wszolek, Z. K., and Gasser, T. (2004). Mutations in LRRK2 cause autosomal-dominant parkinsonism with pleomorphic pathology. *Neuron*, 44(4):601–607.

CHAPTER A

Appendix

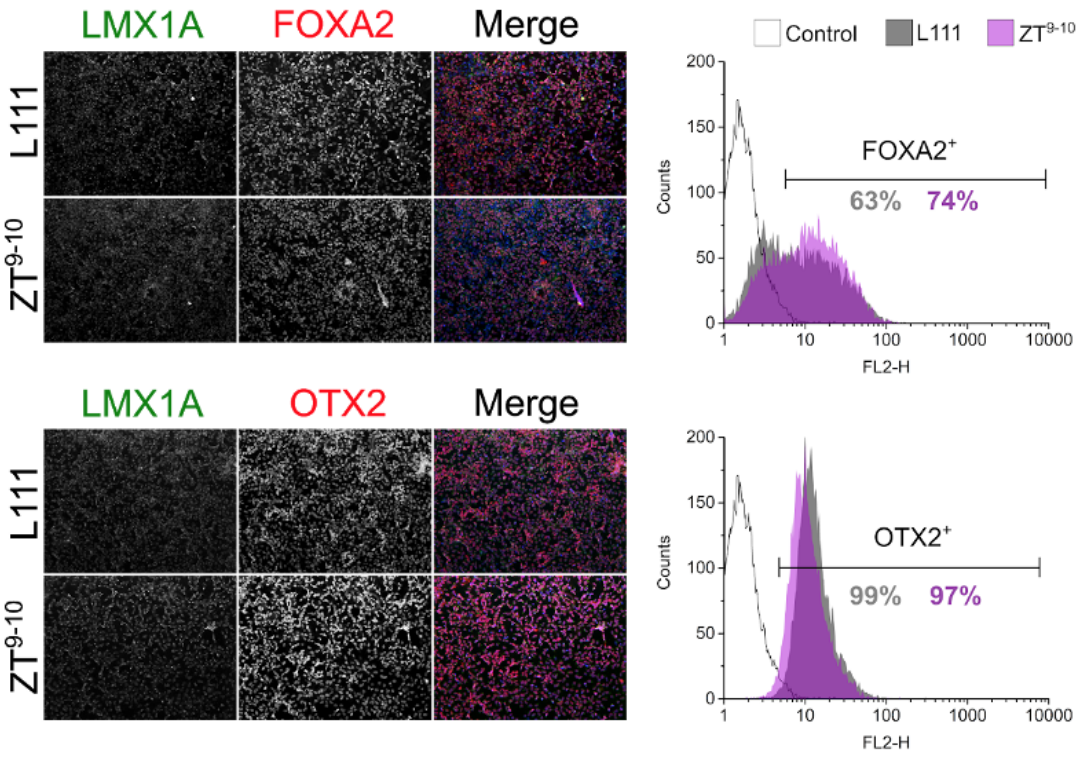

Figure A.1: Differentiation of PSCs to DAPCs is comparably efficient when using ZT-Fn$^{9\text{-}10}$ or Laminin 111 as the culture substrate. Fluorescence micrographs are representative of DAPCs at day 16 post-differentiation cultured on Laminin 111 or ZT-Fn$^{9\text{-}10}$. Cells were stained for ventral midbrain markers *FOXA2* (red), *OTX2* (red) and *LMX1A* (green). Dapi (blue) was used as a nuclear counterstain. Scale bar = 50 µm. Flow cytometry histograms of *FOXA2* and *OTX2* expression in DAPCs cultured on Laminin 111 (grey) or ZT-Fn$^{9\text{-}10}$ (purple). The isotype control profile (white) and gate boundary are shown.

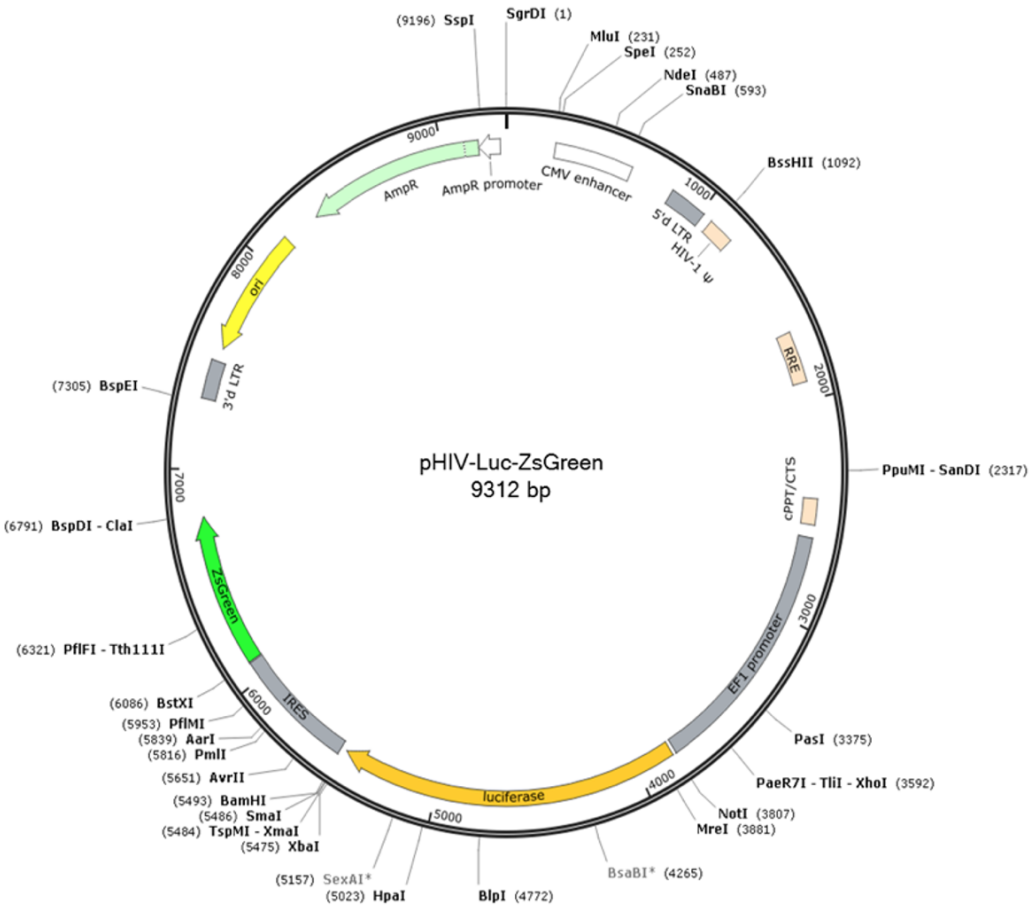

Figure A.2: Schematic illustration of pHIV bicistronic lentivirus containing firefly luciferase and ZsGreen reporters. The Vector was generated by Dr Arthur Taylor, Murray group (Taylor et al., 2020).

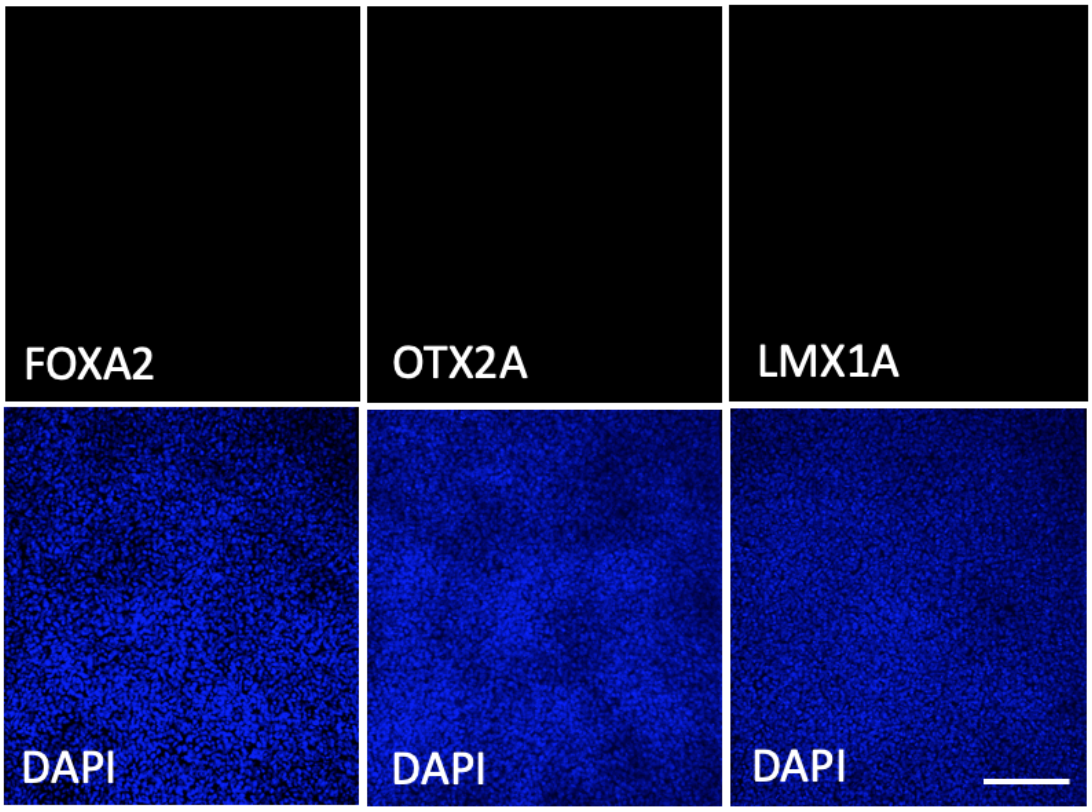

Figure A.3: No primary antibody control immunofluorescence for *FOXA2*, *OTX2A*, and *LMX1A* in DAPCs. DAPCs incubated with the antibody diluent alone and no primary antibody, followed by incubation with secondary antibodies and Dapi.There was no signal detected in the no primary control samples.Scale bars correspond to 100 µm.

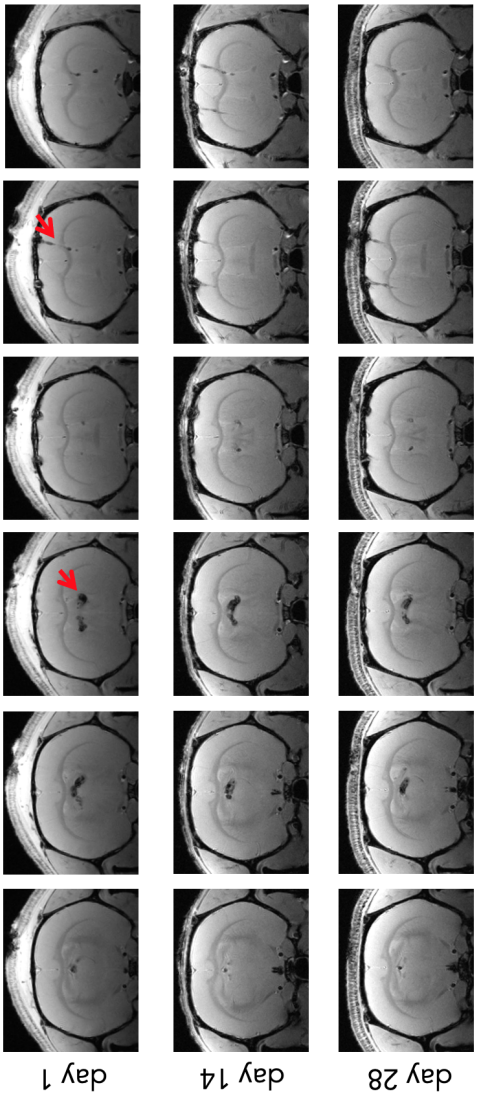

Figure A.4: MRI of rat5 that was misinjected. MRI observation of rat5 was shown that MPIOs^{+} DAPCs could not find in the striatum The MRI images suggest that for this rat the needletrack in dark appears to go into (or very close to) ventricles and the cell deposit was misinjected and ended up in the ventricles (arrowheads).

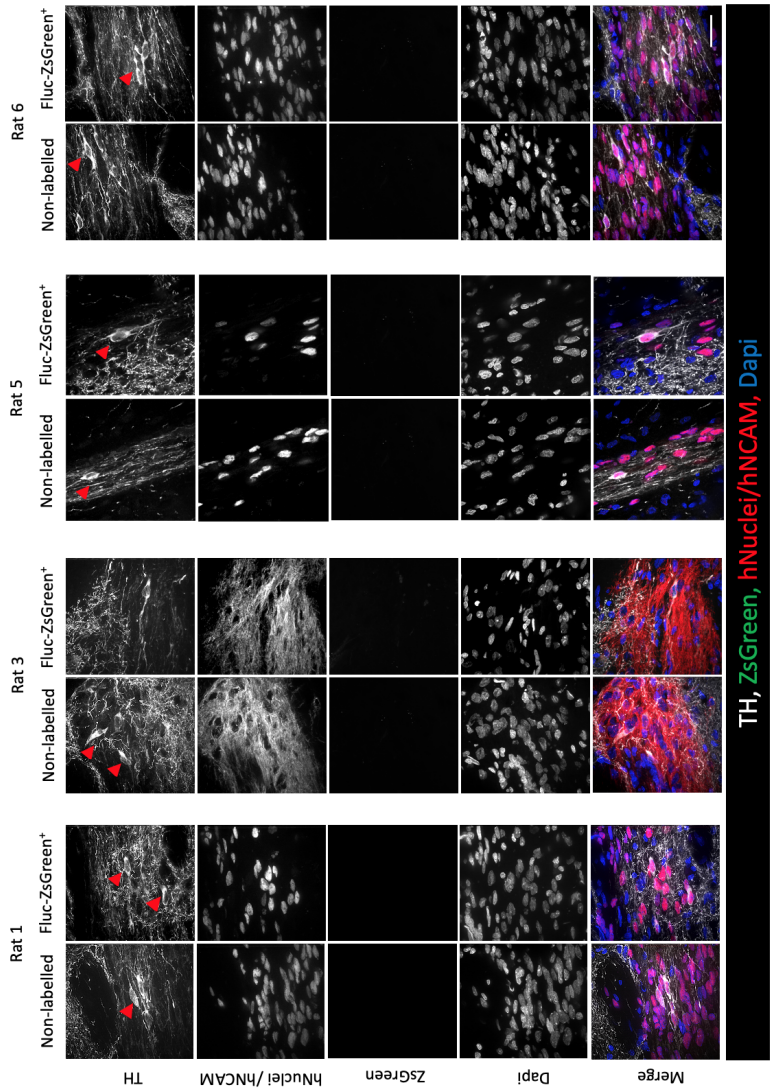

Figure A.5: *TH* **expression in the rat brains grafted for Fluc-ZsGreen labllled DAPCs.** Immunofluorescence microscopy of the injection sites (left hemisphere: nontransduced, right hemisphere: Fluc-ZsGreen$^+$). Cells express a hNCAM or hNuclei, showing that the DAPCs survived in the rats' brains and expressed *TH*, suggesting that they matured into DA neurons. Arrowhead indicates a human cell strongly expressing *TH* while there is no expression of ZsGreen. In the merged images the *TH* is white, ZsGreen is green, hNuclei/hNCAM are red and Dapi is blue. The injection site were found in 4 out of 6 rats that were injected for Fluc-ZsGreen$^+$ DAPCs. Scale bars correspond to 50 µm.

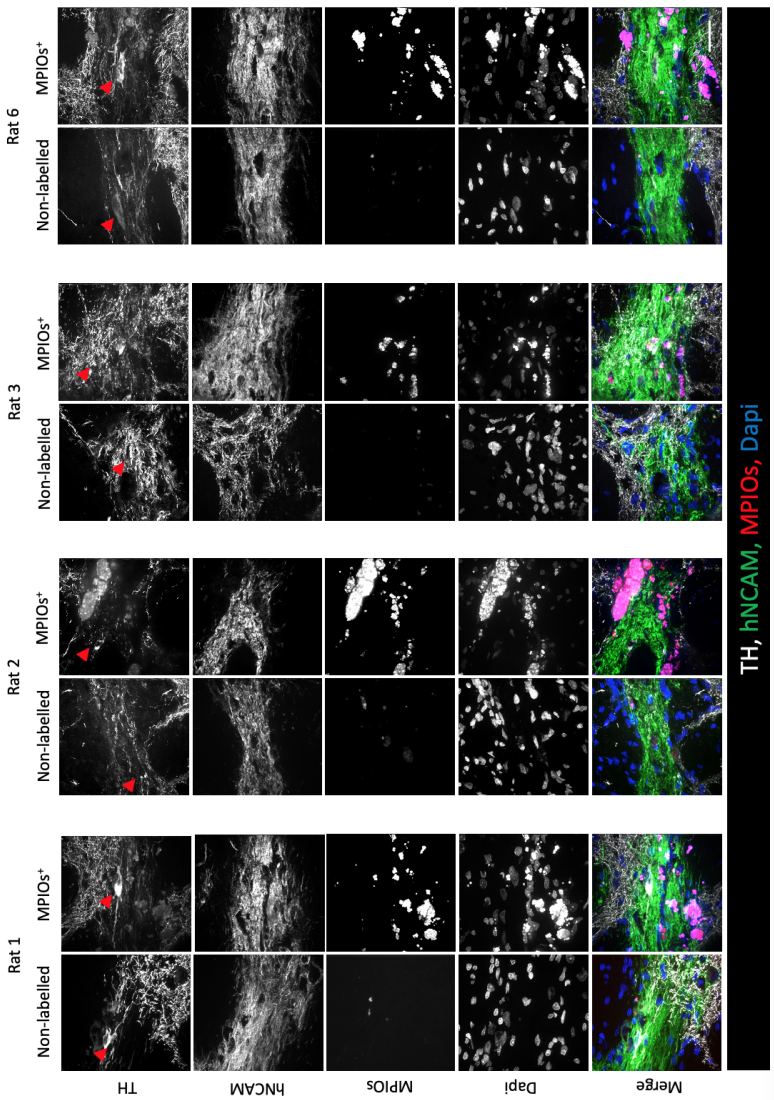

Figure A.6: *TH* **expression in the rat brains grafted for MPIOs lablled DAPCs.** Immunofluorescence microscopy of the injection sites (left hemisphere: nonlabelled cells, right hemisphere: $MPIOs^+$ cells). Cells express human NCAM, showing that MPIO labelled DAPCs survived in the rats' brains and *TH*, suggesting that DAPCs matured into DA neurons. MPIO-specific fluorescence is only seen in the right hemisphere and tends to be localised near to the cell nuclei. In the merged images the *TH* is white, hNCAM is green, MPIOs is red and Dapi is blue. Note that the MPIO fluorophore, Suncoast Yellow, is also excited at 405 nm and bleeds into the Dapi channel. The injection site were found in 4 out of 6 rats that were injected for $MPIOs^+$ DAPCs. Scale bars correspond to 50 µm.

Publications

- **Mousavinejad M**, Skidmore S, Barone FG, Tyers P, Pisupati V, Poptani H, Plagge A, Barker RA, Murray P, Taylor A, Hill CJ. Assessing Human Embryonic Stem Cell-Derived Dopaminergic Neuron Progenitor Transplants Using Non-invasive Imaging Techniques. Mol Imaging Biol. 2020 Oct;22(5):1244-1254. doi: 10.1007/s11307-020-01499-4. PMID: 32378000; PMCID: PMC7497430.

- Hill CJ, Fleming JR, **Mousavinejad M**, Nicholson R, Tzokov SB, Bullough PA, Bogomolovas J, Morgan MR, Mayans O, Murray P. Self-Assembling Proteins as High-Performance Substrates for Embryonic Stem Cell Self-Renewal. Adv Mater. 2019 Apr;31(17): e1807521. doi: 10.1002/adma.201807521. Epub 2019 Mar 13. PMID: 30866118.

MOLECULAR IMAGING AND BIOLOGY

Mol Imaging Biol (2020)
DOI: 10.1007/s11307-020-01499-4

WMIS World Molecular Imaging Society
esmi European Society for Molecular Imaging
Check for updates

RESEARCH ARTICLE

Assessing Human Embryonic Stem Cell-Derived Dopaminergic Neuron Progenitor Transplants Using Non-invasive Imaging Techniques

M. Mousavinejad,[1] S. Skidmore,[1,2] F. G. Barone,[1] P. Tyers,[3] V. Pisupati,[2] H. Poptani,[1] A. Plagge,[1] R. A. Barker,[2,3] P. Murray,[1] A. Taylor,[1] C. J. Hill[1,4]

[1]*Department of Cellular and Molecular Physiology, Institute of Translational Medicine, University of Liverpool, Liverpool, L69 3BX, UK*
[2]*WT-MRC Cambridge Stem Cell Institute, University of Cambridge, Cambridge, UK*
[3]*John van Geest Centre for Brain Repair & Department of Neurology, Department of Clinical Neurosciences, University of Cambridge, Cambridge, UK*
[4]*Centre for Women's Health Research, Department of Women's and Children's Health, Institute of Translational Medicine, University of Liverpool, Liverpool, L8 7SS, UK*

Abstract

Purpose: Human pluripotent stem cell (hPSC)-derived dopaminergic neuron progenitor cells (DAPCs) are a potential therapy for Parkinson's disease (PD). However, their intracranial administration raises safety concerns including uncontrolled proliferation, migration and inflammation. Here, we apply a bimodal imaging approach to investigate the fate of DAPC transplants in the rat striatum.

Procedures: DAPCs co-expressing luciferase and ZsGreen or labelled with micron-sized particles of iron oxide (MPIOs) were transplanted in the striatum of RNU rats ($n = 6$ per group). DAPCs were tracked *in vivo* using bioluminescence and magnetic resonance (MR) imaging modalities.

Results: Transgene silencing in differentiating DAPCs accompanied with signal attenuation due to animal growth rendered the bioluminescence undetectable by week 2 post intrastriatal transplantation. However, MR imaging of MPIO-labelled DAPCs showed that transplanted cells remained at the site of injection for over 120 days. Post-mortem histological analysis of DAPC transplants demonstrated that labelling with either luciferase/ZsGreen or MPIOs did not affect the ability of cells to differentiate into mature dopaminergic neurons. Importantly, labelled cells did not elicit increased glial reactivity compared to non-labelled cells.

Conclusions: In summary, our findings support the transplantation of hPSC-derived DAPCs as a safe treatment for PD.

Key words: Dopaminergic neuron progenitor cells, Human pluripotent stem cell, Parkinson's disease, Non-invasive imaging, Bioluminescence, Magnetic resonance imaging

Introduction

Parkinson's disease (PD) is a neurodegenerative disease that results in part from the progressive loss of dopaminergic (DA) neurons in the substantia nigra. Several groups have shown that human pluripotent stem cell (hPSC)-derived dopaminergic neuron progenitor cells (DAPCs) can generate

Electronic supplementary material The online version of this article (https://doi.org/10.1007/s11307-020-01499-4) contains supplementary material, which is available to authorized users.

Correspondence to: A. Taylor; *e-mail:* taylora@liverpool.ac.uk, C. Hill; *e-mail:* C.J.Hill1@liverpool.ac.uk

Published online: 06 May 2020

mature DA neurons and improve motor function following intrastriatal transplantation in animal models of PD [1, 2]. This has now evolved to the point that the first in human hPSC-based DA neural transplants are being undertaken or planned in patients with PD. However, prior to undertaking larger-scale clinical studies, animal experiments are needed to adequately assess the safety of the therapies. Key safety concerns with such therapies for PD and other central nervous system (CNS) disorders include the risk that the implanted cells could proliferate and form space-occupying masses and/or migrate to off-target sites within the CNS and/or induce major neuroinflammation [3]. In addition to considering the potential risks, it is also important to monitor the long-term viability and differentiation capacity of implanted cells, as to be effective, they must differentiate into the appropriate phenotype and persist in the brain.

An effective strategy for monitoring the proliferation, viability and localisation of implanted cells longitudinally is to employ a non-invasive imaging approach comprising different modalities, such as bioluminescence (BLI), magnetic resonance (MRI) and fluorescence imaging [4, 5]. BLI is the most sensitive live animal imaging technique, enabling relatively small numbers of transplanted cells to be detected [6]. This technique requires that the cells express a luciferase reporter, which means that a signal is only emitted if the cells are alive. An increase in BLI signal over time indicates cell proliferation and potential tumour formation whereas a loss of signal suggests that the cells are no longer viable. A drawback with BLI, however, is that spatial resolution is poor, which means that it cannot be used to determine the location of the implanted cells and/or any resultant masses within the brain. MR imaging, on the other hand, has a very high spatial resolution and can accurately map the position of intracranial lesions [7]. Moreover, by labelling cells prior to administration with an appropriate contrast agent, such as iron oxide particles [8] or ^{19}F-based tracking agents [9], MRI can be used to plot the biodistribution of the cells over time.

Hoehn and co-workers have shown previously that BLI and MR imaging can be used to monitor the viability and intracranial biodistribution of human embryonic stem cell (hESC)-derived neural stem cells following implantation into the mouse striatum [10]. To the best of our knowledge, this bimodal approach has not previously been used to track the tumourigenicity, viability and biodistribution of hESC-derived DAPCs, following intrastriatal administration into the rat brain. A key aim of this study, therefore, was to assess the potential of this bimodal BLI/MR strategy to track hESC-derived DAPCs *in vivo*. In addition to evaluating the effectiveness of the imaging modalities themselves, we also investigated whether the labels used for tracking (*i.e.* a firefly luciferase, Fluc-ZsGreen bicistronic vector for BLI and iron oxide particles for MR imaging [4, 11]) affected the differentiation potential of the cells and/or their immunogenicity following implantation into the rat striatum.

Materials and Methods

hESC Culture and Maintenance

The clinical-grade RC17 hESC line was obtained from Roslin Cells Ltd., UK. Cells were expanded on laminin 521 (0.5 μg/cm^2) (Biolamina) in iPS-Brew XF (StemMACS™). Cells were passaged as small clumps using Versene, a non-enzymatic cell dissociation reagent (ThermoFisher Scientific), and 10 μM of Rho kinase (Rock) inhibitor Y-27632 dihydrochloride (StemMACS, Miltenyi) was added to the medium for the first 24 h after plating. The medium was changed daily, and cells were maintained at 37 °C under 5 % CO_2.

Generation of hESC Reporter Line and Labelling with Iron Oxide Particles

RC17 cells were transduced with a lentiviral vector encoding for the bicistronic expression of the codon-optimised firefly luciferase (luc2) and ZsGreen (*via* an IRES link) under the constitutive promoter elongation factor-α (EF1α). The vector plasmid was a gift from Bryan Welm (Addgene plasmid #39196), and the production and titration of viral particles was carried out using established protocols [11]. In order to transduce the hESCs, colonies of undifferentiated RC17 cells were dissociated into very small clumps consisting of about 10–15 cells using Versene for 5 min. After centrifugation, the cells were counted and seeded onto laminin 521 at a density of approximately 2.5×10^4 cells/cm^2 in the presence of 10 μM Y-27632. Cells were incubated overnight and transduced on the following day with 25×10^4 viral particles (multiplicity of infection of approximately 5) in the presence of polybrene (10 μg/ml). After 24 h, the medium was replaced, and the cells were expanded for 4 days prior to sorting for ZsGreen expression with a BD FACSAria (BD Biosciences) flow sorter. The Fluc-ZsGreen$^+$ cells were collected in iPS-Brew culture medium supplemented with 10 μM Y-27632, seeded on laminin 521 and expanded for subsequent experiments. To assess bioluminescence activity, cells were plated at different densities in black 96-well plates (Thermo Scientific), allowed to settle for 2–4 h and then incubated with medium containing D-luciferin (150 μg/ml, Promega) prior to data acquisition with an IVIS spectrum system (Perkin Elmer).

Micron-sized particles of iron oxide (MPIO) were used as a label for MR detection of DAPCs. Suncoast Yellow MPIOs (Bangs Beads, 1.63 μm nominal diameter, Bangs Laboratories, Inc.) were added directly to the DAPC's cell culture medium at a concentration of approximately 1500 particles/μl for 24 h. After the labelling period, cells were carefully washed with PBS to remove unbound particles, harvested and then used for *in vivo* studies. The extent of MPIO labelling was assessed with a FACSCalibur (BD Biosciences) flow cytometer.

Differentiation into Neural Precursors and Mature Neurons

RC17 cells were differentiated towards mesencephalic DAPCs or terminally differentiated into mature DA neurons as previously described [12]. In brief, DAPCs are obtained after neuralisation, patterning and expansion of the cells for a period of 16 days whereas DA neurons are obtained *via* the maturation of DAPCs for 34 days. Correct caudalization of progenitors towards a midbrain fate was achieved using 0.9 μM GSK3 inhibitor (CHIR99021).

Cell Implantation and In Vivo Imaging

RNU rats (males, 5–6 weeks old) were purchased from Charles River and housed in individually ventilated cages under a 12-h light/dark cycle with *ad libitum* access to standard food and water. All animal experiments were performed under a licence granted through the UK Animals (Scientific Procedures) Act 1986 and were approved by the University of Liverpool ethics committee. All applicable institutional and/or national guidelines for the care and use of animals were followed. All procedures (surgical administration of cells and imaging) were carried out under isoflurane anaesthesia.

Single-cell suspensions prepared in Hanks' Balanced Salt Solution were implanted stereotactically into the left and right hemispheres of the rats' brains. Using the bregma as a reference, the skull was drilled at 0 mm anteroposterior and ±1.5 mm mediolateral, with each hemisphere receiving two deposits of cells at a depth of −5.0 and −4.3 mm from the dura. Each deposit contained 75×10^3 cells in 0.75 μl of PBS, delivered with a microsyringe connected to an infusion pump. The rats were divided into three different experimental groups as outlined in Table 1.

BLI was carried out with an IVIS spectrum system. After inducing anaesthesia, the rats' heads were shaved and the animals received an intraperitoneal injection of luciferin at a dose of 150 mg/kg body weight. Data were acquired 20 min post administration of the substrate with a field of view B (6.5 cm), medium binning, f-stop 1 and exposure time calculated automatically by the acquisition software, up to a maximum of 5 min. All bioluminescence data were normalised to the acquisition conditions and are displayed as radiance (photons/s/cm^2/str).

MRI data were acquired with a Bruker Avance III console interfaced to a 9.4T magnet system (Bruker Biospec 94/20 USR). RF excitation was achieved with an 86-mm resonator and signal detection with a four-channel phased array receive-only rat brain coil. Once the injection site was located using scout images, higher resolution images were acquired with rapid acquisition with relaxation enhancement (RARE) sequence. Following are the parameters used: echo time (TE) = 38 ms, repetition time (TR) = 2700 ms, RARE factor = 8, number of excitations (NEX) = 8, field of view (FOV) = 35 × 35 mm, matrix size = 350 × 350 pixels, slices = 20, slice thickness = 500 μm.

At the experimental endpoint, the rats received an overdose of pentobarbital and were perfused transcardially with PBS followed by 4 % formaldehyde. The brains were harvested, postfixed with 4 % formaldehyde, equilibrated in 30 % sucrose and cryosectioned for microscopy analysis.

RT-qPCR

Cells were washed twice with PBS, and a minimum of 5×10^5 cells were lysed with TRI Reagent (Sigma). Total RNA was extracted according to the manufacturer's protocol, and a NanoDrop was used to determine RNA concentration. To synthesise cDNA, RNA was treated with DNase1 and reverse transcribed using random hexamers (Qiagen) and Superscript III reverse transcriptase (Invitrogen). PCR was performed on a CFX Connect system (Bio-Rad) using SYBR Green JumpStart Taq Ready Mix (Sigma). The genes OTX2, FOXA2 and LMX1A were measured to assess differentiation into DAPCs, with GAPDH being used as a housekeeping gene. Undifferentiated hESCs were used as a control. Relative expression levels of target genes between control and experimental samples were calculated using the $2^{-\Delta\Delta Ct}$ method [13]. Primer sequences are shown in ESM Table 1.

Immunostaining and Histology

Cells were fixed with 4 % formaldehyde for 20 min, permeabilised with 0.1 % Triton X-100 for 20 min and blocked with 1 % bovine serum albumin (BSA) for 30 min. Cryosections (10 μm) from fixed tissues were permeabilised and blocked as described above. Primary antibodies were diluted in 1:1 Triton X-100:BSA according to the dilution factors in ESM Table 2 and incubated for 24 h at 4 °C. Secondary antibodies were diluted 1:1000 in 1:1 Triton X-100:BSA and incubated for 2 h at room temperature. For immunofluorescence, cells were counterstained with DAPI. Images were acquired on a 3i spinning disk confocal microscope CSU-X1 (Intelligent Imaging Innovations) and processed with ImageJ [14]. For immunohistochemistry, tissue sections were incubated with 1.4 mM 3,3′-diaminobenzidine (DAB) and 0.01 % hydrogen peroxide for 15 min, and images were acquired with a Leica DM IL microscope.

Results

hESC Labelling Does Not Negatively Impact on Differentiation Towards DAPCs or Mature Dopaminergic Neurons In Vitro

Flow cytometry analysis of RC17 hESCs 4 days after viral transduction showed that approximately 47 % of the population expressed the reporter gene ZsGreen (ESM

Table 1. Description of the experimental groups

Group	Cells implanted in the left hemisphere	Cells implanted in the right hemisphere	Number of animals	Endpoint
1	Undifferentiated hESCs	Undifferentiated hESCs (Fluc-ZsGreen$^+$)	3	Day 27
2	DAPCs	DAPCs (Fluc-ZsGreen$^+$)	6	Day 91
3	DAPCs	DAPCs (MPIO-labelled)	6	Day 127

Fig. 1a, b). After sorting, a pure population of hESCs expressing the reporter was obtained (Fig. 1a, b), herein defined as Fluc-ZsGreen$^+$ hESCs. Fluc-ZsGreen$^+$ hESCs maintained expression of ZsGreen over multiple passages and were morphologically indistinguishable from non-transduced cells (Fig. 1a, b). To assess whether the introduction of the reporter affected pluripotency, embryoid bodies (EB) were generated and immunostained for markers of embryonic germ layer derivatives. The presence of GATA6 (endoderm), Brachyury (mesoderm) and Nestin (ectoderm) confirmed that the Fluc-ZsGreen$^+$ hESCs remained pluripotent (ESM Fig. 1c).

DAPCs were assessed for the co-expression of the key markers FOXA2, LMX1A and OTX2 on day 16 of differentiation. Quantification of mRNA *via* RT-qPCR revealed significant upregulation of all these markers (Fig. 1c), which was confirmed *via* immunofluorescence (Fig. 1d). However, fluorescence microscopy also revealed that not all cells expressed ZsGreen after differentiation into DAPCs (Fig. 1d). DAPCs were further differentiated into mature DA neurons and immunostained (differentiation day 50) to detect the classic DA neuron marker, tyrosine hydroxylase (TH). Immunofluorescence demonstrated that the transduced RC17-derived DA neurons expressed TH (Fig. 1e), but ZsGreen was no longer detectable at this differentiation stage.

Flow cytometric analysis of DAPCs showed that only 51 % of these cells expressed ZsGreen, implying a significant loss of reporter gene expression when compared to undifferentiated hESCs (Fig. 1f), and complete loss once the cells had matured to dopaminergic neurons (DAs) (Fig. 1e). Measurement of the light output (bioluminescence) revealed that the expression of luciferase corresponded to that of ZsGreen; that is, bioluminescence was strong before differentiation (37 p/s/cell), significantly reduced as cells differentiated towards DAPCs (17 p/s/cell) and extremely weak when they became mature DAs (<1 p/s/cell) (Fig. 1g).

Taken together, these results show that the introduction of the genetic reporter did not affect hESC pluripotency nor their ability to differentiate to DAPCs and DA neurons. However, reporter gene expression was progressively lost as the cells differentiated towards DA neurons. Despite the reduction in light emission in DAPCs, we reasoned that it would still be possible to detect them in rodents *in vivo*, enabling their tracking and assessment of viability/tumourigenicity in the early post-transplant period, but that it would not be possible to detect the mature DA neurons.

In Vivo Imaging Reveals Absence of DAPC Tumourigenicity and Long-Term Intracranial Distribution

In addition to assessing the ability of BLI and MRI to detect the implanted cells, a further objective of the *in vivo* studies was to investigate whether the presence of either the Fluc-ZsGreen reporter or the MPIOs affected (i) the tumourigenicity of the cells, (ii) the ability of the hESC-derived DAPCs to differentiate into mature DA neurons *in vivo* or (iii) the immunogenicity of the human cells. To this end, three groups of rats were set up. Group 1, which served as a control group for tumour formation, comprised of three rats that had Fluc-ZsGreen$^+$ hESCs implanted into the right striatum and unlabelled hESCs into the left striatum (Fig. 2a); group 2 comprised of six rats that had DAPCs derived from Fluc-ZsGreen$^+$ hESCs implanted into the right striatum and unlabelled cells into the left striatum (Fig. 2d); group 3 comprised of six rats that had MPIO-labelled hESC-derived DAPCs implanted into the right striatum and unlabelled hESC-derived DAPCs implanted into the left striatum (Fig. 4c).

hESCs and DAPCs Follow Distinct Fates In Vivo, Irrespective of the Introduction of a Reporter Gene

Optical imaging of animals that received undifferentiated hESCs on the administration day and on days 14 and 27 post administration revealed great variability in the bioluminescence signal. On the administration day, just one of the animals displayed a signal, which was very weak, suggesting that Fluc expression was not robust enough for sensitive detection in all animals. Bioluminescence was progressively lost from this rat but detected in a different animal at a later time point (ESM Fig. 2a).

MR imaging of these rats at the experimental endpoint (day 27) displayed a large area of atypical hyperintense contrast surrounding the injection site, which was present in both brain hemispheres of all animals (Fig. 2b and ESM Fig. 2b). Histological analysis of the tissue showed that this area consisted of a large number of tightly packed cells as evidenced by strong nuclear (haematoxylin) staining in the same area (Fig. 2b), suggesting an abnormal growth of cells. Immunofluorescence microscopy of these samples revealed that the masses in both hemispheres consisted of human cells, as evidenced by positive staining for a human-specific

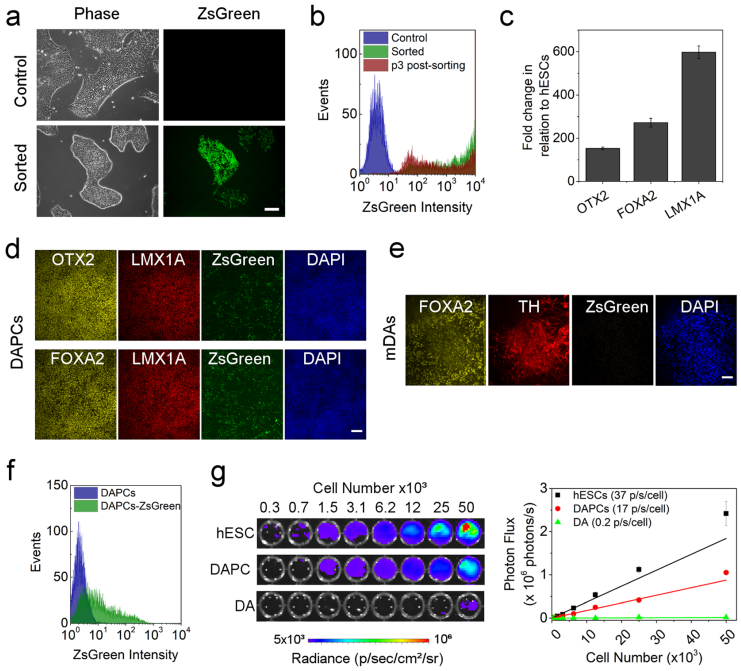

Fig. 1. Effect and stability of the Fluc-ZsGreen reporter gene in hESCs. a Phase contrast and fluorescence microscopy of the control and Fluc-ZsGreen$^+$ hESCs. Cells were imaged three passages post sorting. **b** ZsGreen expression, as measured *via* flow cytometry, of the control and sorted hESCs. The green fluorescence of the sorted cells is stable for several passages. **c** Expression of OTX2, FOXA2 and LMX1A in DAPCs obtained from Fluc-ZsGreen$^+$ hESCs. **d**, **e** Fluorescence microscopy of DAPCs and DAs obtained from Fluc-ZsGreen$^+$ hESCs (differentiation days 15 and 50, respectively). Cells were immunostained for OTX2, FOXA2, LMX1A and TH. **f** Flow cytometry shows that differentiation into DAPCs reduces ZsGreen expression (approximately 47 % of the cells expressing the construct). **g** BLI of different numbers of Fluc-ZsGreen$^+$ hESCs, DAPCs and DAs and the corresponding photon flux. Data are representative of three independent experiments. Error bars represent SD, and the solid line the linear fit of the data. Scale bars in micrographs correspond to 100 µm.

nuclear antigen (hNuclei). Interestingly, however, not all cells in the masses that formed in the right brain hemisphere (Fluc-ZsGreen$^+$ hESCs) expressed ZsGreen, suggesting that some of the hESCs lost expression of the reporter (Fig. 2c). The hESC-derived masses did not display a teratoma-like tissue architecture when examined by haematoxylin and eosin staining (data not shown). Instead, many of the cells expressed β-III tubulin, suggesting that transplantation of these cells in the rat brain promoted differentiation to ectodermal lineages (ESM Fig. 2c). The growths were also negative for OCT4, confirming that cells had differentiated in the brain (ESM Fig. 2d). Taken together, these results indicate that undifferentiated hESCs form mass lesions, irrespective of the introduction of the Fluc-ZsGreen reporter.

For rats implanted with DAPCs (group 2) (Fig. 2d), four of six animals displayed a bioluminescence signal on the administration day (Fig. 2e and ESM Fig. 3a), which was not detectable at the subsequent imaging points (days 14, 28, 56 and 91). In contrast to hESCs, administration of DAPCs resulted in no abnormal MR contrast at the experimental endpoint (day 91, Fig. 2f), with all animals exhibiting normal brain structures and the needle track being the only remarkable feature.

Human cells were still present at the injection site in both hemispheres, as evidenced by hNuclei positivity (Fig. 3a). Importantly, the areas containing human cells were also positive for TH, suggesting maturation of some DAPCs in the rats' brains within the experimental period

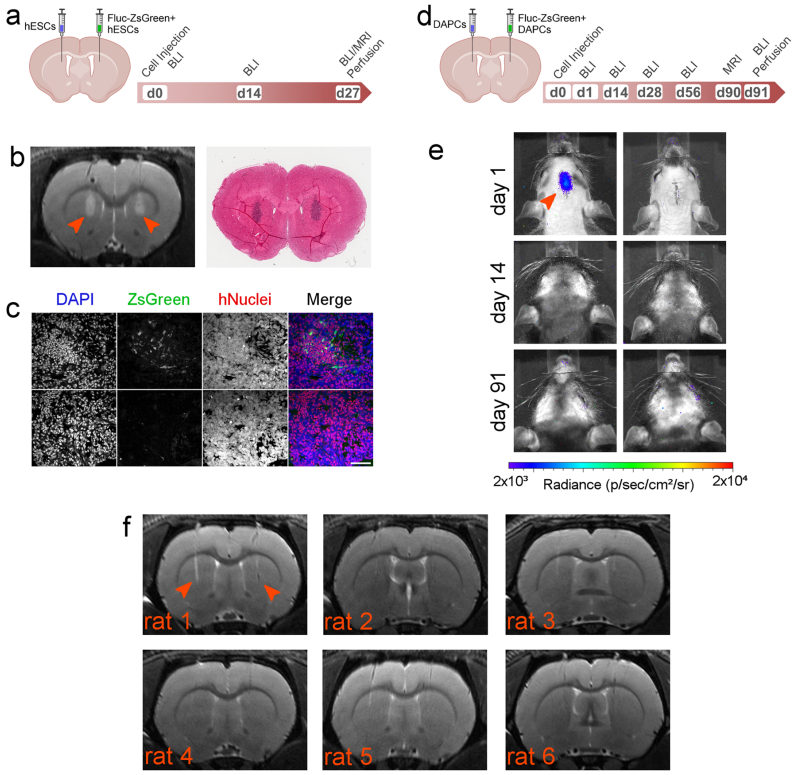

Fig. 2. Long-term fate of hESCs and DAPCs. a Schematic of injection and experimental timeline of hESC administration and imaging. **b** Representative RARE MRI scan (day 27) and corresponding histological section (H&E staining) of a rat that received undifferentiated hESCs (left hemisphere: non-transduced, right hemisphere: Fluc-ZsGreen$^+$). Both sides display a large area of hyperintense contrast at the injection site (arrowheads) which was confirmed to correspond to tightly packed cell nuclei *via* histology. **c** Fluorescence microscopy of areas of abnormal growth in the right hemisphere. In all cases, the growth corresponded to cells of human origin, as evidenced by expression of a human nuclear antigen. The level of ZsGreen expression was heterogeneous within the growths, with areas of strong expression (top) and areas where ZsGreen was lost (bottom). Scale bar = 50 µm. **d** Schematic of injection and experimental timeline of DAPC administration and imaging. **e** BLI of two of the six rats that received DAPCs as imaged on days 1, 14 and 91. Most, but not all, rats displayed a signal on the injection day, but this was lost by day 14, and no signal was seen at any other time points. The left panel is representative of rats that displayed signal on day 1, and the right panel representative of rats that did not display a signal on any of the days. Data for the other rats and time points are shown in the ESM. Note that this rat strain can display cycles of thin hair growth, as seen in some images. **f** RARE MRI scans (day 90) of all six rats that received DAPCs (left hemisphere: non-transduced, right hemisphere: Fluc-ZsGreen$^+$). No abnormal features are seen, apart from the needle track that is still visible in some animals (indicated arrowheads in the first rat only).

(91 days). Not all human cells robustly expressed TH, likely because a period of >20 weeks is necessary for the maturation of all DAPCs. The injection sites were also positive for a human-specific NCAM (hNCAM) antigen (Fig. 3b), providing further evidence that human cells had integrated with the rat brain and displayed neural lineage commitment, irrespective of whether they had been genetically modified.

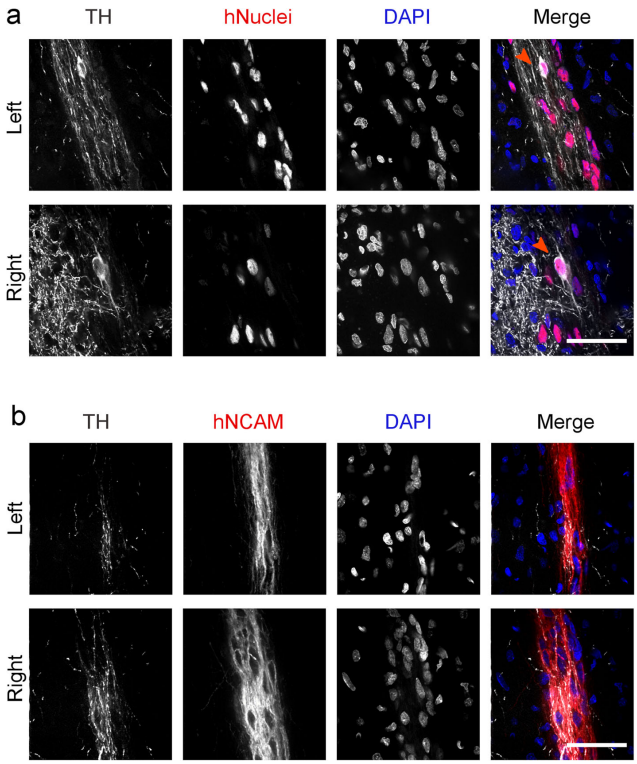

Fig. 3. DAPC integration with the rat brain. a Immunofluorescence microscopy of the injection sites (left hemisphere: non-transduced, right hemisphere: Fluc-ZsGreen$^+$). Cells express a human nuclear antigen, showing that the DAPCs survived in the rats' brains and expressed TH, suggesting that they matured into DAs. Arrowhead indicates a human cell strongly expressing TH. **b** Immunofluorescence of a similar area but using an antibody against human NCAM as a means to confirm the human origin of the cells. Scale bars correspond to 50 μm.

MPIO Labelling Enables Assessment of the Intracranial Distribution of Implanted Cells

Flow cytometry analysis of MPIO-labelled DAPCs suggested that approximately 72 % of DAPCs were labelled with the particles, as evidenced by yellow fluorescence originating from MPIOs (Fig. 4a). We also detected a shift in the side scatter of DAPCs after labelling with MPIOs, providing further evidence for the internalisation of the particles (Fig. 4b).

Rats implanted with MPIO-labelled DAPCs (group 3) (Fig. 4c) were imaged only *via* MR as neither of the hemispheres received cells with the genetic reporter. Monitoring of this group for up to 4 months post implantation confirmed that DAPC implantation does not lead to tumour formation, with all rats displaying normal brain structures at all time points. In five out of six rats, hypointense contrast was seen in the right brain hemisphere (Fig. 4d and ESM Fig. 3b). This was an expected consequence of the MPIO labelling, which enabled us to monitor the delivery and intracranial distribution of DAPCs. Remarkably, the distribution of the administered DAPCs appears to remain stable throughout the 4 months that the animals were monitored for, with no obvious change in the area with hypointense contrast, suggesting that the DAPCs were confined to the areas into which they were initially deposited. In one rat, no hypointense contrast was observed in the target area. Further analysis of the

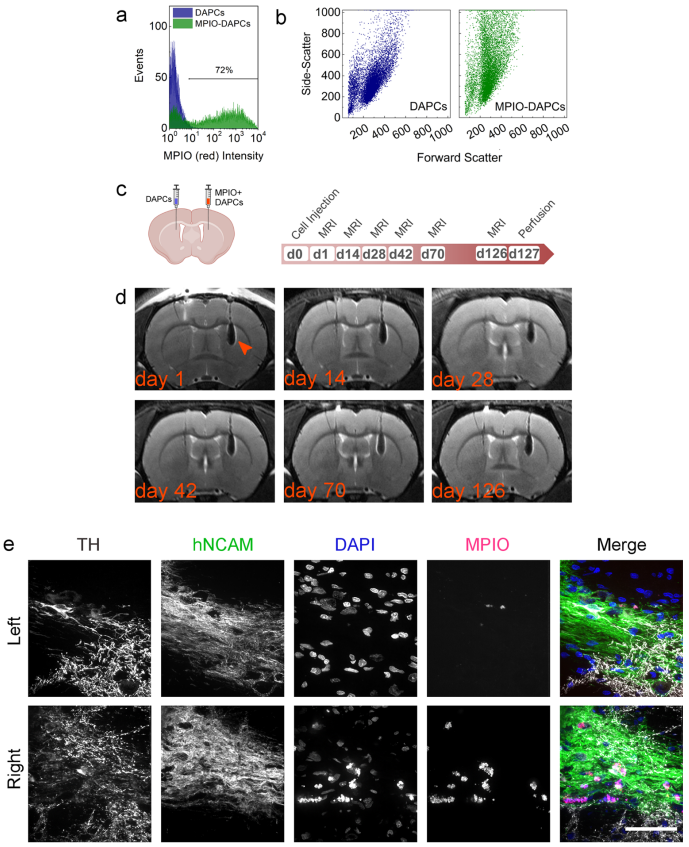

Fig. 4. MPIO tracking of DAPCs in the rat brain. a Yellow fluorescence of unlabelled and MPIO-labelled DAPCs. **b** Forward *vs.* side scatter plot of unlabelled and MPIO-labelled DAPCs. **c** Schematic of injection and experimental timeline of DAPC administration and magnetic resonance imaging. **d** Representative RARE MRI scans of a rat that received MPIO-labelled DAPC (left hemisphere: unlabelled, right hemisphere: labelled) as imaged on day 1, 14, 28, 42, 70 and 126 post administration. Hypointense contrast, indicative of a reduction in relaxation time as caused by MPIO labelling, is seen in the right hemisphere throughout the experimental period (indicated with an arrowhead in the first image). No abnormal growth is observed in either of the hemispheres. **e** Immunofluorescence microscopy of the injection sites. Cells express human NCAM, showing that MPIO-labelled DAPCs survived in the rats' brains and TH, suggesting that DAPCs matured into DAs. MPIO-specific fluorescence is only seen in the right hemisphere and tends to be localised near to the cell nuclei. Note that the MPIO fluorophore, Suncoast Yellow, is also excited at 405 nm and bleeds into the DAPI channel. Scale bar = 50 µm.

scans revealed that for this animal, the needle had been inserted at an angle, with the cells delivered to the ventricle leading to them becoming lodged at a different anatomical location (ESM Fig. 3c).

As observed before, immunofluorescence staining at the injection sites confirmed the presence of human cells that expressed TH, reinforcing the point that these cells were able to integrate within the rat brain and differentiated into mature DAs, irrespective of the MPIO labelling (Fig. 4e). In the right hemisphere, MPIOs were found in the same areas as the administered human cells and appeared to localise to perinuclear regions.

Intense Staining for GFAP Is Observed Surrounding the Human Cell Implants

A previous study showed that the implantation of Fluc$^+$ hESC-derived neural stem cells into the mouse striatum caused marked glial reaction in the host brain, as evidenced by intense immunostaining for glial fibrillary acidic protein (GFAP), a marker of reactive astrocytes [10]. To investigate whether Fluc-ZsGreen or MPIOs contributed to this reaction, sections from group 2 and group 3 rats were immunostained for GFAP. Qualitative analysis showed an increase in GFAP staining around the human implants, but no differences in staining intensity were observed around the implants comprising unlabelled human cells or MPIO-labelled cells (Fig. 5a and ESM Fig. 4a) and cells derived from Fluc-ZsGreen$^+$ hESCs (Fig. 5b and ESM Fig. 4b). Consistent with the expression profile of ZsGreen in mature DA neurons *in vitro* (Fig. 1e), the expression of ZsGreen in the brain sections was barely detectable (Fig. 5b and ESM Fig. 4b).

Discussion

Our study assessed the effectiveness of BLI and MR imaging to monitor the tumourigenicity, viability and intracranial biodistribution of hESC-derived DAPCs following stereotactic injection into the rat striatum. In most animals, BLI could only detect Fluc-ZsGreen$^+$ cells shortly after administration and was not effective for monitoring tumourigenicity and cell viability in the longer term. MR imaging, on the other hand, could detect tumours arising from undifferentiated hESCs and could monitor the intracranial biodistribution of MPIO-labelled hESC-derived DAPCs over the full time-course of our experiments.

The inability to detect cells with BLI likely resulted from a number of factors. First, at the initial imaging session, the rats were only 6 weeks old. During the intervening 2 weeks before the next imaging session, the rats grew considerably and became more pigmented (see ESM Fig. 3a), causing the intensity of the emitted light to be reduced; this likely explains why after day 1, bioluminescence could only be

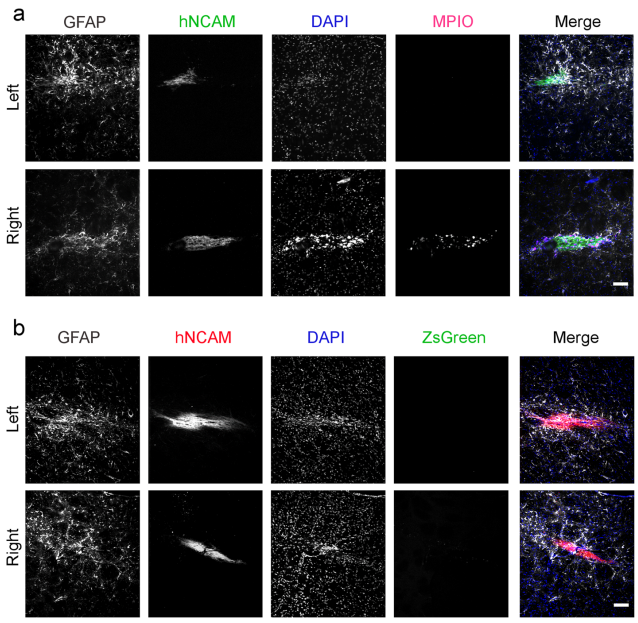

Fig. 5. Glial reaction at the injection sites. a Immunofluorescence microscopy of brains from rats that received MPIO-labelled DAPCs (left hemisphere: unlabelled; right hemisphere: labelled). The presence of human cells is identified with hNCAM staining, and the intensity of GFAP staining is stronger in these areas. MPIOs are only seen in the right hemisphere. **b** Immunofluorescence microscopy of brains from rats that received Fluc-ZsGreen$^+$ DAPCs (left hemisphere: untransduced control cells; right hemisphere Fluc-ZsGreen$^+$ cells). Scale bars correspond to 100 μm.

detected in a rat that had developed a large Fluc-ZsGreen$^+$ hESC-derived mass (ESM Fig. 2a, rat 3). Bernau *et al.* found that Fluc$^+$ human foetal neuronal progenitors implanted into the rat striatum could be imaged with BLI for 3 months [15]. However, they implanted 9×10^5 Fluc$^+$ cells into the left hemisphere compared with only 1.5×10^5 cells in our study. An additional problem was that in comparison with undifferentiated hESCs, we found that the expression levels of the reporter genes decreased by ~50 % in Fluc-ZsGreen$^+$ hESC-derived DAPCs and could not be detected at all in the mature DA neurons. It is well recognised that ESC differentiation is accompanied by increased levels of DNA methylation, leading to gene silencing, and that the pattern of silencing is cell type specific [16]. The choice of promoter also affects the extent of silencing. A previous study comparing the activity of five constitutive promoters, EF1α, human β-actin (ACTB), cytomegalovirus (CMV), phosphoglycerate kinase (PGK) and ubiquitinC (UbC) in differentiating hESCs, reported that EF1α was the most stable, with expression levels in EBs being reduced to ~50 % of those in undifferentiated hESCs [17]. Our observation that Fluc-ZsGreen expression was undetectable in the mature DA neurons, both *in vitro* and *in vivo*, was unexpected. Tennstaedt *et al.* have shown that a EF1α:Fluc-GFP$^+$ neural stem cell line derived from hESCs could be detected with BLI for 6 weeks following injection into the mouse brain without any noticeable decrease in bioluminescence intensity [18]. However, the neural stem cells used in the Tennstaedt study have a different phenotype to hESC-derived DAPCs, and there is no evidence that they differentiate into the DA lineage [18]. Likewise, there is no evidence that the Fluc$^+$ human foetal neuron progenitors used in the aforementioned Bernau *et al.* study differentiate into the DA lineage in the rat brain [15]. Indeed, as far as we are aware, there are no studies that show Fluc expression in hESC-derived DA neurons *in vivo* when Fluc is under the control of a constitutive promoter. In future studies, a cell type-specific promoter, such as FOXA2, which is expressed in both DAPCs and mature DA neurons [19], could prove more effective than the EF1α promoter for monitoring viability longitudinally, especially if used with the highly sensitive AkaLuc luciferase in combination with the substrate Akalumine [20]. However, one advantage of our system is that the loss of signal is due to differentiation. This could be used to show that the grafted cells have indeed followed the correct pathway post implantation rather than dedifferentiated back into an ESC-like phenotype.

Four weeks after implantation of undifferentiated hESCs, MR imaging could detect a cell mass in both cerebral hemispheres, irrespective of whether the cells had been transduced with the Fluc-ZsGreen reporter (ESM Fig. 2b). However, no cell masses were detected at any time point following administration of hESC-derived DAPCs, suggesting that in contrast to the undifferentiated hESCs, the DAPCs are non-tumourigenic. Cells labelled with MPIOs could be detected at all time points using longitudinal MR imaging. In addition, we found that the cells remained at the injection site and did not appear to migrate to other brain regions. From a safety perspective, the lack of migration is important to prevent cells integrating into intact neural circuits causing side effects (*e.g.* epilepsy) [21].

Previous studies have shown that labelling cells with iron oxide nanoparticles can inhibit differentiation to specific lineages [22, 23]. In our study, we did not find any evidence that the bicistronic Fluc-ZsGreen reporter or the MPIOs inhibited the differentiation of hESC-derived DAPCs into TH$^+$ DA neurons. The final aim of our study was to investigate whether the reporter or the MPIOs increased glial reactivity to the grafted cells. It is known that the implantation of cells into the brain induces a glial response [24], as evidenced by increased numbers of reactive GFAP$^+$ astrocytes surrounding the grafts [10]. Transplantation of both labelled and unlabelled DAPCs elicited a marked glial reaction at the injection site, as expected. However, there was no notable difference in the scale of glial response, suggesting that neither Fluc-ZsGreen nor MPIOs increased the glial reaction to the DAPCs [25].

Conclusions

In summary, we have demonstrated that hESC-derived DAPCs can be labelled with luminescence and contrast-enhancing reporters for *in vivo* cell tracking. Following intracranial transplantation in the rat striatum, our findings support the safe implementation of DAPC-derived therapies for the treatment of PD.

Acknowledgements. All *in vivo* imaging was carried out in the Centre for Preclinical Imaging, University of Liverpool. R.A.B is an NIHR Senior Investigator.

Funding Information. We gratefully acknowledge the support by the Medical Research Council, Engineering and Physical Sciences Research Council and Biotechnology and Biological Sciences Research Council funded UK Regenerative Medicine Platform "Safety and Efficacy, focussing on Imaging Technologies Hub" (MR/K026739/1) and Pluripotent Stem Cell Hub. F.G.B. is funded by a Wellcome Trust PhD studentship.

Compliance with Ethical Standards

Conflict of Interest

The authors declare that they have no conflict of interest.

References

1. Grealish S, Diguet E, Kirkeby A, Mattsson B, Heuer A, Bramoulle Y, van Camp N, Perrier AL, Hantraye P, Björklund A, Parmar M (2014) Human ESC-derived dopamine neurons show similar preclinical efficacy and potency to fetal neurons when grafted in a rat model of Parkinson's disease. Cell Stem Cell 15:653–665
2. Kriks S, Shim JW, Piao JH, Ganat YM, Wakeman DR, Xie Z, Carrillo-Reid L, Auyeung G, Antonacci C, Buch A, Yang L, Beal MF, Surmeier DJ, Kordower JH, Tabar V, Studer L (2011) Dopamine neurons derived from human ES cells efficiently engraft in animal models of Parkinson's disease. Nature 480:547–U177
3. Heslop JA, Hammond TG, Santeramo I, Tort Piella A, Hopp I, Zhou J, Baty R, Graziano EI, Proto Marco B, Caron A, Sköld P, Andrews PW, Baxter MA, Hay DC, Hamdam J, Sharpe ME, Patel S, Jones DR, Reinhardt J, Danen EHJ, Ben-David U, Stacey G, Björquist P, Piner J, Mills J, Rowe C, Pellegrini G, Sethu S, Antoine DJ, Cross MJ, Murray P, Williams DP, Kitteringham NR, Goldring CEP, Park BK (2015) Concise review: workshop review: understanding and assessing the risks of stem cell-based therapies. Stem Cells Transl Med 4:389–400
4. Scarfe L, Taylor A, Sharkey J, Harwood R, Barrow M, Comenge J, Beeken L, Astley C, Santeramo I, Hutchinson C, Ressel L, Smythe J, Austin E, Levy R, Rosseinsky MJ, Adams DJ, Poptani H, Park BK, Murray P, Wilm B (2018) Non-invasive imaging reveals conditions that impact distribution and persistence of cells after in vivo administration. Stem Cell Res Ther 9:332
5. Mezzanotte L, Iljas JD, Que I, Chan A, Kaijzel E, Hoeben R, Löwik C (2017) Optimized longitudinal monitoring of stem cell grafts in mouse brain using a novel bioluminescent/near infrared fluorescent fusion reporter. Cell Transplant 26:1878–1889
6. Tennstaedt A, Aswendt M, Adamczak J, Hoehn M (2013) Noninvasive multimodal imaging of stem cell transplants in the brain using bioluminescence imaging and magnetic resonance imaging. In Imaging and tracking stem cells: methods and protocols, Ed. Turksen K. pp 153–166
7. Jost SC, Collins L, Travers S, Piwnica-Worms D, Garbow JR (2009) Measuring brain tumor growth: combined bioluminescence imaging-magnetic resonance imaging strategy. Mol Imaging 8:245–253
8. Taylor A, Herrmann A, Moss D et al (2014) Assessing the efficacy of nano- and micro-sized magnetic particles as contrast agents for MRI cell tracking. PLoS One:9
9. Galisova A, Herynek V, Swider E et al (2019) A trimodal imaging platform for tracking viable transplanted pancreatic islets in vivo: F-19 MR, fluorescence, and bioluminescence imaging. Mol Imaging Biol 21:454–464
10. Tennstaedt A, Mastropietro A, Nelles M, Beyrau A, Hoehn M (2015) In vivo fate imaging of intracerebral stem cell grafts in mouse brain. PLoS One 10:e0144262
11. Taylor A, Sharkey J, Plagge A, Wilm B, Murray P (2018) Multicolour in vivo bioluminescence imaging using a NanoLuc-based BRET reporter in combination with firefly luciferase. Contrast Media Mol I
12. Nolbrant S, Heuer A, Parmar M, Kirkeby A (2017) Generation of high-purity human ventral midbrain dopaminergic progenitors for in vitro maturation and intracerebral transplantation. Nat Protoc 12:1962–1979
13. Livak KJ, Schmittgen TD (2001) Analysis of relative gene expression data using real-time quantitative PCR and the $2^{-\Delta\Delta CT}$ method. Methods 25:402–408
14. Schneider CA, Rasband WS, Eliceiri KW (2012) NIH image to ImageJ: 25 years of image analysis. Nat Methods 9:671–675
15. Bernau K, Lewis CM, Petelinsek AM, Benink HA, Zimprich CA, Meyerand ME, Suzuki M, Svendsen CN (2014) In vivo tracking of human neural progenitor cells in the rat brain using bioluminescence imaging. J Neurosci Methods 228:67–78
16. Suelves M, Carrio E, Nunez-Alvarez Y, Peinado MA (2016) DNA methylation dynamics in cellular commitment and differentiation. Brief Funct Genomics 15:443–453
17. Norrman K, Fischer Y, Bonnamy B, Sand FW, Ravassard P, Semb H (2010) Quantitative comparison of constitutive promoters in human ES cells. PLoS One 5:e12413
18. Tennstaedt A, Aswendt M, Adamczak J, Collienne U, Selt M, Schneider G, Henn N, Schaefer C, Lagouge M, Wiedermann D, Kloppenburg P, Hoehn M (2015) Human neural stem cell intracerebral grafts show spontaneous early neuronal differentiation after several weeks. Biomaterials 44:143–154
19. Domanskyi A, Alter H, Vogt MA, Gass P, Vinnikov IA (2014) Transcription factors Foxa1 and Foxa2 are required for adult dopamine neurons maintenance. Front Cell Neurosci 8
20. Iwano S, Sugiyama M, Hama H, Watakabe A, Hasegawa N, Kuchimaru T, Tanaka KZ, Takahashi M, Ishida Y, Hata J, Shimozono S, Namiki K, Fukano T, Kiyama M, Okano H, Kizaka-Kondoh S, McHugh TJ, Yamamori T, Hioki H, Maki S, Miyawaki A (2018) Single-cell bioluminescence imaging of deep tissue in freely moving animals. Science 359:935–939
21. Wijeyekoon R, Barker RA (2009) Cell replacement therapy for Parkinson's disease. Biochim Biophys Acta Mol basis Dis 1792:688–702
22. Kostura L, Kraitchman DL, Mackay AM, Pittenger MF, Bulte JWM (2004) Feridex labeling of mesenchymal stem cells inhibits chondrogenesis but not adipogenesis or osteogenesis. NMR Biomed 17:513–517
23. Kolecka MA, Arnhold S, Schmidt M, et al. (2017) Behaviour of adipose-derived canine mesenchymal stem cells after superparamagnetic iron oxide nanoparticles labelling for magnetic resonance imaging. BMC Vet Res 13
24. Cicchetti F, Barker RA (2014) The glial response to intracerebrally delivered therapies for neurodegenerative disorders: is this a critical issue? Front Pharmacol 5
25. Purushothuman S, Marotte L, Stowe S, Johnstone DM, Stone J (2013) The response of cerebral cortex to haemorrhagic damage: experimental evidence from a penetrating injury model. PLoS One 8:e59740

Erschienen in: Advanced Materials ; 31 (2019), 17. - 1807521
https://dx.doi.org/10.1002/adma.201807521

Self-Assembling Proteins as High-Performance Substrates for Embryonic Stem Cell Self-Renewal

Christopher J. Hill, Jennifer R. Fleming, Masoumeh Mousavinejad, Rachael Nicholson, Svetomir B. Tzokov, Per A. Bullough, Julius Bogomolovas, Mark R. Morgan, Olga Mayans, and Patricia Murray**

The development of extracellular matrix mimetics that imitate niche stem cell microenvironments and support cell growth for technological applications is intensely pursued. Specifically, mimetics are sought that can enact control over the self-renewal and directed differentiation of human pluripotent stem cells (hPSCs) for clinical use. Despite considerable progress in the field, a major impediment to the clinical translation of hPSCs is the difficulty and high cost of large-scale cell production under xeno-free culture conditions using current matrices. Here, a bioactive, recombinant, protein-based polymer, termed ZT^{Fn}, is presented that closely mimics human plasma fibronectin and serves as an economical, xeno-free, biodegradable, and functionally adaptable cell substrate. The ZT^{Fn} substrate supports with high performance the propagation and long-term self-renewal of human embryonic stem cells while preserving their pluripotency. The ZT^{Fn} polymer can, therefore, be proposed as an efficient and affordable replacement for fibronectin in clinical grade cell culturing. Further, it can be postulated that the ZT polymer has significant engineering potential for further orthogonal functionalization in complex cell applications.

The generation of substrates that preserve pluripotency in human stem cells and direct their controlled differentiation is intensely pursued.[1,2] Such substrates are of critical value to stem-cell-based applications, such as those concerning the modeling of disease, drug discovery, the screening of toxicants, and personalized therapies in regenerative medicine for conditions like age-related macular degeneration and Parkinson's disease.[3,4] Human pluripotent stem cells (hPSCs), specifically human embryonic stem cells (hESCs) and induced pluripotent stem cells (iPSCs), are of critical significance in these pursuits.[5] Biomedical applications of hPSCs require large-scale ex vivo culture. Therapeutic uses require, in addition, xeno-free conditions to avoid risk of zoonotic transmission. Meeting these combined requirements is challenging as hPSCs are typically cultured on costly animal-derived substrates of undefined and variable batch-to-batch composition. In particular, hPSCs are commonly cocultured with mouse fibroblast feeder cells or grown on Matrigel, a complex mixture of extracellular matrix (ECM) proteins secreted by mouse sarcoma cells that consists primarily of laminin, collagen IV, and entactin.[6] Recently, substrates based on the recombinant eukaryotic expression of ECM proteins such as laminin or vitronectin have been introduced.[7,8] These successfully support hPSC self-renewal,[9,10]

Dr. C. J. Hill, M. Mousavinejad, R. Nicholson, Dr. M. R. Morgan, Prof. P. Murray
Department of Cellular and Molecular Physiology
Institute of Translational Medicine
University of Liverpool
Nuffield Building, Crown Street, Liverpool L69 3BX, UK
E-mail: P.A.Murray@liverpool.ac.uk
Dr. C. J. Hill, Prof. O. Mayans
Department of Biochemistry
Institute of Integrative Biology
University of Liverpool
Crown Street, Liverpool L69 7ZB, UK
E-mail: Olga.Mayans@uni-konstanz.de
Dr. J. R. Fleming, Prof. O. Mayans
Department of Biology
University of Konstanz
78457 Konstanz, Germany
Dr. S. B. Tzokov, Prof. P. A. Bullough
Department of Molecular Biology and Biotechnology
The Krebs Institute
University of Sheffield
Sheffield S10 2TN, UK
Dr. J. Bogomolovas
Department of Medicine
UCSD
La Jolla, CA 92093, USA
Dr. J. Bogomolovas
Department of Cognitive and Clinical Neuroscience
Central Institute of Mental Health
Medical Faculty Mannheim
Heidelberg University
68159 Mannheim, Germany

but have high purchase costs. Together with the expense of clinical grade culture media, this limits the upscaling of hPSC expansion (e.g., in large-scale 3D culture systems using microcarriers[11]) using these substrates. Chemical substrates carrying conjugated peptides are also available, like Synthemax. However, in addition to their high cost, their use in therapeutic applications might raise potential safety concerns. For example, Synthemax is made of carboxylic acid-carrying acrylate, to which peptides derived from vitronectin are attached using chemical crosslinking.[12] It successfully supports hPSC expansion[12] but it has been observed to lead to genetic abnormalities in long-term cell cultures.[13] In summary, the need for economic and safe translational materials persists.

The protein polymer ZT[14] holds promise to meet the need for an economical, homogeneous, and functionally adaptable cell substrate of controlled composition. ZT exploits the complexation of the protein telethonin (Tel) with the two N-terminal immunoglobulin (Ig) domains from titin, Z1Z2, which occurs naturally in human sarcomeres. Tel is "sandwiched" between two antiparallel Z1Z2 doublets, forming a robust intermolecular β-sheet that spans the three components[15] (**Figure** 1A). Both Tel and Z1Z2 can be overexpressed recombinantly in bacteria with a high yield. The ZT polymer is based on a Z1Z2–Z1Z2 fusion tandem (Z_{1212}) that causes the spontaneous propagative assembly of Z1Z2:Tel complexes.[14] ZT components can be readily functionalized by genetically encoding functional moieties into the building blocks prior to their assembly. This strategy affords exact control on the position and stoichiometry of exogenous elements in the polymer. As proof of principle, ZT was engineered to display an affinity motif N-terminal to Tel that recruited gold nanoparticles to the polymer with nanoscale periodicity.[14] Moreover, the isolated Z1 domain showed that its CD loop permits the grafting of lengthy peptide motifs without causing fold perturbations, serving as an accessible and functional epitope.[16] Thereby, the ZT polymer can allow the incorporation of functional moieties in a controllable fashion.

Here, we aimed to exploit the polymeric nature, scaffolding capabilities, and ease of production of the ZT polymer to develop an economic substrate for culturing hESCs. Specifically, we aimed to mimic the efficiency of human fibronectin in supporting hESC self-renewal in serum-free conditions.[17,18] In fibronectin, the small peptide RGD in domain Fn10 is the critical integrin-binding motif mediating cell adhesion, spreading, and migration.[19] Accordingly, RGD peptide mimetics are frequently employed as adhesive moieties on substrates for cell culture applications.[20,21] hESCs do not attach to RGD peptides,[18] but a proteolytic 120 kDa fibronectin fragment containing the complete Fn10 domain successfully supported their self-renewal.[18] Building on this knowledge and on the fact that fibronectin supports cell attachment with higher efficacy than RGD alone,[22] we have assessed the mimetic potential of the ZT polymer functionalized with RGD and Fn10 moieties.

First, we established that the ZT polymer remains unaltered upon display of exogenous bioreactive motifs. For this, we created two functionalized Z_{1212} variants by genetically fusing DNA sequences: 1) a Z_{1212} tandem carrying the fibronectin GRGDS motif in the CD loop of the second Z1 domain ($Z_{1212}{}^{RGD}$) (Figure 1A,B) and 2) a Z_{1212} chimera where the Fn10 domain from fibronectin had been fused C-terminally to the tandem ($Z_{1212}{}^{Fn}$) via the same GETTQ linker sequence originally used to join Z1Z2 doublets[14] (Figure 1C). In $Z_{1212}{}^{RGD}$, the GRGDS sequence has higher affinity for integrins than the core RGD motif alone, with the flanking residues known to enhance cell attachment.[23,24] This resulted ultimately in the substitution of four native Z1 residues for a seven-residue peptide (Figure 1B). For comparison, a biologically inactive RGE version[22] was created ($Z_{1212}{}^{RGE}$).

The variants $Z_{1212}{}^{RGD}$, $Z_{1212}{}^{RGE}$, and $Z_{1212}{}^{Fn}$ proved undemanding to produce recombinantly in *Escherichia coli* cultures. Pure, stable, and monodisperse samples of all variants were produced in high yields equivalent to the wild type protein Z_{1212} (>40 mg L^{-1} culture) (Figure S1A,B, Supporting Information). To test the capability of the variants to self-assemble, and given that the Z1Z2/Tel complex is the fundamental assembly unit of the ZT polymer, we considered that complexation of Tel by modified Z1Z2 samples at the native 2:1 ratio was evidence of undisrupted assembly in these variants. Therefore, we produced $Z1Z2^{RGD}$/Tel and $Z1Z2^{Fn}$/Tel complexes by in cellulo co-expression, studied their migration in size exclusion chromatography (SEC), and measured their molecular mass by SEC-coupled multi-angle laser light scattering (MALLS), confirming the expected 2:1 association (Figure S1C–E, Supporting Information). Next, we mixed the polymerizing Z_{1212} variants ($Z_{1212}{}^{RGD}$, $Z_{1212}{}^{RGE}$, and $Z_{1212}{}^{Fn}$) with Tel and confirmed assembly by native-PAGE (Figure S1F,G, Supporting Information) and electron microscopy (Figure 1D); the resulting polymers are here denoted as ZT^{RGD}, ZT^{RGE}, and ZT^{Fn}, respectively. Taken together, these results proved that the Z_{1212} building block could be successfully functionalized in both internal (CD loop) and external (C-terminus) positions, maintaining its structural integrity and its polymerization capability.

The conformation of the RGD motif influences the selectivity and affinity of the integrin receptors it engages and, thereby, its efficiency in cell adhesion.[22,24–26] Thus, we studied whether the RGD motif inserted in Z1 resembles the motif in the native Fn10. In Fn10, the motif is located within the FG β-hairpin loop that resembles a distorted type II' β-turn with high intrinsic flexibility.[25,27] To confirm the degree of structural mimicry achieved by the loop engineered in Z1, we elucidated the crystal structure of $Z_{1212}{}^{RGD}$ at 3.0 Å resolution (Table S1, Supporting Information). The structure confirmed that the fold of Z1 is not altered by the inserted sequence, with the structure closely matching that of wild-type Z1 (rmsd = 0.47 Å to Z1 in Protein Data Bank (PDB) entry 2A38[28]) (Figure 1E). The inserted SSGRGDSS sequence formed a loop protruding from the surface of Z1 as expected, in quasi β-turn conformation and with evident signs of flexibility (Figure S2, Supporting Information), thereby reproducing the features of the native motif in fibronectin. Comparison of crystal structures for modified Z1 and Fn10 (PDB IDs: 1FNA, 1FNF, and 4MMX) showed that the engineered RGD motif locally adopts a similar conformation (Figure 1F,G). These data confirm the ability of the introduced sequence to emulate the native RGD motif.

We then tested whether the functionalized ZT polymer promoted spreading of murine mesenchymal stromal cells (mMSC) by comparing the relative efficiency of cell attachment to the ZT^{RGD} and ZT^{Fn} polymers. For this analysis, we employed the clonally-derived mMSC line D1, which tolerates a variety of RGD-based substrata.[29–31] We cultured mMSCs on nonadhesive

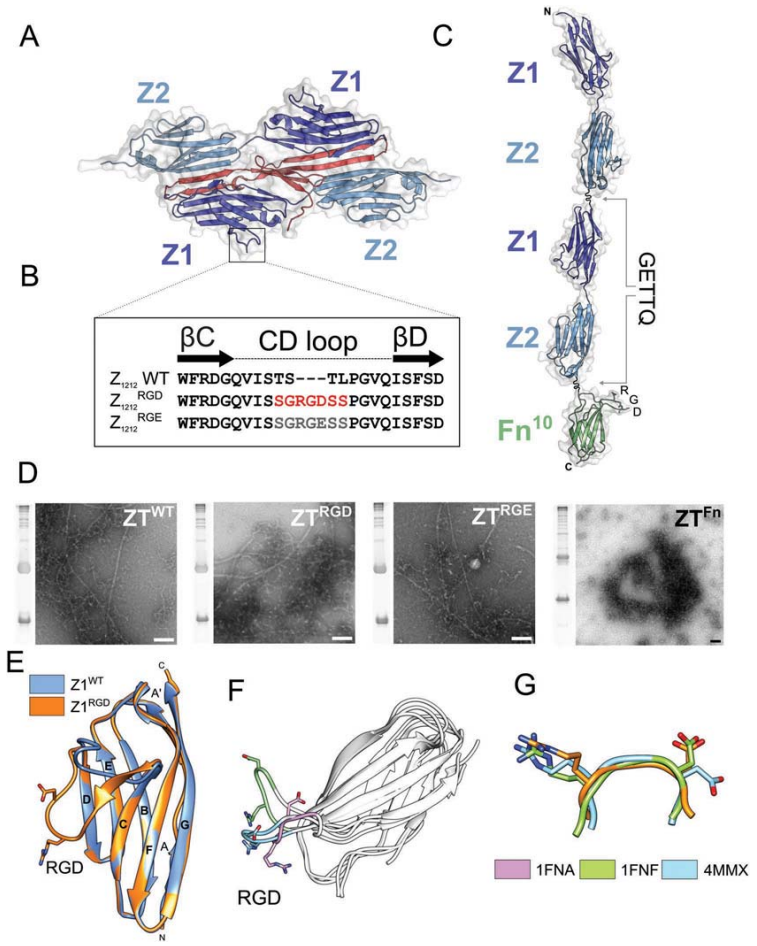

Figure 1. The functionalized ZT polymer. A) Crystal structure of the "sandwich" complex formed by two antiparallel Z1Z2 Ig-doublets from titin (blue) and Tel (red) (PDB: 1YA5[15]). The CD loop of domain Z1 is boxed. B) Sequence of the native and modified CD loop. The residues introduced are colored red. C) Z_{1212} protein carrying a C-terminally fused domain Fn10 from human fibronectin (PDB: 1FNF,[25] green). Fusion of naturally-occurring protein moieties in this chimera uses a GETTQ linker sequence. The native RGD motif located within the FG loop of Fn10 is displayed. D) Transmission electron microscopy images of ZT^{WT}, ZT^{RGD}, ZT^{RGE}, and ZT^{Fn} polymers postassembly (scale bars correspond to 100 nm). E) Crystal structure of the GRGDS modified Z1 domain superimposed on wild-type Z1 (PDB 2A38[28]). F) Superimposition of crystal structures of domain Fn10 from fibronectin (PDB codes are given). The conformational flexibility of the RGD loop (colored) is manifest. G) Superimposition of the RGD loop in Z1 (orange) with those from Fn10 structures shows that the motif incorporated in Z1 adopts a near-native conformation at the local level (structure 1FNA is excluded as its conformation is unique).

polystyrene plates coated with the ZT^{RGD}, ZT^{RGE}, and ZT^{Fn} polymers under serum-free conditions and quantified cell attachment and dispersion. At 2 h culture, mMSCs showed adherence to both ZT^{RGD} and ZT^{Fn} in a concentration-dependent manner, confirming the accessibility of both RGD and Fn10 moieties within the polymer (**Figure 2**A,B). However, consistently more

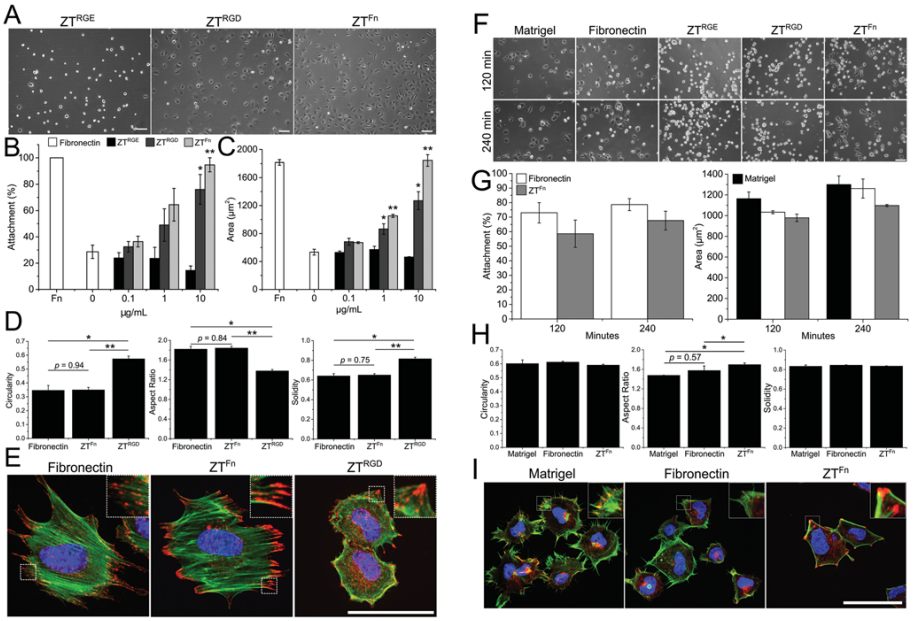

Figure 2. Murine MSC and human ESC adhesion and spreading on ZT substrates. A) Representative phase-contrast micrographs of mMSCs cultured for 2 h under serum-free conditions on nontreated plastic coated with ZT polymers at 10 μg mL^{-1} (scale bar = 100 μm). B,C) Effect of ZT^{RGE} (non-bioactive), ZT^{RGD}, and ZT^{Fn} substrates on mMSC adhesion (B) and spreading (C). Cell attachment is expressed as a percentage of the positive control (fibronectin at 10 μg mL^{-1}) that was taken as 100%. The average area of cells grown on fibronectin is included for comparison. Statistical significance in (B) and (C) is in reference to a nontreated surface (0 μg mL^{-1}). D) Comparisons of the average circularity, aspect ratio, and solidity of cells grown on nontreated plastic coated with fibronectin, ZT^{RGD}, or ZT^{Fn}, all samples at 10 μg mL^{-1}. E) Representative confocal microscopy images of cells stained for F-actin (green), paxillin (red), and DAPI (blue) following attachment to different substrates. Zooms of boxed areas are shown in the upper right of the respective image. F) Representative phase-contrast images of HUES7 cells cultured for 2 and 4 h on ZT^{RGD}, ZT^{Fn}, and control substrates. Scale bar = 100 μm. G) Quantification of cell attachment and spreading is shown by the bar charts. Cell attachment is expressed as a percentage of the positive control (Matrigel) that was taken as 100%. H) Comparisons of the average circularity, aspect ratio, and solidity of cells plated on plastic plates coated with Matrigel, fibronectin, or ZT^{Fn} at 10 μg mL^{-1}. I) Representative confocal microscopy images of cells stained for F-actin (green), paxillin (red), and DAPI (blue) following attachment to different substrates. Zooms of boxed areas are shown in the upper right of the respective image. (Error bars represent the standard error on the mean (SEM), $n = 3$. Scale bar = 50 μm if not otherwise stated. Throughout, $^{*}p < 0.05$, $^{**}p < 0.01$, and $^{***}p < 0.001$).

cells attached to ZT^{Fn} than to ZT^{RGD}. As expected, the non-bioactive ZT^{RGE} did not support cell attachment. mMSC spreading was quantified by calculating the average cell area for all conditions (Figure 2C). Spreading was significantly increased on ZT^{RGD} and ZT^{Fn} compared to the plastic control, but ZT^{Fn} showed the best performance. In addition, cell profiles were used to determine the average circularity (or area-to-perimeter ratio), aspect ratio (AR), and solidity of mMSCs plated on human plasma fibronectin, ZT^{RGD} or ZT^{Fn} (Figure 2D). Values were remarkably equivalent for cells grown on ZT^{Fn} or fibronectin, while differences were observed in cells plated on ZT^{RGD}. Higher circularity and solidity values for mMSCs cultured on ZT^{RGD} correlated with a symmetric spreading on this substrate, while the higher AR and lower solidity of cells cultured on ZT^{Fn} or fibronectin indicate anisotropic spreading. By using a competitive inhibition assay that employed a linear GRGDS peptide, we confirmed that the observed effects on cell attachment are due to the respective specificities of the engineered ZT^{RGD} and ZT^{Fn} polymers for integrin binding (Figure S3, Supporting Information). To further investigate attachment, we examined the impact of the different substrates on cytoskeletal organization and adhesion complexes (Figure 2E). Focal complexes were observed on all substrates. However, mMSCs plated on fibronectin or ZT^{Fn} displayed well-developed stress fiber networks, while cells attached to ZT^{RGD} exhibited fewer stress fibers and a cortical actin distribution. Taken together, cell adhesion and spreading data indicated that the loop-grafted GRGDS motif was insufficient to support effective mMSC attachment, but that the interaction of cells with the ZT^{Fn} polymer mimicked that of full-length human fibronectin.

To assess the capability of ZT^{Fn} to support cell growth in potential clinical applications, we then tested this polymer on human HUES7 cells, proving that hESCs attach to and proliferate on ZT^{Fn}. HUES7 cells neither attach nor spread on materials functionalized with RGD peptides, but they can be cultured on fibronectin or large proteolytic fragments thereof.[18] Accordingly, we confirmed that HUES7 cells did not adhere to ZT^{RGD} (Figure 2F) or to the Fn10 domain alone (in the absence of the polymerized ZT) (Figure S4, Supporting Information). However, they attached successfully to the ZT^{Fn} polymer. Moreover, the extent of HUES7 cell attachment and spreading on ZT^{Fn} was comparable to that on human plasma fibronectin (both substrates used at comparable amounts; Figure S5, Supporting Information). Cell attachment and spreading on both fibronectin and ZT^{Fn} were only moderately lower than those obtained from the complex matrix Matrigel (Figure 2G). We concluded that the ZT^{Fn} polymer comparatively resembled the performance of native fibronectin in supporting hESC growth and spreading.

We further compared the effect of ZT^{Fn}, fibronectin, and Matrigel on cell growth. As our long-term goal is to support the clinical application of hPSCs, we focused this test on established biological substrates, naturally produced by living cells and composed only of biodegradable, folded protein components that have not undergone chemical treatment. We did not employ chemical substrates (e.g., Synthemax) as comparative controls to ZT^{Fn} because of their more distant composition. The results showed that, while average cell circularity and solidity were consistent between substrates, the average AR of cells plated on ZT^{Fn} was significantly higher than that of cells cultured on fibronectin and particularly higher than Matrigel, reflecting the asymmetric spreading on ZT^{Fn} (Figure 2H). F-actin and paxillin staining showed that focal adhesions were present in HUES7 cells grown on Matrigel and ZT^{Fn}, but were less common on fibronectin (Figure 2I). Filopodia-like projections were abundant in cells cultured on Matrigel and in some cells grown on fibronectin, but cells grown on ZT^{Fn} lacked projections and exhibited a geometric morphology with well-defined actin stress fibers (Figure 2I). Intriguingly, the observed increase in actin filamentation was sustained following prolonged culture on ZT^{Fn} (Figure S6A, Supporting Information). Despite their morphological differences, cells grown on ZT^{Fn} retained an ESC phenotype following single cell dissociation as confirmed by nuclear OCT4 and NANOG expression (Figure S6B, Supporting Information). Cells on all substrates successfully began to form colonies after 24 h (Movies S1–S3, Supporting Information) and robustly expressed pluripotency markers (Figure S7A, Supporting Information). Additionally, focal adhesions were found to contain focal adhesion kinase (FAK) phosphorylated at tyrosine 397 (pY397), confirming the activation of signaling pathways downstream of integrin engagement (Figure S7B, Supporting Information).

To better characterize the molecular mode of action of ZT^{Fn}, we set out to identify the integrins it engages. As fibronectin attachment is largely dependent on $\alpha5\beta1$ and $\alpha V\beta3$,[32] we tested first the involvement of these integrins in HUES7 cells plated on ZT^{Fn}. While we detected $\alpha5\beta1$ in focal adhesions (**Figure 3**A), we did not detect $\alpha V\beta3$ (Figure S8A,B, Supporting Information). Unexpectedly, targeting the αV subunit alone produced robust focal adhesion-like staining, as did an antibody against subunit $\beta5$ unique to the $\alpha V\beta5$ heterodimer (Figure 3B). Thus, we concluded that HUES7 cell attachment to ZT^{Fn} is mediated by $\alpha V\beta5$ and $\alpha5\beta1$ integrins present in cell adhesion complexes (Figure 3C). After 2 days of culture, the cells continued to engage $\alpha V\beta5$ (Figure S9, Supporting Information). On the contrary, cells grown on Matrigel and fibronectin were negative for both αV and $\beta5$ adhesion-specific staining (Figure S8B, Supporting Information). Currently, there is no robust evidence for the binding of $\alpha V\beta5$ to fibronectin; therefore, its engagement by ZT^{Fn} was unexpected. Integrin $\alpha V\beta5$ is a well-characterized receptor of the RGD motif in the somatomedin-B domain from vitronectin.[33,34] Accordingly, $\alpha V\beta5$ mediates hPSC attachment to vitronectin,[35,36] and attachment of hiPSC lines IMR90 and Gibco episomal line to the synthetic vitronectin-based peptide acrylate, Synthemax.[12] In agreement with our finding, we observed that the morphology of cells grown on ZT^{Fn} strikingly emulated that of cells grown on vitronectin (Figure S10, Supporting Information). Both cells cultured on vitronectin and ZT^{Fn} also displayed increased stress fiber formation and large focal adhesions containing FAK pY397 (Figure S10, Supporting Information). The larger size of focal adhesions formed on the ZT^{Fn} substrate caused the cells to migrate more slowly in comparison to Matrigel and fibronectin substrates, as a close relationship exists between the size of focal adhesions and cell migration speed (Figure 3D).[37] Slow migration was reproduced by cells cultured on vitronectin (Figure 3D). Upon prolonged culture on all substrates, cells formed colonies. Colonies grown on Matrigel exhibited $\alpha5\beta1$ expression in distinct fibrillar patterns while expression of this integrin was lost on ZT^{Fn} (Figure S9A, Supporting Information). Yet, colonies grown on ZT^{Fn} continued to express $\alpha V\beta5$ (Figure S9B, Supporting Information). It is remarkable to observe that the presentation of the Fn10 domain in the context of the ZT^{Fn} polymer induces a preferential switch to $\alpha V\beta5$. It can be concluded that not only the chemical composition of the bioreactive motif but also the geometry of its presentation to the cell is critical for integrin selectivity. This finding adds to the previous observation that the specific conformation of fibronectin on different synthetic surfaces dramatically influenced integrin binding.[38]

To investigate whether the observed difference in integrin engagement affected cell phenotype, we assessed the ability of ZT^{Fn} to promote survival of single HUES7 cells. We found that hESCs maintain a pluripotent phenotype following prolonged culture on ZT^{Fn}, which supported clonal expansion with an efficacy comparable to fibronectin and only moderately reduced relative to Matrigel (**Figure 4**A). Cell proliferation was somewhat reduced on ZT^{Fn} compared to Matrigel, but was not significantly different from fibronectin (Figure 4B). Finally, we assessed the ability of ZT^{Fn} to maintain the long-term self-renewal of HUES7 cells. For this, the cells were cultured in mTeSR1 medium (without ROCK inhibitor, a compound used to extend cell survival[39]) for up to 18 passages. The cells were passaged every 5–6 days as clumps containing 50–200 cells; they were cultured on ZT^{Fn} for ≈4 months in total with no noticeable negative effects. The cells grew as colonies with typical morphologies, including a high nuclear-to-cytoplasmic ratio and prominent nucleoli. Cells also retained nuclear expression of OCT4 and NANOG (Figure S11A, Supporting Information). Relative gene expression analysis of pluripotency markers OCT4, NANOG, and SOX2 was used to compare cells cultured on Matrigel with those cultured on fibronectin or ZT^{Fn} for 1, 5, and

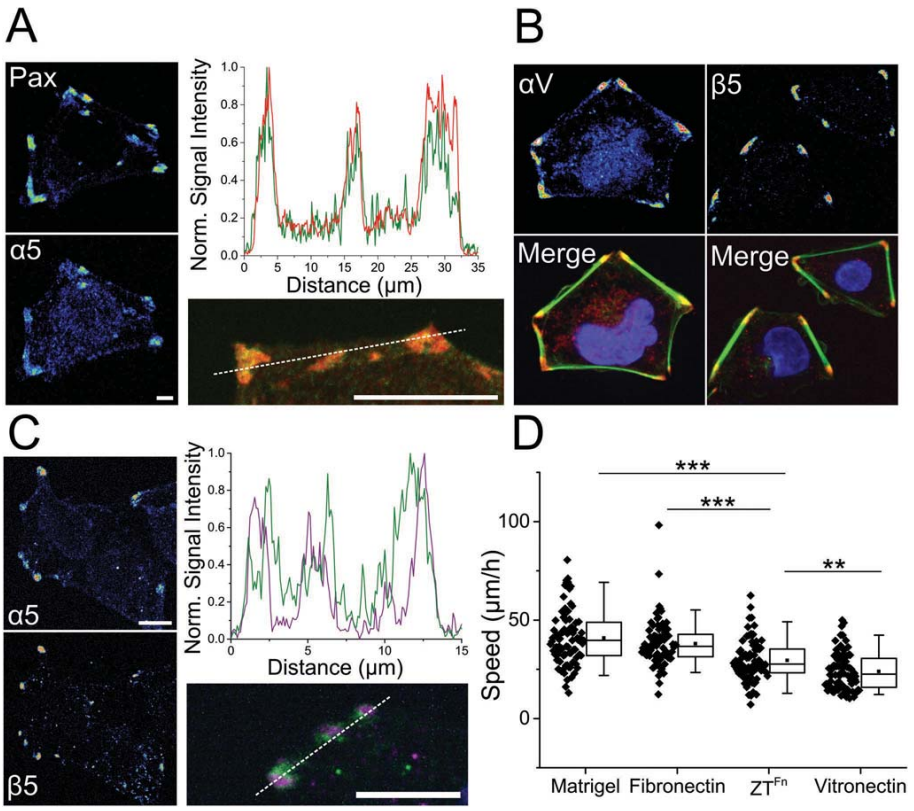

Figure 3. Integrin engagement and migration of human ESCs on ZT^{Fn}. A) Representative pseudocolored confocal microscopy images show paxillin (red) and $\alpha 5$ integrin subunit (green) costaining of HUES7 cells following 4 h culture on ZT^{Fn}. The fluorescence intensity line scan profile was generated from the merged image shown below. Scale bars = 10 μm. B) Staining of αV and $\beta 5$ integrin subunits (red). The merged images show counterstaining for F-actin (green) and DAPI (blue). Scale bar = 50 μm. C) Pseudocolored microscopy images show costaining of $\alpha 5$ (green) and $\beta 5$ (purple) subunits in HUES7 cells cultured on ZT^{Fn}. A fluorescence intensity profile is shown for the merged image. Scale bars = 10 μm. D) Box-and-whisker plots of cell migration. Boxes show the median (middle line), mean (square), 25th and 75th percentiles (box ends), and 5th and 95th percentiles (whiskers) ($n = 80$).

10 passages. *NANOG* and *SOX2* transcript levels were found to be significantly decreased in cells cultured on fibronectin at passage 10 (Figure 4C). Although NANOG expression was also downregulated in cells cultured on ZT^{Fn} at passage 10 relative to Matrigel, expression was significantly higher compared to fibronectin (Figure 4C). Cells cultured on ZT^{Fn} or fibronectin for 13 passages were used to form embryoid bodies that contained derivatives of the three embryonic germ layers in vitro (Figure S11B in Supporting Information). Positive staining for Brachyury (mesoderm), GATA6 (GATA-binding factor 6, endoderm), and Nestin (ectoderm) confirmed that HUES7 cells remained pluripotent following their long-term culture on ZT^{Fn}.

In conclusion, we show that the ZT polymer is a chimeric composite of recombinant human proteins, with high functionalization capability.[14] Neither loop grafting nor domain fusion reduced the bacterial production yield of Z_{1212} variants, an important consideration for large-scale applications. We show that the functionalized ZT system is compatible with standard cell culture techniques and that it serves as an efficient substrate for the long-term self-renewal of pluripotent hESCs, being a viable substitute for natural fibronectin and other commonly used matrices for hPSC culture. The material is produced in bacteria; it is scalable and predictably compatible with 3D culture systems. In this regard, the incorporation of natural ECM proteins with 3D

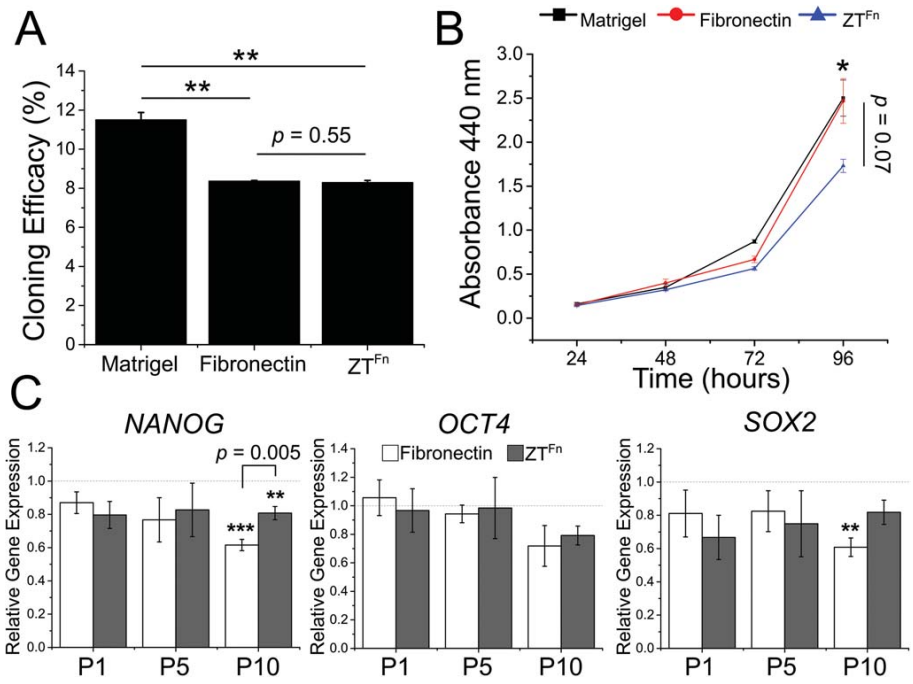

Figure 4. Human ESC clonal culturing and self-renewal on ZT^{Fn}. A) Clonogenic survival of cells plated on Matrigel, fibronectin, and ZT^{Fn} at a density of 2.5×10^3 cm^{-2}. B) Proliferative capacity of HUES7 cells cultured on Matrigel, fibronectin, or ZT^{Fn} over 4 days. Error bars represent SEM ($n = 4$). C) Quantitative RT-qPCR analysis of NANOG, OCT4, and SOX2 expression levels in HUES7 cells cultured on fibronectin or ZT^{Fn} for 1, 5, and 10 passages relative to cells cultured on Matrigel. Error bars represent SEM ($n = 3$).

materials using crosslinking is established in the bibliography. For example, fibronectin has been photocrosslinked into hyaluronic acid 3D hydrogels for endothelial cell culture.[40] As the ZT polymer is composed of folded protein domains that closely resemble those of fibronectin, its incorporation in 3D systems via chemical crosslinking can be expected to be an equally feasible goal. In summary, economical substrates of controlled composition such as the ZT^{Fn} polymer will be essential for further advancement in the clinical translation of PSC-based therapies.

Acknowledgements

The authors thank Yevheniia Nesterenko and the Electron Microscopy Unit of Universität Konstanz for EM images of ZT^{Fn}. The authors thank the Diamond Light Source for synchrotron radiation time. This research was supported by the BBSRC (Biotechnology and Biological Sciences Research Council), JRI Orthopaedics (BB/I01666X/1), and the Wellcome Trust (204401/z/16/z). J.R.F. was supported by an EU Marie Sklodowska-Curie Individual Fellowship (TTNPred, 753054). The authors thank the HUES cells facility, Melton Laboratory, Harvard University, MA (USA) for providing the HUES7 cell line. The mMSC cell line was purchased from ATCC. C.J.H., O.M., and P.M. conceived the study. C.J.H., O.M., M.R.M., and P.M. designed experiments. C.J.H. and J.B. performed molecular cloning. C.J.H produced and characterized protein constructs and assemblies. C.J.H., S.B.T., and P.A.B. carried out electron microscopy studies. C.J.H., J.R.F., and O.M. analyzed protein structure. C.J.H., M.M., and R.N. performed cell-based experiments and data analysis. C.J.H. performed confocal imaging. C.J.H., O.M., P.M., and M.R.M. wrote the manuscript. The coordinates and X-ray diffraction data for the crystal structure of Z_{1212}^{RGD} have been deposited with the Protein Data Bank (www.rcsb.org) with accession code 6FWX.

Conflict of Interest

The authors declare competing financial interests: C.J.H., O.M., and P.M. disclose a pending patent on the use of Fn10 as a chimeric fusion protein of the ZT system.

Keywords

biomaterials, protein engineering, protein self-assembly, self-renewal, stem cells

[1] C. M. Madl, S. C. Heilshorn, *Annu. Rev. Biomed. Eng.* **2018**, *20*, 21.
[2] Z. Liu, M. Tang, J. Zhao, R. Chai, J. Kang, *Adv. Mater.* **2018**, *30*, 1705388.
[3] R. S. Thies, C. E. Murry, *Development* **2015**, *142*, 3614.
[4] Y. Avior, I. Sagi, N. Benvenisty, *Nat. Rev. Mol. Cell Biol.* **2016**, *17*, 170.
[5] Y. Shi, H. Inoue, J. C. Wu, S. Yamanaka, *Nat. Rev. Drug Discovery* **2017**, *16*, 115.
[6] C. S. Hughes, L. M. Postovit, G. A. Lajoie, *Proteomics* **2010**, *10*, 1886.
[7] E. Sanjar, S. Jin, *World J. Stem Cells* **2015**, *7*, 243.
[8] Y. Fan, J. Wu, P. Ashok, M. Hsiung, E. S. Tzanakakis, *Stem Cell Rev. Rep.* **2015**, *11*, 96.
[9] A. B. J. Prowse, M. R. Doran, J. J. Cooper-White, F. Chong, T. P. Munro, J. Fitzpatrick, T. L. Chung, D. N. Haylock, P. P. Gray, E. J. Wolvetang, *Biomaterials* **2010**, *31*, 8281.
[10] T. Miyazaki, S. Futaki, H. Suemori, Y. Taniguchi, M. Yamada, M. Kawasaki, M. Hayashi, H. Kumagai, N. Nakatsuji, K. Sekiguchi, E. Kawase, *Nat. Commun.* **2012**, *3*, 1236.
[11] C. Kropp, D. Massai, R. Zweigerdt, *Process Biochem.* **2017**, *59*, 244.
[12] Z. Melkoumian, J. L. Weber, D. M. Weber, A. G. Fadeev, Y. Zhou, P. Dolley-Sonneville, J. Yang, L. Qiu, C. A. Priest, C. Shogbon, A. W. Martin, J. Nelson, P. West, J. P. Beltzer, S. Pal, R. Brandenberger, *Nat. Biotechnol.* **2010**, *28*, 606.
[13] J. W. Lambshead, L. Meagher, J. Goodwin, T. Labonne, E. Ng, A. Elefanty, E. Stanley, C. M. O'Brien, A. L. Laslett, *Sci. Rep.* **2018**, *8*, 701.
[14] M. Bruning, L. Kreplak, S. Leopoldseder, S. A. Muller, P. Ringler, L. Duchesne, D. G. Fernig, A. Engel, Z. Ucurum-Fotiadis, O. Mayans, *Nano Lett.* **2010**, *10*, 4533.
[15] P. Zou, N. Pinotsis, S. Lange, Y.-H. Song, A. Popov, I. Mavridis, O. M. Mayans, M. Gautel, M. Wilmanns, *Nature* **2006**, *439*, 229.
[16] M. Bruning, I. Barsukov, B. Franke, S. Barbieri, M. Volk, S. Leopoldseder, Z. Ucurum, O. Mayans, *Protein Eng., Des. Sel.* **2012**, *25*, 205.
[17] M. A. Baxter, M. V. Camarasa, N. Bates, F. Small, P. Murray, D. Edgar, S. J. Kimber, *Stem Cell Res.* **2009**, *3*, 28.
[18] D. M. Kalaskar, J. E. Downes, P. Murray, D. H. Edgar, R. L. Williams, *J. R. Soc., Interface* **2013**, *10*, 20130139.
[19] A. J. Zollinger, M. L. Smith, *Matrix Biol.* **2017**, *60–61*, 27.
[20] L. Perlin, S. Macneil, S. Rimmer, *Soft Matter* **2008**, *4*, 2331.
[21] S. L. Bellis, *Biomaterials* **2011**, *32*, 4205.
[22] P. Rajagopalan, W. A. Marganski, X. Q. Brown, J. Y. Wong, *Biophys. J.* **2004**, *87*, 2818.
[23] M. D. Pierschbacher, E. Ruoslahti, *Nature* **1984**, *309*, 30.
[24] T. G. Kapp, F. Rechenmacher, S. Neubauer, O. V. Maltsev, E. A. Cavalcanti-Adam, R. Zarka, U. Reuning, J. Notni, H. J. Wester, C. Mas-Moruno, J. Spatz, B. Geiger, H. Kessler, *Sci. Rep.* **2017**, *7*, 39805.
[25] D. J. Leahy, I. Aukhil, H. P. Erickson, *Cell* **1996**, *84*, 155.
[26] E. Ruoslahti, B. Obrink, *Exp. Cell Res.* **1996**, *227*, 1.
[27] A. L. Main, T. S. Harvey, M. Baron, J. Boyd, I. D. Campbell, *Cell* **1992**, *71*, 671.
[28] M. Marino, P. Zou, D. Svergun, P. Garcia, C. Edlich, B. Simon, M. Wilmanns, C. Muhle-Goll, O. Mayans, *Structure* **2006**, *14*, 1437.
[29] N. Huebsch, P. R. Arany, A. S. Mao, D. Shvartsman, O. A. Ali, S. A. Bencherif, J. Rivera-Feliciano, D. J. Mooney, *Nat. Mater.* **2010**, *9*, 518.
[30] Y. Lei, S. Gojgini, J. Lam, T. Segura, *Biomaterials* **2011**, *32*, 39.
[31] M. Mehta, C. M. Madl, S. Lee, G. N. Duda, D. J. Mooney, *J. Biomed. Mater. Res., Part A* **2015**, *103*, 3516.
[32] M. R. Morgan, A. Byron, M. J. Humphries, M. D. Bass, *IUBMB Life* **2009**, *61*, 731.
[33] J. P. Kim, K. Zhang, J. D. Chen, R. H. Kramer, D. T. Woodley, *J. Biol. Chem.* **1994**, *269*, 26926.
[34] I. Schvartz, D. Seger, S. Shaltiel, *Int. J. Biochem. Cell Biol.* **1999**, *31*, 539.
[35] S. R. Braam, L. Zeinstra, S. Litjens, D. Ward-van Oostwaard, S. van den Brink, L. van Laake, F. Lebrin, P. Kats, R. Hochstenbach, R. Passier, A. Sonnenberg, C. L. Mummery, *Stem Cells* **2008**, *26*, 2257.
[36] T. J. Rowland, L. M. Miller, A. J. Blaschke, E. L. Doss, A. J. Bonham, S. T. Hikita, L. V. Johnson, D. O. Clegg, *Stem Cells Dev.* **2010**, *19*, 1231.
[37] D. H. Kim, D. Wirtz, *FASEB J.* **2013**, *27*, 1351.
[38] B. G. Keselowsky, D. M. Collard, A. J. García, *J. Biomed. Mater. Res., Part A* **2003**, *66A*, 247.
[39] K. Watanabe, M. Ueno, D. Kamiya, A. Nishiyama, M. Matsumura, T. Wataya, J. B. Takahashi, S. Nishikawa, S. Nishikawa, K. Muguruma, Y. Sasai, *Nat. Biotechnol.* **2007**, *25*, 681.
[40] S. K. Seidlits, C. T. Drinnan, R. R. Petersen, J. B. Shear, L. J. Suggs, C. E. Schmidt. *Acta Biomater.* **2011**, *7*, 2401.